MICROSTRUCTURE AND MECHANICAL PROPERTIES OF FRICTION WELDED CAST AND FORGED STEEL BARS

by

Yusuf Tolga Sunay

B.S. in M.E., Istanbul Technical University, 2003

Submitted to the Institute of Graduate Studies in
Science and Engineering in partial fullfillment of
the requirements for the degree of
Master Science

Graduate Program in Mechanical Engineering

Boğaziçi Univeristy

2005

ACKNOWLEDGEMENTS

I wish to thank to Prof. Sabri Altıntaş for his invaluable guidance and help during preparation this dissertation. I want to mention his patience, giving me hope even in the dead-ends.

I also would like to thank to Dudullu KOSGEB for their help. Besides I am grateful to my family for their support during this study.

ABSTRACT

MICROSTRUCTURE AND MECHANICAL PROPERTIES OF FRICTION WELDED CAST AND FORGED STEEL BARS

Friction welding has been represented as a technological solid-state joining process widely used for dissimilar material combinations with high joint strength, short mass production time and low energy characteristics. This study investigates the factors affecting the joint performance of friction-welded joints, investment cast AISI 1050-AISI 304 and forged AISI 1050-AISI 304 material pairs. The influence of manufacturing method of specimens under changing process parameters were examined both metallurgically and mechanically. An experimental set-up was designed and conducted for experiments. Later, the tensile and microhardness tests were carried out and 2^3 factorial design was performed in order to evaluate effects of the process parameters.

Statistical approach showed that friction pressure and forge pressure are the most viable parameters for forged parts while these are friction time, friction pressure and forge pressure for cast parts in order to maximize the tensile strength. The same procedure was applied to hardness values of the weld interface and it was found that friction time and friction time are both effective in hardness, however, the increase in these parameters leads to decrease in hardness. Therefore it was concluded that higher values of friction time and friction pressure are beneficial from the perspective of hardness whose high values can create notch effect at the interface. Additionally, correlation between the microstructure and mechanical properties was tested by macrographs, optical microstructure, SEM and EDS analysis. The recrystallization and mechanical mixed layer (MML) were observed in both groups and it was confirmed that the reason of high hardness values is that of mechanically mixed layer, oppositely, low hardness values belong to recrystallization phenomena. Among these both groups, forged AISI 1050-AISI 304 friction weldments exhibited superior mechanical properties with lower hardness and higher tensile values compared to investment cast AISI 1050-AISI 304 group.

ÖZET

SÜRTÜNME KAYNAKLI DÖKME VE DÖVME ÇELİKLERİN MİKROYAPISI VE MEKANİK ÖZELLİKLERİ

Sürtünme kaynağı farklı malzeme tiplerinin kaynaklanmasında kullanılan, yüksek dayanım, hızlı üretim ve düşük enerji maliyeti gibi özellikleri ile öne çıkan bir katı hal birleştirme tekniği olarak tanımlanmaktadır. Bu çalışma hassas dökülmüş AISI 1050-AISI 304 sürtünme kaynaklı parçalar ile dövülmüş AISI 1050-AISI 304 sürtünme kaynaklı parçalarda kaynak kalitesini etkileyen parametreleri incelemektedir. Üretim yöntemlerinin sürtünme kaynağında değişen proses parameterleri altında ki etkisi hem metalurjik hem de mekanik olarak araştırılmıştır. Bu amaçla bir deney düzeneği tasarlanmış ve imal edilmiştir. Bu tesisatta gerçekleştirilen deneylerden sonra çekme ve mikrosertlik ölçümleri tamamlanarak elde edilen sonuçlar 2^3 faktöriyel tasarım ile analiz edilmiştir.

İstatiksel analiz sürtünme basıncı ve yığma basıncının dövme parçalarda bunlara ek olarak sürtünme zamanının da hassas dökme parçalarda etkili olduğunu sergilemiştir. Aynı yöntem mikrosertlik sonuçları için uygunladığında ise sürtünme zamanı ve sürtünme basıncı her iki deney grubu içinde en önemli parametreler olarak bulunmuştur. Burada üzerinde dikkatle durulması gereken nokta anılan parametrelerin sertlikle ters orantılı olduğudur. Yani bu parametrelerin yüksek değerde alınması yüksek sertliği dolayısıyla çentik etkisini önlemesi yönünden yararlı olacaktır. Bütün bunlara ek olarak yapılan mikroyapı incelemeleri, SEM ve EDS analizleri her iki deney grubu içinde kaynak ara yüzeyinde yeniden kristallenme ve mekanik olarak karışmış bir tabaka (MML) olduğunu göstermektedir. Ara yüzeydeki yüksek sertlik değerleri mekanik olarak karışmış tabakayla, düşük sertlik değerleri ise yeniden kristallenen kısımla açıklanabilir.

Yukarıda bahsedilen bilgiler ışığında, düşük sertlik ve yüksek dayanım özellikleri ile dövme AISI 1050 çeliğinin AISI 304 ile olan sürtünme kaynağının dökme AISI 1050 çeliğinin kaynağına kıyasla daha başarılı olduğu gözlemlenmiştir.

TABLE OF CONTENTS

LIST OF FIGURES

LIST OF TABLES

LIST OF SYMBOLS/ABBREVATIONS

A	Friction time term in mathematical model
B	Friction pressure term in mathematical model
C	Forge pressure term in mathematical model
d	Specimen diameter
d_1	Diameter of AISI 1050 steel
d_2	Diameter of AISI 304 steel
d_p	Piston diameter
f	Friction coefficient
F	Entire elementary friction force
M	Entire moment of the forces
M_{brake}	Brake moment
M_{motor}	Motor moment
n	Relative rotation speed (rpm)
N	Entire power
N_{motor}	Motor power (kW)
p	Unit pressure
P_{fr}	Friction pressure (MPa)
P_{pump}	Gear pump pressure
P_u	Upset pressure
r	Unit radius
t_{fr}	Friction time (sec)
t_u	Upset time (sec)
x	Factors
z	Repetitions
β	Coefficients of variables
η	Optimization parameter
σ	Contrast

ANOVA	Analysis of variance
C	Investment Cast AISI 1050-AISI 304 material combination
DOE	Design of experiments
F	Forged AISI 1050- AISI 304 material combination
HAZ	Heat affected zone
MML	Mechanically mixed layer
PADZ	Partially deformed zone
PDZ	Plastic deformed zone
SSQ	Sum of squares

1. INTRODUCTION

Recently the major trend in material research is to make products more functional, powerful and reliable. As the trend towards functional and reliable materials continues, the introduction of more environmental-friendly materials with wider variety of functions will bring more growth in the market. Thus, it is a serious problem to select materials within a limited range. Therefore, possible solutions should be found for the development of new material and modification of the existing materials. But, it takes too much time to develop new materials and it also requires multiple processes to test the reliability of them. Various methods of joining dissimilar materials have been introduced both to meet the needs of users and to enhance the added value of new materials while keeping the merits of the existing materials intact. Friction welding can be used to join metals of differing thermal and mechanical properties [1].

Taking these into consideration, the joint performance depends on the material combination, process parameters; however there is still no exact information about the effect of the manufacturing method on the weld quality. Thus, present study investigates the effect of investment casting and forging processes on the microstructure and mechanical properties of friction weldments. To do that, friction time, friction pressure and forge pressure were selected as representative, within range, respectively, 10-14 sec,12-14 bar, 25-40 bar. 2^3 factorial design was carried out from the standpoint of tensile test and hardness at the interface. Investment cast AISI 1050 and forged AISI 1050 were successfully joined to AISI 304 steel under the optimized process parameters. Later the results were confirmed by the microstructural examination.

The present study aims to analyze the following properties:

- The influence of investment casting and forging processes on the microstructure and mechanical properties of friction weldments of steels, AISI 1050 and AISI 304
- The behavior of the joints of investment cast group and forged group under optimized conditions.

2. LITERATURE REVIEW

The idea of using heat generated by friction for forming and joining metals is not new. In 1891 an American machinist Bevington obtained a patent for "An improved method of shaping or forming and welding metal tubes and other articles" using heat generated by friction, although the process was not exploited. Klostock and Neelands in 1941 patented a method of friction welding by which seam welds could be made using a rotating welding road, but this again was not developed. During World War II friction welding was used for welding plastic components in Germany and in USA. However, the real credit for developing friction welding into commercial must be credited to a Russian machinist, Chukidov, who demonstrated and patented it in 1956. Much of the early development work was carried out in Russia and progress was made recently in many other countries. Friction welding was first introduced to the UK in 1961 by the Welding Institute [2].

Friction welding is a process in which the heat for welding is produced by direct conversion of mechanical energy to thermal energy at the interface of the workpieces without the application of electrical energy, or heat from other sources, to the work pieces [3]. In its simplest form, friction welding involves holding two components in axial alignment. One of these components rotates and the other is applied pressure. The friction developed at the interface raises the interfacial temperature until the metal is adequately plastic for welding, with sufficient metal behind the interface becoming softened to permit the bars to be forced together. During this period metal is slowly extruded from the weld region to form an upset. When sufficient heating has taken place, the relative rotation is arrested while the axial load is either maintained or increased to consolidate the solid state weld [4].

Several arrangements are possible for friction welding. A very efficient and economic utilization of the heat introduced into the welded area is possible with some of the schemes because of the strictly localized heat generation on the surfaces to be welded.

In other words, in friction welding it is possible to induce heat only in those areas of the pieces where it is needed for welding [5].

Because of the high quality of the weld obtained friction welding has been widely accepted in the aerospace industry as well as automobile industry for the welding of critical parts [6].

2.1. Friction Welding Theory

When two rough surfaces are rubbed together under sufficient pressure as in friction welding, the high spots collide with each other and are worn down. As they break each other down, the oxide films are ruptured and metal to metal contact is made. Discrete bonds are formed at these points. If relative movement is continued, these bonds are shared and new ones formed. The mechanical energy involved in this operation is transformed into thermal energy and surfaces heat up. As the temperature increases, the compressive strength of the metal decreases and it becomes easier to deform the forging surfaces. The high spots quickly disappear and an increasing area of surface is in a condition to bond. Assuming the rate of the heat input is in excess of that conducted away from the interface the joint will increase in temperature and become more plastic until the compressive strength of metal is unable to withstand the applied pressure. The surface area under the pressure will then increase and the metal will be upset: being forced out of the joint to form a collar. This movement of metal, if sufficient, carries away oxides and other contaminants out of the weld zone. Should any liquid phase be produces during this period, the drop in friction due to its superior lubrication freezes it almost immediately. The process is therefore temperature self-regulating and micro examination of joints have shown that liquid metal has not been involved in the actual joining process. Continuous torque measurements during friction have reflected this liquid-solid cycle of regulation. By this time joint is now complete and process of continuous shear is taking place in the weld zone. If the movement is stopped at this point, a weld will be obtained. A simultaneous increase in pressure will increase the upset and reduce the thickness of the weld zone [7].

2.2. Classification of Friction Welding

The two most widely used friction welding techniques are direct drive and inertia welding. These differ in the method by which energy is supplied the former employing a direct drive route using electric or hydraulic motors, while inertia is a stored energy technique generally using a system of flywheels. Both processes, however, utilize rotation to provide relative motion between the components. Orbital friction welding, on the other hand, uses an orbiting motion with the advantage that non-round components can also be joined. The presently used system of orbital friction welding involves the rotation of both components at a common speed in the same direction with a small off-axis displacement to provide the relative motion. Deceleration is induced by the return of the off-axis component into axial alignment with its mating component. Another advantage of this third technique is the uniform velocity across the contacting surfaces, thereby avoiding temperature gradients .Classification of friction welding methods depending on the drive mechanism is shown in Figure 2.1 [8].

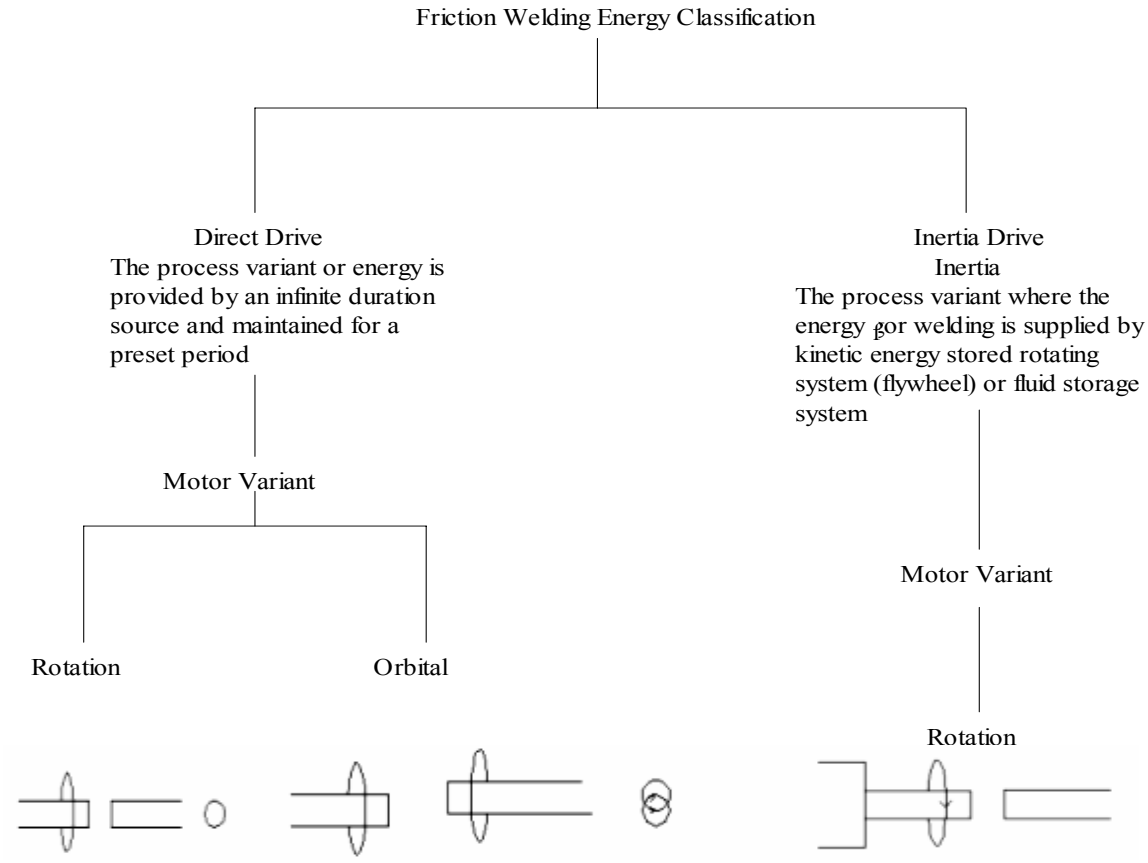

Figure 2.1. Classification of friction welding [8]

2.2.1 Direct Drive Friction Welding

Continuous drive friction welding, which is also referred as direct drive friction welding, requires a machine resembling an engine lathe equipped with an efficient spindle braking system, a means of applying and controlling axial pressure and a weld cycle timer and control. The equipment is simple in principle, but machines are complex when of a size capable of welding large workpieces [3]. Figure 2.2 shows a schematic presentation of direct drive friction welding.

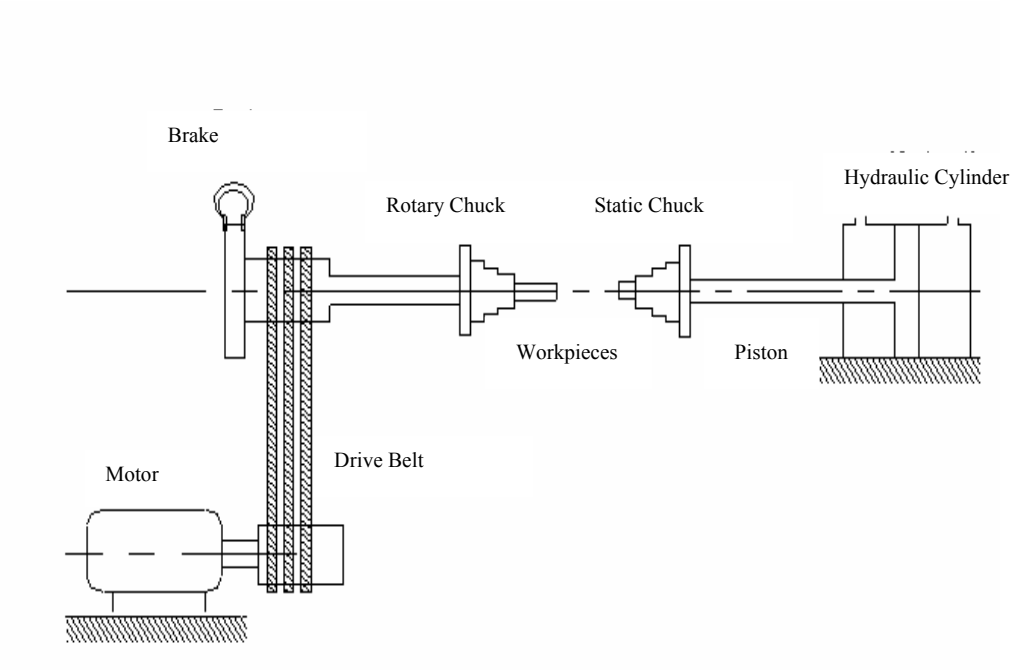

Figure 2.2. Schematic diagram of direct drive friction welding [7]

Process: The stages of friction welding are shown in Figure 2.3 [9]. In the first stage, one component is rotated while the other is advanced into pressure contact with it. Heat is produced at the faying surfaces. Overheating of metals can't occur as the weld zone temperature is always stabilized below melting point seen in Figure 2.3 b). In the third stage softened material begins to extrude in response to the applied pressure, creating an annular upset as shown in Figure 2.3 c). Later heat is conducted away from the interfacial area for forging to take place as illustrated in Figure 2.3 d). Rotation is stopped and a forge force is applied to complete the weld. The joint undergoes hot working to form a homogenous, full-surface, full diameter, high integrity weld [9].

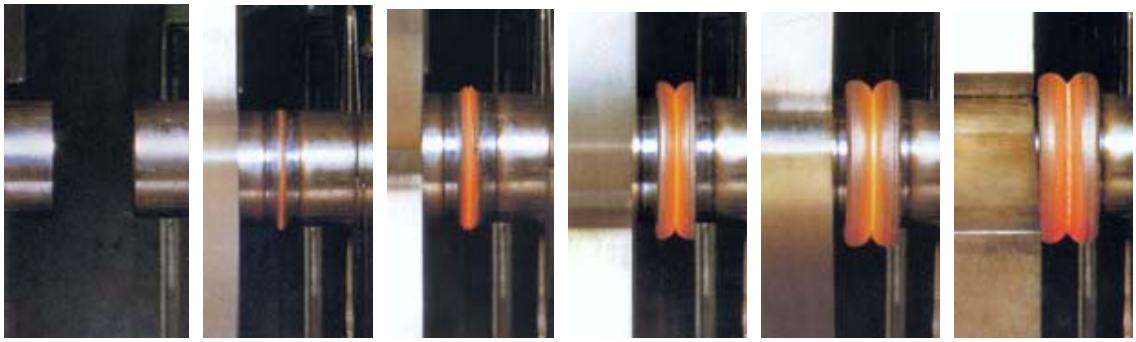

a) Start b) Friction c) Extrude d) Heat conduction e) Stop the rotation f) Forging

Figure 2.3. Stages of direct drive friction welding [9]

Process Variables: There are a number of variables associated with this method.

- Rotational speed
- Heating pressure
- Forging pressure
- Heating time
- Braking time
- Forge delay time
- Forging time

In practice, some of these variables may be inherent in the machine design, such as braking time. If constant pressure is used, the forging variables do not apply. The three important variables with this equipment are speed, pressure, and heating time [10].

The function of rotation is to produce a relative velocity at the faying surfaces. For steels, the tangential velocity should be in the range of 76 to 107 m/min (250 to 350 ft/min). This is true for both solid and tubular workpieces. Tangential speeds below 76 m/min (250 ft/min) produce very high torques that cause work clamping problems, non-uniform upset, and metal tearing. Production machines are designed usually to operate with speeds of 92 to 198 m/min (300 to 650 ft/min). For example, a spindle speed of 600 rpm can be used to weld steel products of 5 to 10 cm. diameters [10].

While high rotational speeds can be used, axial thrust and duration of heating must be carefully controlled to avoid overheating of the weld zone. This may be an advantage, however, when welding quench hardenable steels to control cooling rate and possible cracking [10].

For certain dissimilar metal combinations, low velocities can minimize the formation of brittle intermetallic compounds. From a weld quality standpoint, speed is not generally a critical variable.

The effective pressure ranges are no necessarily narrow for heating and forging, although the selected pressures should be reproducible for any specific operation. The pressure controls the temperature gradient in the weld zone, the required drive power, and the axial shortening. The specific pressure depends upon the metals being joined and the joint geometry. Pressure can be used to compensate for heat loss to a large mass, as in the case of tube-to plate welds [10].

Heating pressure must be high enough to hold the faying surfaces in intimate contact to avoid oxidation. Joint quality is improved many metals, including steels, by applying forging force at the end of the heating period. For steels, a wide range of pressures applicable for making sound welds. In the case of mild steel, heating pressures of 310 to 600 bar (4500 to 8700 psi) and forging pressures of 759 to 1517 bar (11 000 to 22 000 psi) are acceptable. Commonly used values are 552 and 1380 bar (8000 and 20 000 psi) respectively. High-hot-strength alloys, such as stainless steels and nickel-base alloys will require higher forging pressures [10].

If a “preheat” effect is desired to achieve a slower cooling rate, a pressure of about 207 bar (3000 psi) is applied for a brief period. The pressure is then increased to that required for welding.

For a particular application, heating time is determined during set-up or from previous experience. Excessive time limits productivity and wastes material. Insufficient time may result in uneven heating as well as entrapped oxides and unbonded areas at the interface.

Heating time can be controlled in two ways. The first is with a suitable timing device that stops rotation at the end of the preset time. Preheat and forging functions could be incorporated with heating time using a sequence timer [10].

The second method is to stop rotation after a predetermined axial shortening. This method is set to consume a sufficient length to assure adequate heating prior to upsetting. Variations in surface condition can be accommodated without a sacrifice in weld quality [10].

The change of process parameters during welding is represented in Figure 2.4 [11]. As seen in Figure 2.4., when the welding speed decreases to zero, then forge pressure is applied to consolidate the weld.

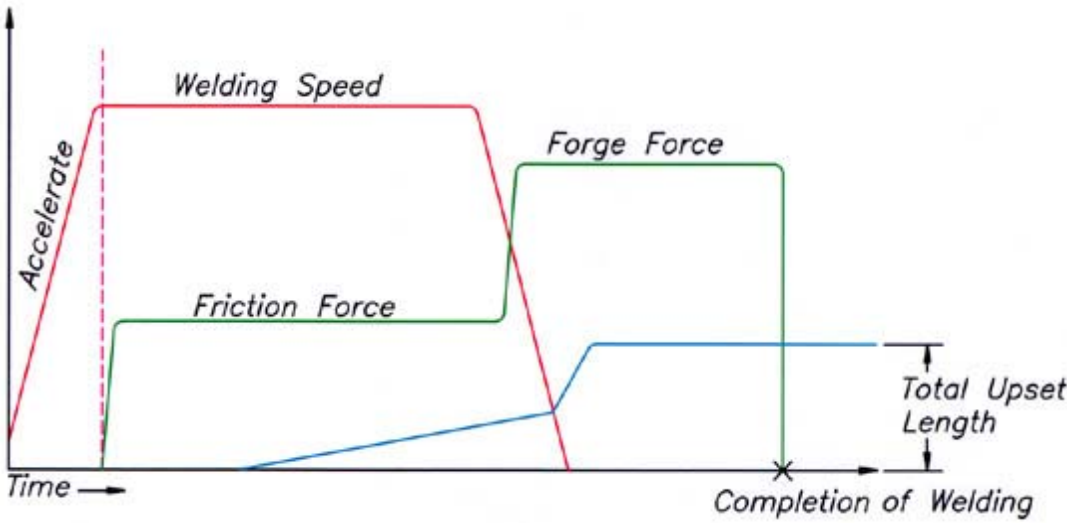

Figure 2.4. Changes in process parameters during operation [11]

2.2.2 Inertia Friction Welding

The idea behind inertia friction welding amount of kinetic energy can be stored in a freely rotating flywheel and complete converted into frictional welding heat without the use of clutches, brakes and time or distance programs. As in direct drive friction welding, one workpiece is clamped in a non-rotating vise or fixture, and the other workpiece is clamped in a chuck mounted to a rotating spindle [12].

The welding machine is similar in construction to a continuous drive friction welding machine, with the rotating spindle mounted in the headstock. Flywheel size is adjusted by adding or removing flywheel disks [3]. The schematic representation of inertia drive friction welding machine is shown in Figure 2.5.

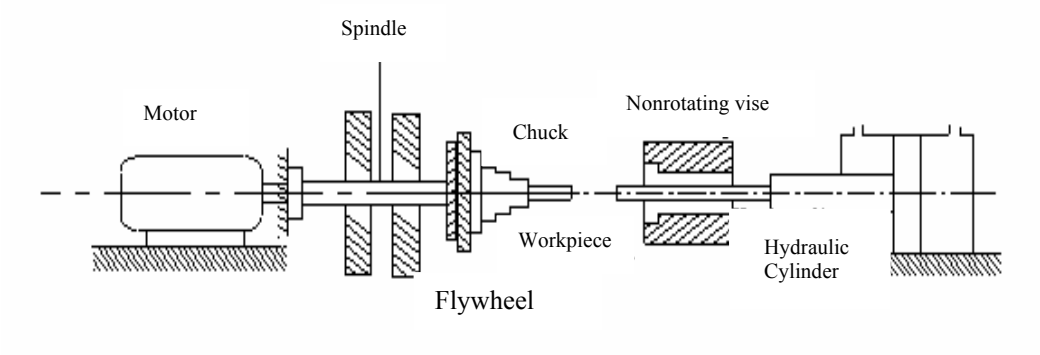

Figure 2.5. Schematic diagram of inertia friction welding [12]

Process: In inertia-drive friction welding, a flywheel and the totaling part are mounted in a spindle, which is driven to the desired speed. The drive source is then disengaged, and the two parts make contact under a preset axial force. The free-rotating fly-wheel decelerates under either the same applied force later under a larger force. Meanwhile, kinetic energy stored in the flywheel and spindle is converted to frictional heat at the abutting surfaces. The weld is complete when the flywheel comes to a stop. A subsequent higher forging force may be used after the flywheel has stopped [13]. Changes in process parameters during operation are shown in Figure 2.6 [11].

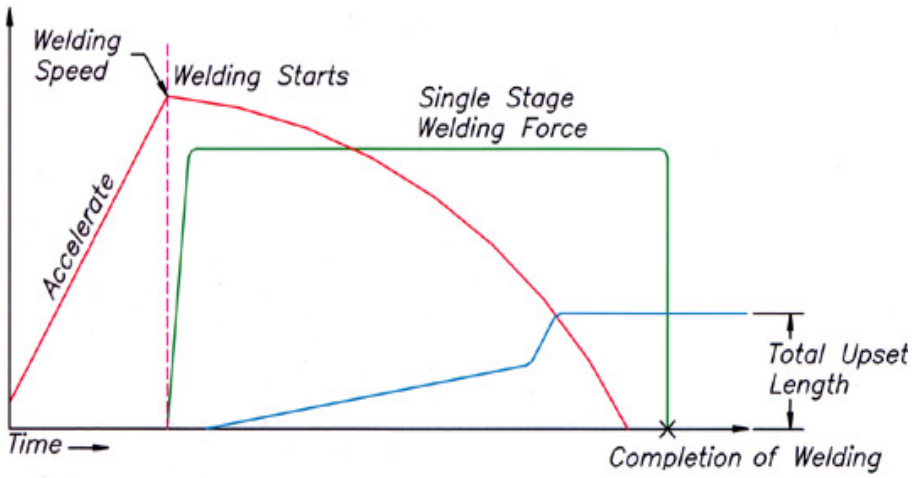

Figure 2.6. Changes in process parameters during operation [11]

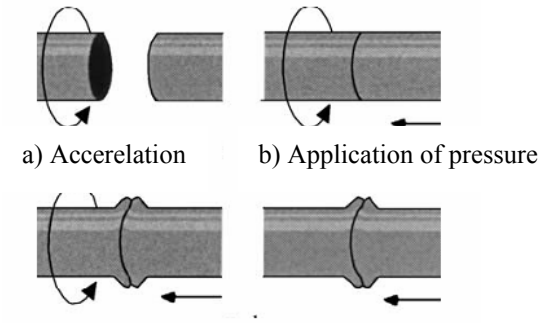

Figure 2.7. Stages of inertia friction welding [14]

Process Variables: The stages of inertia friction welding are shown in Figure 2.7. The major process parameters contributing to the welding machine setting are: inertial energy of the flywheel and forging pressure [14].

2.3. Modes of Friction Welding

With the most friction welding applications, one of the two workpieces is rotated about an axis of symmetry with the faying surfaces normal to that axis. This means that in the normal case, one of the two workpieces must be circular in cross section at the joint location. Typical arrangements for single and multiple welding operations are shown in Figure 2.8 a)–Figure 2.8 e). Figure 2.8 a) depicts the conventional and most commonly used mode in which one workpiece rotates while the other remains stationary. Figure 2.8 b) shows another mode in which both workpieces are rotated but in opposite directions. This procedure would be suitable for producing welds in small diameter workpieces where very high relative speeds are needed. Figure 2.8 c) shows still another mode where two stationary workpieces push against a rotating piece positioned between them. This setup might be desirable if the two end parts are long or are of such an awkward shape that rotation would be difficult or impossible by the other modes. A similar situation, shown in Figure 2.8 d), involves two rotating pieces pushing against a long stationary piece at the middle. The same principle can be applied to the making of two welds back-to-back at the same time with one rotating spindle at the center, as shown in Figure 2.8 e), for the purpose of improving productivity. This operation usually would be fully automated for mass production or coupling is rotated and compressed as it is heated. An internal expanding mandrel supports the pipe walls and prevents penetration of upset metal into the bore of the

pipe. The two pipes of Figure 2.8 f) have beveled ends and are butted together and clamped securely in place. A solid ring with a composition similar to that of the pipe is positioned within the joint groove. The ring is beveled so that it will make initial contact at the apex of the joint groove. This is done to promote metal flow from this point outward and to reduce the initial high torque. After the necessary heat is developed from friction, ring rotation is terminated while the compressive load on the ring is maintained or increased to consolidate the joint. Orbital motion may be used to weld non-circular parts as shown in Figure 2.8 g). The work pieces are aligned with the faying surfaces in contact and under pressure. One piece is then moved in a small circular motion relative to and in contact with faying surface of the other piece, with neither piece rotating about its central axis. This variation provides uniform tangential velocity over the total interface area [10].

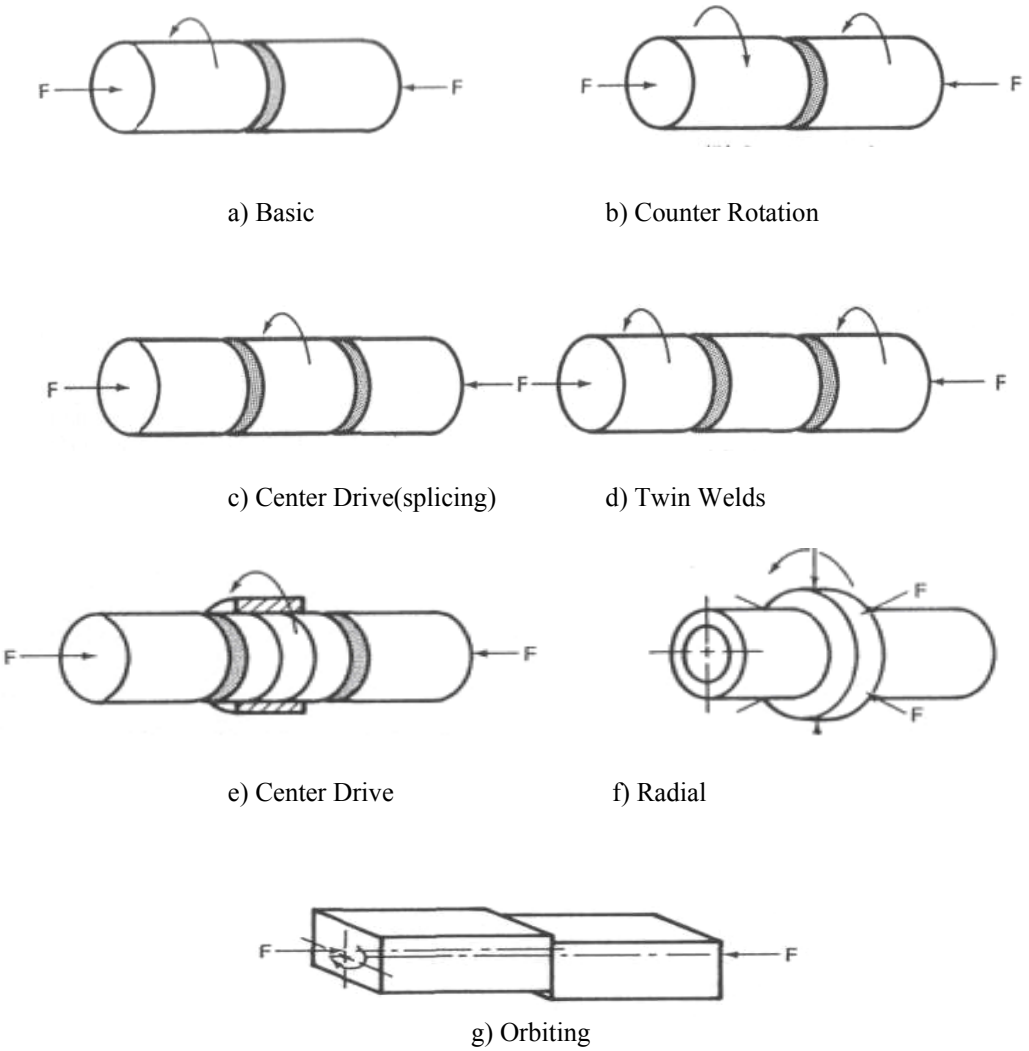

a) Basic b) Counter Rotation

c) Center Drive(splicing) d) Twin Welds

e) Center Drive f) Radial

g) Orbiting

Figure 2.8. Modes of friction welding [10]

2.4. Weldability of Different Materials by Friction Welding

The friction weldability of commonly encountered metals and alloys is conveniently assessed by dividing them into five groups [15].

Group A comprises materials such as mild steel, fully-austenitic stainless steel, commercially pure metals, and solid solutions with no adverse metallurgical reactions between the constituents. Mechanical properties are greatly affected by the heat affected zone of the weld, which is characterized by grain refinement due to hot working.

Group B comprises heat-treated alloys such as hardenable steels and precipitation hardening aluminum alloys. Mechanical properties will be affected by the thermal cycle during welding, but they can be restored by suitable post-weld heat treatment to restore ductility, toughness or strength dependent on service requirements.

Group C covers the combinations which form brittle alloys or intermetallic compounds at the weld interface. The intermetallic layer can generally be controlled to a thickness of only a few microns.

Group D materials produce sound joints as-welded which show diffusion effects during heat treatment or service at elevated temperatures.

Finally Group E includes a few combinations which do not generally give good results. Some of the constituents may inhibit successful welding, such as graphite flakes in gray cast iron, lead or sulphur in free cutting steels, and porosity in sintered parts. Excessive inclusion content can reduce the joint's mechanical properties particularly because of reorientation of the grain flow at the weld [15].

The materials chart for friction weldability of material is given in Figure 2.9 [9].

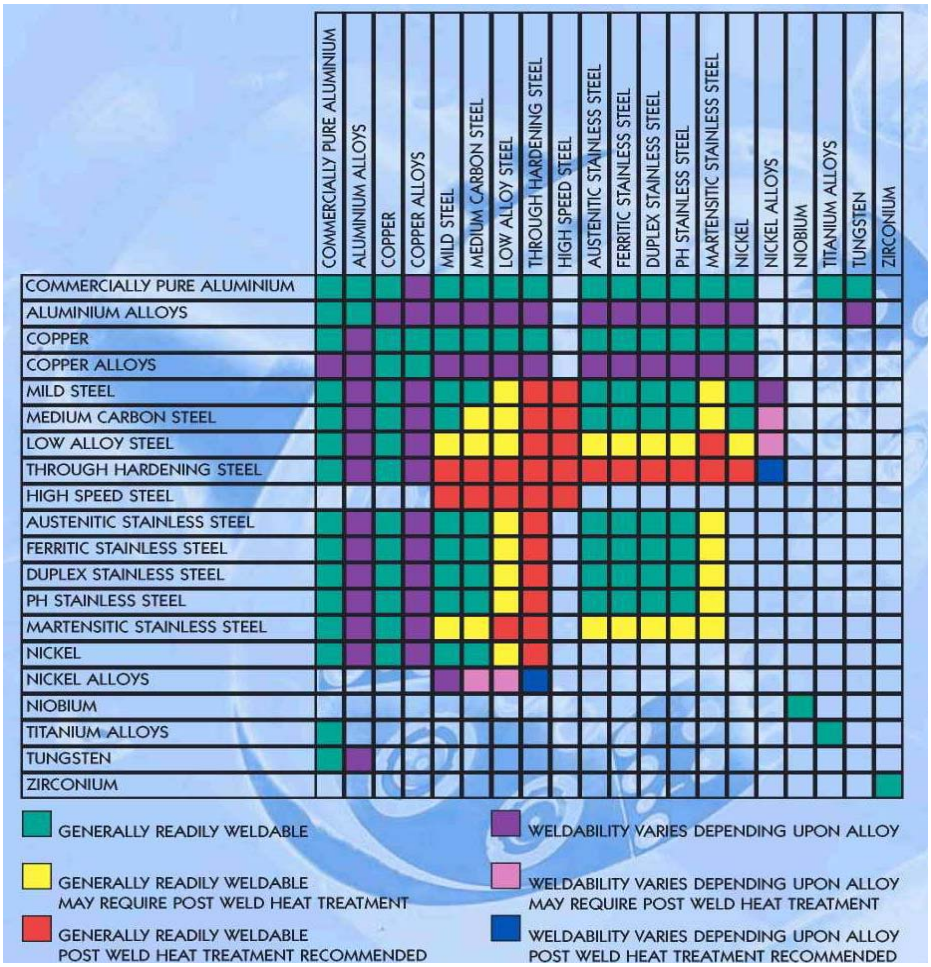

Figure 2.9. Materials chart for weldability [9]

2.5. The Mechanism of Friction Welding

Friction welding can be considered as two operations which take place successively; frictional heating of the interface, by relative movement in the plane of welding combined with pressure normal thereto: followed by forging without relative movement. An arrest stage thus obviously separates the two operations, because so long as relative movement persists no joint can form, and after its arrest there is no further heating. During the heating phase, softened material begins to extrude outwardly in response to the applied pressure. In order to maintain that pressure, relative axial movement (called “burn-off”) must be allowed, and it is a future of the process that the rate of burn-off is generally uniform. During arrest the interface temperature, hitherto substantially constant, will begin to fall as the heat losses by radiation and conduction start to exceed the frictional heating. Relative movement must thereafter be completely arrested and a forging pressure applied, to bond

the components fully and hot-work the interface before the fully and hot-work the interface before the joint is too cool. The importance of the arrest stage thus varies greatly with joint size and configuration. Thin-walled tubes in particular need very rapid arrest to be successfully welded, whereas large-diameter solid welds retain their heat arrest rate being consequently less important [15].

The burn-off of material during the heating the phase is highly significant in relation to weld quality. Impurities in the surfaces to be welded, irregularities initially preventing their full metal-to-metal contact and oxides formed while the contact is only partial, are all expelled if the amount of burn-off is sufficient. Joints of satisfactory integrity can thus be made even when the surfaces to be welded are rough as cast or forged, out-of-square as sawn or cropped, oxidized, or contaminated with typical cutting fluids and lubricants. This contrasts sharply with the costs of weld preparation for arc-welding [15].

Heat is generated only precisely at the surfaces to be welded, and evenly around the cross-section. The only other-interface-seeking processes involve resistance welding: i.e. flash-butt and magnetically-impelled arc. Both initially involve local fusion, whereas the friction weld is inherently self-regulating. As the material approaches its melting point the effective coefficient of friction drops, and with it the rate of heat input. The temperature is thus stabilized well below the melting point. The friction weld is truly a solid-state, with a total absence of cast structures. The forging pressure is chosen to bond the joint fully,(usually the welded area substantially exceeds the original joint area) and to refine the grain size by hot working. Friction welding is very to tolerant of process parameter variations in most cases suiting processes well to the realities of workshop production [15].

2.6. Heat Liberation during Friction Welding

It was noted before that the temperature conditions of machine connections subjected to friction are very important. Many scientists agree that binding due to friction produces an increase in the temperature of the connection [5].

Even more important is the heat liberation during friction welding. In this case, the temperature conditions determine not only the entire aggregate of the phenomena taking place on the friction surfaces, but also the efficiency of the process, strength characteristics of the welded connection and, finally, the parameters of the welding equipment .The temperature conditions during welding depend in turn on the intensity of heat liberation (power). The heat liberation diagram for friction welding is shown in Figure 2.10 [5].

The analytic expression for the heat power, applicable to the most simple friction welding method, can be obtained by investigating the heat liberation process on an elementary friction surface area, bounded by the radius r and $r+ dr$ [5].

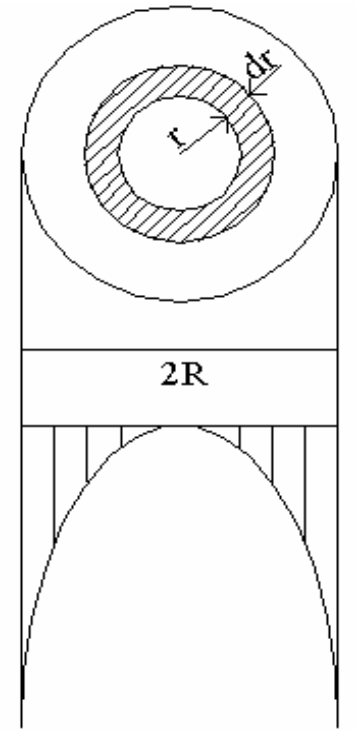

Figure 2.10. Heat liberation diagram for friction welding [5]

The elementary friction force acts on this infinitely small area with:

$$dF = pdS = 2\pi pfrdr \tag{2.1}$$

The moment of this force around the rotation axis (point 0) is

$$dM = rdF = 2\pi pfr^2 dr \tag{2.2}$$

If this dependence is disregarded and friction coefficient is const., is assumed, one obtains, as the first approximation, the following expression by integration:

For the moment of the forces acting on the entire friction surface with the radius R,

$$M \approx \frac{2}{3}\pi pfR^3 \tag{2.3}$$

For the corresponding power

$$N \approx \frac{2}{3}\pi pfnR^3 \tag{2.4}$$

For the average unit power in relation to the nominal unit friction area

$$N_{unit} \approx \frac{2}{3} pfnR \tag{2.5}$$

where F is entire elementary friction force, M is entire moment of the forces, p is unit pressure, n is relative rotation speed, f is friction coefficient, N is power and r is unit radius, R is total radius.

On the basis of the above expressions, it can be concluded that for a given pair of surfaces, the intensity of heat liberation during friction welding is determined by the relative rotation speed and the unit pressure, as well as by the size of the cross section of the welded pieces and the friction coefficient [5].

If one disregards the heat dissipation into the surrounding medium and if one considers the direction of the thermal current as parallel to the axis of the welded details, then the unit pressure required for welding should not depend on the cross-sectional area.

The rotation speed or the axial unit pressure must be changed for different diameters of the detail. This also shows that the total force required for welding is proportional to the cross section of the welded detail.

Nevertheless, in order to assure oneself of the correctness of these conclusions, one should first establish the correctness of the above indicated assumption in regard to the independence of the friction coefficient from the parameters of the process even for approximate computations, i.e., one must determine whether the changes of the friction coefficients due to parameter variations of the welding process are sufficiently small to be disregarded [5].

2.7. Basic Requirements for Friction Welding Equipment

The experience gained from research on friction welding development and operation of friction welding equipment form the basis for the formulation of the fundamental special requirements of such equipment. These requirements can be divided into two groups:

i) Operational requirements
ii) Design requirements

Operational requirements include the following:

- Meeting of the basic operational specifications of the friction welding process (rotation speed, axial load);
- Provision for the required pressure cycle;
- Provision for rigid control of the duration of the process (length of upset) ;
- Provision for swift stopping of the relative rotation at the end of the heating period [5].

Basic design considerations are:

- Minimum flywheel moments for the rotating parts to facilitate swift stopping;

- Adequate rigidity of the load-carrying components of the machine to eliminate radial displacement of the welded specimens during operation of the machine, and damping of radial vibrations created by the welding process;
- Reliable gripping of the welded specimen in the machine which will withstand the maximum friction moment and the axial force without movement or rotation of the specimen [5].

In many cases, there exists the additional requirement for welding specimens of unlimited length. In such a case, the spindle of the headstock and the chuck gripping the stationary specimen must be designed with a central opening.

While the overall design of machine is determined in some measure by the part to be the welded, the mechanical aspects of the design are determined by upsetting forces required, the torque transmission and the amount of vibration damping needed [5].

Also, a number of general requirements are applicable to friction welding machines: high efficiency, maximum flexibility, minimum weight, small tolerances, ease of operation, low power consumption, simple servicing, etc.

2.7.1. Swift Stopping of the Relative Rotation

This problem is of importance only when welding details of comparatively small diameter. Generally, when welding large diameter specimens (for steel above 25 mm, for copper and aluminum above 40 mm), as experience has shown, forced braking is not required, since the slow rotation speeds correspond to a low kinetic energy of the rotating masses (energy is a function of the square of the velocity). An increase in its absorption is sufficient for braking under these conditions, since there is a greater frictional moment when large diameters are joined [5].

Four principal techniques of swift stopping of the relative rotation of the specimens are used in machines designed for welding of bodies of a relatively small diameter:

- Forced braking of the entire driving mechanism including the rotating specimen, for example, by electromagnetic braking, reversing.
- Disconnection of the chuck holding the rotating specimen from other parts of the drive, for example, by an electromagnetic coupling (braking with the moment of the friction surfaces of the specimens or using a separate brake).
- Release of the originally stationary specimen at the end of the heating cycle (the moment acting on it induces rotation) and the relative speed of the specimens becomes zero; cooling and creation of the final connection takes place with both specimens rotating [5].
- Release of the stationary specimen at the end of the welding cycle followed by forced rotation as a result of engagement with a separate drive or the same drive (for both specimens).

Machines which utilize one of the first two techniques are more flexible in their operation, since one of the specimens can be of a practically unlimited length, diameter and mass [5].

Of all the techniques mentioned above, braking of the motor should be given preference from the standpoint of design and operational reliability. However, it should be noted that this complicates the operating conditions of the motor (the rise in temperature of the motor is increased).

Two artificial techniques that increase the braking effect should be mentioned:

- Application of a stepped pressure cycle increases the axial load and the moment acting on the friction surfaces producing a greater braking moment;

- Use of a machine where both specimens rotate in opposite directions. Each specimen rotates at half of the relative rotation speed. This method accelerates the braking process, since the kinetic energy is a function of the square of the speed [5].

2.7.2. Requirements for Gripping Devices

To reduce costs and to simplify the machine, manual gripping of the detail should be used on machines producing custom products or small quantities. In all other cases, loading of the machine should be accomplished by fast acting devices not requiring physical exertion of the operator [5].

All gripping devices must be extremely reliable in holding the specimen. The slightest dislocation of the detail to be welded in the chuck during the welding process leads to welding of the specimen to the gripping device or wear and damage of the device. The welding requirements for specimens of unlimited length very often make it impossible to utilize the supports for transmitting the axial reactions from the gripping devices. Such "supportless" gripping devices must resist considerable axial force to allow the detail to rotate. The gripping devices should be designed for the maximum friction moment which can be 2-2,5 times larger than the computed on the basis of the installed power [5].

Chuck requirements are critical because of the high torques as well as the axial and radial forces transmitted. Hydraulically operated chucks generate the forces which prevent the parts from slipping through. Special attention must also be given to the bearings [16].

2.7.3. Automation of the Welding Cycle

The necessity of adhering to the specified pressure cycle and of strict conformity with the required duration of the process is mandatory for all friction welding machines, since this eliminates any influence of the qualifications and habits of the welder from the quality of the welded connection. This capitalizes on one of the basic advantages of friction welding: the simplicity with which a high degree of uniformity in the quality of welded connections is obtained [5].

2.7.4. Damping Vibrations

Friction generates vibrations which must be dampened by the design of the machine and the choice of the process variables. This, in turn has direct influence on the weld quality and the life of the machine. To obtain satisfactory results, extensive investigations regarding the generation and damping vibrations are necessary [16].

2.8. Advantages and Limitations of Friction Welding

2.8.1. Advantages

Friction welding solves many of the problems encountered in electric butt welding and eliminates the particular disadvantage of the flash in flash welding. Although many of the manufacturing hazarding flash welding has been partially overcome, the shower sparks has limited the use of these machines in modern production installations, particularly in the light of new safety regulations. The sparks also raise considerable problems with machine and cleaning. Clamping and current transfer limit the desired accuracy of the completed weld. Some advantages of friction welding are:

- Lower electrical power requirements: There is no single phase, short time peak electrical load during the welding process. With lower power demand and power consumption the process frequently can be considered installations where flash butt welding would be impossible. Power costs in some applications were 70% to 80% lower than the other processes [17].
- Better use of floor space: Because friction welding produces no flashes or shower of sparks, the machines can be installed closer to the operators manufacturing areas.
- Material savings: The smaller loss of length in friction welding and the possibility combining materials not suitable for welding by electrical methods has provided substantial material cost savings.
- Easier work piece preparation: Clamping prior to welding is, in most cases, much simpler and the weld surface conditions are less critical than those required for electrical than those required for electrical flash butt welding [17].

- Less adjustment to maintain dimensional tolerance. The electrical flash butt process requires highly conductive and relatively soft clamping devices that must have frequent machining and adjustment to maintain tolerances. Chuck linings of friction welding machines are hardened and ground to provide better accuracy and longer service life.
- Adaptable to automatic processes: In many applications, automatic loading and unloading of the machine, as well as indexing of the parts and transfer to other operations is possible.
- Better control of welding variables: The reliability of weld is influenced by neither the welding current nor the electrical resistance at the welded joint. These critical variables in electric welding are dependent upon the part, the welding machine and the electrical power available at the time of welding. With friction welding, the dependent variables can easily be controlled and adjusted by the production operators.
- Eliminations of weld inclusions: Friction welding largely eliminates the inclusion of foreign matter in the weld area. During friction welding process, any interface impurities such as surface oxides, grease and oil remain trapped, which do not permit the close interface contact necessary for full bonding [17].
- What is more, often combinations that can be friction welded cannot be joined by other welding techniques because of formation of brittle phases which make the joint poor in mechanical properties [18].

2.8.2. Limitations

At least one of the components had to be circular section. Secondly as a result of welding, a collar or" flash" of metal of the metal is produced. In some cases this collar is acceptable but in other applications it is necessary to remove it by post weld machining. This could process difficult if the collar is situated inside a long tube [19]. Additionally, the end preparation of the workpieces reasonably good alignment and the leaving of tolerance for a specific set of welding conditions are critical [20].

Apart from the cost of equipment, which must be suitable for the intended joints, the friction welding process has some costs in tooling and set-up that must be taken into

account when calculating the cost per weld. Tight concentricity requirements, when needed, may be difficult to meet. Also finishing operations may be requested which sum up to the total cost [21].

2.9. Joint Design for the Friction Welding Process

Weld joint design used in friction welding are generally less critical than those required for other welding methods. Saw-cut, sheared and even flame-cut surfaces can be joined successfully, thereby reducing and eliminating operations prior to welding. In general, grease paint and other contaminants on the weld surfaces do not pose a problem since they are expelled from the interface during the weld cycle. Exceptions include mill scale and some cold forging lubricants. Center drills and other small concavities can serve to trap contaminants in the weld and should be avoided. When joining materials of significantly differing mechanical properties, interface preparation can become critical, such as aluminum to steel [22].

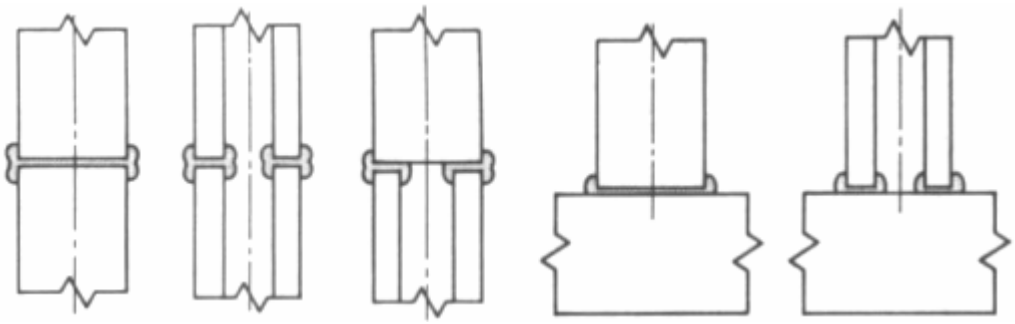

a) Rod b) Tube c) Rod to tube d) Rod to plate e) Tube to plate

Figure 2.11. Friction welding joint designs [10]

The nature of friction welding suggests that the face of at least one of the workpieces must be essentially round, except in case of orbital welding. These configurations for friction welding are shown in Figure 2.11. The rotated workpiece should be somewhat concentric in shape because it is revolved at relatively high speed [10]. Flat joints are the most common and can be classified as bar to bar, tube to tube, bar to tube, bar to plate and tube to plate as shown in Figure 2.11. These classifications refer to the joint itself and not to the shape of the parts [3]. Bar to bar and tube to tube joints can used where material

requirements change along components length [10]. In the friction welding of circular bars the rubbing velocity is zero at the centre and increases linearly with the radius [23].

Tube-to-plate welds are not as strong as tube-to-tube welds, because rounding of the end of the tube during heating and upsetting reduces weld effectiveness. Fatigue life of the tube-to-plate weldment increases with removal of the sharp notch at the tube base before the part is put to use. On some metals, when heating is too slow, or when excessive weld energy is applied, the upset metal flows up and around the outside of the tube and forms, in effect, a tube within a tube [10].

On tubular welds, the upset is extruded equally toward the bore and toward the periphery. When weld upset cannot be permitted to remain in the bore and cannot be reached for removal after welding, a trap must be incorporated into the joint design [3].

Conical joints are usually designed with the faces at 45 to 60 degrees to the axis of rotation. For low-strength metals, large angles are preferred to support the axial thrust required to produce adequate heating pressure. One advantage of an angled joint over a 90 degree joint of equivalent interface area is that the change in tangential velocity across the interface is less [3].

Some joints between dissimilar metals with widely different mechanical or thermal properties are better produced with appropriate adjustment of faying surface area. The metal of lower strength or lower thermal conductivity may have a larger faying surface area. For applications where the flash cannot be removed conveniently, clearance for it can be provided in one or both workpieces [3].

2.10. Applications of Friction Welding

2.10.1. Transportation Industry

In the past, application of the process to the transportation industry has received a great deal of attention because friction welding may simplify or cheapen the part, or make procurement of components easier. As a result of this successful work, friction welding is

now extensively used in the mass production of a variety of parts [24]. In many automotive applications it is necessary to use different stress loads on various types of materials. In some cases the requirement of two types of metal on one part such as a valve serves the requirement of “putting the right metal in the right place”, say, using a stronger material for the stem and a heat tolerant material for the head. Figure 2.12 shows an example of these exhaust valves [26]. Other applications include, differential spools, drive shafts, axles, front wheel drive shaft joints, wheels and rims, certain camshaft and crankshaft applications. Depending on the application, the parts can be welded in a pre-weld configuration or a semi-finished condition [25].

Figure 2.12. Friction welding example: exhaust valves [26]

Friction welding is also being used to weld together relatively simple forgings to make complex shapes. This means that friction welding can be incorporated into a quantity production forging line giving the advantages of increased output, simplified parts and part standardization. A variety of products can thus be made by using various combinations of standard components [26].

Figure 2.13. Friction welding example: drive shafts [26]

Further benefits can be obtained by using friction welding, as material cost savings can be achieved because of standardization, and also because forging quality steels are only required whose components are to be shaped by forging processes. This is particularly significant in the manufacture of drive shafts. The friction welding example of drive shafts is represented in Figure 2.13 [26]. A one piece forged shaft requires premium quality steel throughout, so that the flange of the shaft can be shaped by a hot heading operation. When friction welding is used, however or, a flange forging is produced in the premium material whereas the shank of the shaft is made from normal bar stock material, or could be made from a different steel to give further benefits. The application of friction welding to this type of component results in a 15% overall cost reduction [4].

Figure 2.14. Friction welding example: gearbox shaft [26]

The ability to standardize parts has become particularly apparent in the manufacture of gearbox shafts. An application of such an example is shown in Figure 2.14. Gear blanks produced from bar cutoffs or stampings, load onto a transfer machine for welding. Precision forgings and stampings can be used with friction welding often reducing machining costs [26].

2.10.2. Hydraulic-Oil-Gas Industry

Hydraulic cylinders and valves are prime candidates for friction welding. The cylinders can be completely machined and the caps can be weld on afterwards providing for cost reductions and minimal inventory requirements. For irregular shapes, the cylinder can be welded to a larger piece of material to reduce cost and machine time. [24]. Figure 2.15 represents a friction welded hydraulic cylinder with collar [27].

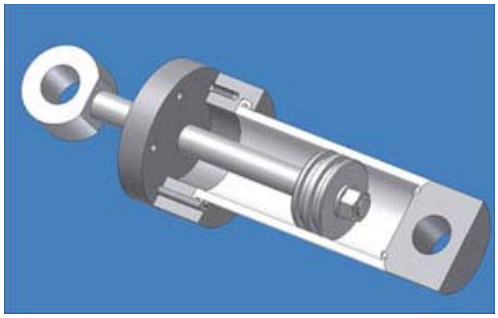

Figure 2.15. Friction welding example: hydraulic cylinder [27]

Figure 2.16 shows a practical example made of stainless steel and carbon steel which is the most popular combination of friction welding of dissimilar metals [29]. These materials are commonly friction welded to obtain mechanical parts, such as immersion pump shafts with adequate strength and ductility. Carbon steel (gear part) is employed for regions where wear resistance is required and stainless steel (shaft part) for regions where corrosion resistance is required; components similar to the example are employed as mixing shafts for food and pharmaceutical processing machine sand for various pump shafts [28].

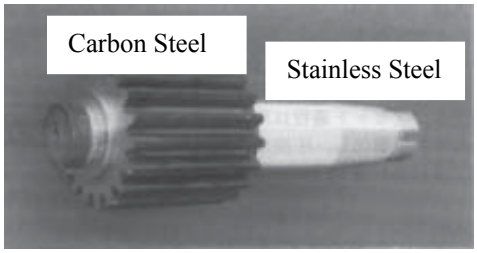

Figure 2.16. Friction welding example: gear pump shaft [28]

Figure 2.17 shows an example of friction welding, say, diesel engine piston [11]. That is highly preferred application of friction welding.

Figure 2.17. Friction welding example: diesel engine piston [11]

A natural application for friction welding is in the attachment of tool joints to drill-pipes or for similar assemblies that are used in the hydrocarbon and mineral exploration industries. Several application studies of friction welding to this type of component, which involves attaching two screw-up couplings, i.e., a male or pin at one end and a female or box at the other. High quality joints have been produced between SAE 4140 tool joints and low alloy or mild steel pipe, using, for example, weld times of 45 seconds for 100 mm outer diameter [4]. Machines capable of accepting pipes of 9 m. to12 m. length utilizing special powered clamps have been developed [30]. A schematic representation of friction welding locations in drill pipes is shown in Figure 2.18.

Figure 2.18 Friction welding example: drill pipes [31]

2.10.3. Electronic Industry

Displacement sensors which are made by friction welding includes austenitic free cutting stainless steel AISI 303 for good machinability and Ni-base magnetic material (Ni content: 47 %). These sensors are employed for position control of servo valves and detection of the press position in a press machine; the joint diameter, within the range of 3–8 mm, is selected according to usage. Conventionally, magnetic and non-magnetic materials have been either produced by being fastened using bolts, by cutting a screw thread or have been joined by means of brazing. These manufacturing techniques gave a significantly lower joint strength than that of the base metal, dispersion in the achieved strengths and problems of joint reliability. However, since the process was changed to friction welding, the production time reduced, the costs reduced and the sensor performance stabilized [28].

Fixing bolt for a semiconductor case produced by friction welding includes oxygen-free copper and stainless steel. In friction welding there is no formation of a non-bonded area, as there is with other joining processes such as brazing, and there are advantages of a high joint strength and little thermal effect [28].

2.10.4. Aerospace and High Tech Industry

Full strength inertia welded parts are used in a wide variety of aerospace applications. Because of the localized weld, many critical heat treated and finish ground parts can be welded with minimal distortion. Items such as turbine wheels and shafts, pressure vessels, landing gear struts, ballscrew assemblies, actuator components, gear blanks and gear assemblies are just a few examples [24].

For instance for the turbochargers itself is produced using a precision investment casting for the turbine head and a forged shaft, which at the weld area is drilled for some 13 mm to reduce the surface area for the welding process [25].

The material combinations are:

- Steel shaft (forging)
- Turbine (precision casting)

The direct connection of these two parts by solid state bond by the method provides a stronger connection that can be obtained through silver brazing reduces rejection percentage as compared to brazing and reduces the cost of manufacture [32]. The component itself is safety critic. It revolves in the turbocharger casting at more than 30000 revolutions per minute and runs in hydrostatic bearings. At this speed, the component has to be welded effectively and balanced. Any out-of-tolerance will cause vibration and ultimately failure [25]. Figure 2.19 shows such a friction welded turbocharger with appearance of collar inside [28].

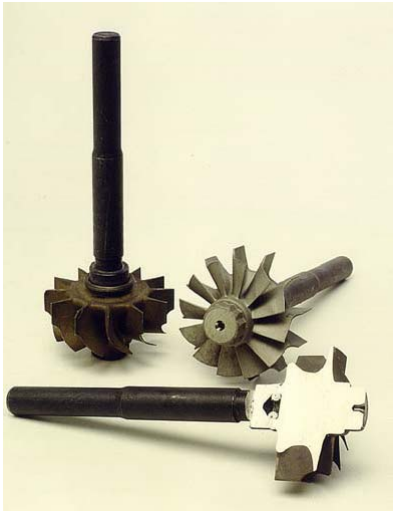

Figure 2.19. Friction welding example: turbocharger [26]

2.10.5. Other Applications of Friction Welding

Friction welding is also used of bimetal electrical connections that are employed in power transmission and in electrochemical processing plants. For example, factory bonded copper/aluminum transition pieces are produced on both job shop and production basis. The process is particularly suited for making joints in these materials, but research has shown that the quality of the surfaces prior to welding is critical [4].

Ideally, the faying surface of the copper should be machined smooth and square to the rotational axis and all organic contamination must be effectively removed by degreasing or by chemical etching prior to the start of welding. Even when rigorous cleaning procedures have been applied, care must be taken to ensure that the ends are not contaminated with finger grease when the parts are loaded into the machine. Although the degree of contamination is fundamental to the formation of a sound weld, this presents no significant problem in the manufacture of consistent and reliable high quality welds [4].

Copper aluminum transition pieces are essential components where copper has been replaced by aluminum for transmission cables, because effective and reliable mechanical connections cannot be produced between aluminum parts. Conductivity is adversely affected by the growth of insulating oxides, the susceptibility to corrosion and because of creep of aluminum under the points of high stress, such as screw points. Thus, there has

become a need for transition pieces which are capable of joining aluminum conductors to other copper conductors in existing electrical equipment, without the need for equipment redesign [33].

Additionally aluminum and its alloys have specific strength, high heat conductivity, and high recyclability, while stainless steels are more conventional materials. The demand for aluminum-stainless steel joints has therefore increased in many areas including cryogenic application, spacecraft and high vacuum chambers and cooking utensils owing to superior properties [33]. Many types of friction welded aluminum-copper joints are represented in Figure 2.20 [24].

Figure 2.20. Aluminum-copper transition joints [24]

2.11. Weld Quality

The manufacture of metal seals, pressure devices, sensors, and many other metal components require precision welding. The sealing, shaping, or joining technique must be extremely reliable because it is necessary to maintain the integrity of the product. The weld process must also be accomplished without interfering with the cosmetics or function of the product [34].

2.11.1. Inspection and Testing

Process control is best performed by random destructive or proof testing of either production welds or specimens welded with the production machines. The frequency of testing is usually determined by service requirements, customer specifications, or company quality control procedures. Destructive inspection may include metallographic examination as well as tensile, impact or bend tests [10].

2.11.2. Non-destructive Testing

Nondestructive testing methods are not generally acceptable for determining friction weld quality and soundness. However, ultrasonic techniques may be effective for the detection of subsurface discontinuities such as incomplete fusion at or near the center of the weld. A straight beam ultrasonic test conducted perpendicular to the weld interface gives the most reliable results. This test can be applied if one end of the weldment is accessible to the ultrasonic transducer. Lack of bonding at the inside surface of a tube-to-tube weld may be detected by ultrasonic inspection using the angle beam technique [10].

Amount of Upset: Figure 2.21 shows a friction welded material pair with different size and shape of upset. In friction welding, it is recognized that the amount of upset during friction welding is closely related to the mechanical properties of the welded specimen. Therefore, the amount of upset in friction welding is an important criterion by which to judge appropriate friction welding conditions, that is to say, to guarantee the mechanical properties of the welded parts. However, the upsetting process of friction welding is extremely complicated because the heating and cooling process is non-uniform and the deformation process is very complicated. Therefore, the amount of upset cannot be easily determined. Even now, friction welding conditions in order to attain good mechanical properties of the welded parts are obtained by a trial and error according to the shape, size and the material used. Thus, if appropriate friction welding conditions of each material, to which the amount of upset are closely related, can be estimated beforehand, the great extension of the usefulness and application limits of friction welding will be expected [35].

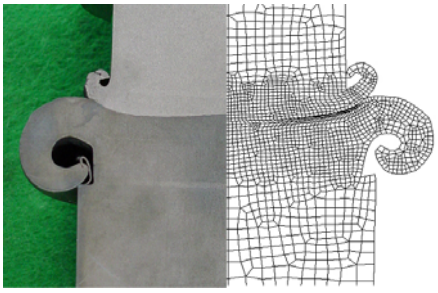

Figure 2.21. Weld quality control: amount of upset [36]

2.11.3. Destructive Testing

Bend Test: The former diameter and the acceptable bend angle will depend on the material strength and the acceptance specification. A bend test is considered to be acceptable if no cracks occur in the weld region up to the given bend angle. In some cases, a limited amount of cracking may be permitted in accordance with national standards [37].

Tensile Test: For tensile tests, strength is evaluated in accordance with the specification and the position of the fracture is noted (heat affected zone, parent metal). When the fracture occurs in the weld, the appearance, size and the number of defects are determined visually. When defects exist in the fractal surface, they must not exceed an agreed percentage of the initial area of the specimen. For these non-conventional specimens, yield point, elongation and reduction of area are not determined or are only measure to provide additional test data.

Impact Test: Notch toughness tests are made only when specifically required. When selecting the notch position either into the weld or into the HAZ (heat affected zone), special consideration must be given to each case. The weld position is located by etching [37].

Metallographic Examination: Metallographic examination may be used in support of the above mechanical tests or must be used where those tests cannot be applied. Acceptance criteria will form part of the technical specification. The surface prepared for examination must represent the whole cross section. The cut plane passes perpendicularly to the plane of the weld. Each specimen must be prepared for examination in both the

polished and etched condition. The metallographic quality of the joint will be evaluated as a function of the presence of oxides or other layers of contamination, lack-of-bond defects, cold joints, weld flaws and cracks, cavities, inclusions, overheating structure, possibly also hardness and microhardness (in the weld and in the heat affected zone) as defined in the specification e.g. by comparative standards, etc.

If metallographic examination reveals defects in the parent metal, this must not be considered as cause for the rejection of the weld, but may indicate that the material or batch of material is unsuitable for the particular procedure [37].

3. OPTIMIZATION OF PROCESS PARAMETERS IN FRICTION WELDING

A major difficulty in parameter optimization is the large number of variables involved. The usual single factor experiment (run on the principle of varying one factor at a time while keeping the others constant) is tedious and unsatisfactory in complex systems such as friction welding where the number of possible influencing factors is large. Statistical design of a multi-factorial experiment, on the other hand, involves simultaneous variation of all factors, greatly reducing the number of trials while still enabling mathematically reliable estimates to be made of the optimum conditions [38].

3.1. Introduction

The design of experiments (DOE), also called the statistical design of experiments, is a tool for determining the significance of different factors affecting process quality, and for calculating optimal settings for controllable factors [39]. Statistical design of experiments (DOE) involves understanding how different factors to a system, whether concerning product or process, affect the output and subsequently identify the critical factors and their optimal settings. It has emerged as the premier technique in the product and process development cycle for quality improvement and is widely being used by practitioners in the industries. If these methodologies are properly applied, significant benefits in terms of effectiveness, cost, optimization and efficiency can be achieved [40].

3.1.1. Fundamentals of DOE

In DOE terminology, input parameters, variables and structural assumptions composing a model are called factors and output measures are called responses. Selection of factors depends on the goal of the experiment. During an experiment, values of one or more factors change; therefore, each factor requires at least two levels [41].

There are several phases, as listed here:

- Identification of factors that may affect the outcome of the experiment and responses that give a measure of the outcome.
- Choosing an appropriate experimental design, either for screening or response surface modeling.
- Generation of a design matrix, determining which experiments will be conducted.
- Conducting the experiments.
- Fitting the data and generating plots that describing the trends in the results.
- Drawing conclusions and planning the next step.

3.2. Types of Experimental Design

Experimental designs are used to investigate industrial systems or processes. A typical process model is given in Figure 3.1. Purposeful changes are made to the controllable input factors of a process so as to observe and identify the reasons for changes that may be observed in the output responses. The noise factors are considered as random factors that cannot be controlled. Experimental data are used to derive a statistical empirical model linking the outputs and inputs. These empirical models generally contain first-order terms [42].

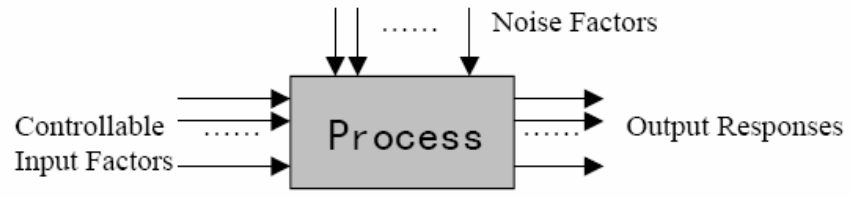

Figure 3.1. The components of process [43]

One common design of experiments (DOE) approach is full factorial design; testing all combinations of factors at each setting. Two-level factorial design is a statistically-based method that involves simultaneous adjustment of experimental factors at only two levels: high and low. The two-level design approach offers a parallel testing scheme that's much more efficient than one-factor-at-a-time [43]. For example, eight experiments would

be needed to examine all combinations of 3 factors at 2 levels each. This is called a 2^3 full factorial design. These experiments can be visualized as the eight corners of a cube and that representation is shown in Figure 3.2. The letters indicate which factors are set to their high value; the rest of the factors are set to their low values. The experiment in which factors A and C are set high and factor B is set low is shown as "ac" in the graph. The settings used for experiments are called treatment conditions [44].

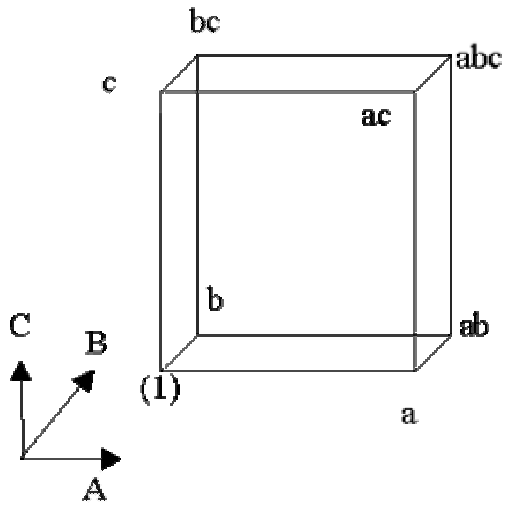

Figure 3.2. 2^3 factorial design cube [45]

3.2.1. Theory of 2^3 Factorial Design

The mathematical model with *z* repetitions per cell in a completely randomized design is:

$$Y_{ijk} = \mu + A_i + B_j + AB_{ij} + C_k + AC_{ik} + BC_{jk} + ABC_{ijk} + E_{ijkv} \qquad (3.1)$$

where i; j; k= (0;1) and v=(1;:::; z).

The usual reactions are:

$$\sum_{i=0}^{1} A_i = \sum_{j=0}^{1} B_j = \sum_{i=0}^{1} AB_{ij} = \sum_{j=0}^{1} AB_{ij} = \sum_{k=0}^{1} C_k = ...\sum_{k=0}^{1} ABC_{ijk} = 0 \qquad (3.2)$$

which implies that,

$$A_1 = -A_0,\ B_1 = -B_0,\ AB_{11} = -AB_{10} = -AB_{01} = AB_{00}, \tag{3.3}$$

$$C_1 = -C_0, \text{ (and further on until)}$$

$$ABC_{000} = -ABC_{100} = -ABC_{010} = ABC_{110} = -ABC_{001} = ABC_{101} = ABC_{011} = -ABC_{111} \tag{3.4}$$

The effects of the experiment (which give the difference in response when a factor is changed from low level to high level) are:

$$A = 2A_1, B = 2B_1, AB = 2AB_{11}, C = 2C_1, ..., ABC = 2ABC_{111} \tag{3.5}$$

The standard order for the 2^3=8 different experimental conditions (factor combinations) is:

$$(1),\ a,\ b,\ ab,\ c,\ ac\ ,\ bc,\ abc \tag{3.6}$$

where the introduction of the factor C is done by multiplying c onto the terms for the 2^2 experiment and adding the resulting terms to the sequence.

$$\begin{aligned}
[I] &= [+(1) + a + b + ab + c + ac + bc + abc] \\
[A] &= [-(1) + a - b + ab - c + ac - bc + abc] \\
[B] &= [-(1) - a + b + ab - c - ac + bc + abc] \\
[AB] &= [+(1) - a - b + ab + c - ac - bc + abc] \\
[C] &= [-(1) - a - b - ab + c + ac + bc + abc] \\
[AC] &= [+(1) - a + b - ab - c + ac - bc + abc] \\
[BC] &= [+(1) + a - b - ab - c - ac + bc + abc] \\
[ABC] &= [-(1) + a + b - ab + c - ac - bc + abc]
\end{aligned} \tag{3.7}$$

Yates' algorithm is mainly used for the DOE and it helps user to calculate the main effects which seem as main effects in the equation. Yates' algorithm is performed as

below, but the operation on the columns should now be done 3 times as there are 3 factors [45].

The calculation matrix in the form of effects is as Equation 3.8.

$$\begin{bmatrix} I \\ A \\ B \\ AB \\ C \\ AC \\ BC \\ ABC \end{bmatrix} = \begin{bmatrix} +1 & +1 & +1 & +1 & +1 & +1 & +1 & +1 \\ -1 & +1 & -1 & +1 & -1 & +1 & -1 & +1 \\ -1 & -1 & +1 & +1 & -1 & -1 & +1 & +1 \\ +1 & -1 & -1 & +1 & +1 & -1 & -1 & +1 \\ -1 & -1 & -1 & -1 & +1 & +1 & +1 & +1 \\ +1 & -1 & +1 & -1 & -1 & +1 & -1 & +1 \\ +1 & +1 & -1 & -1 & -1 & -1 & +1 & +1 \\ -1 & +1 & +1 & -1 & +1 & -1 & -1 & +1 \end{bmatrix} \begin{bmatrix} (1) \\ a \\ b \\ ab \\ c \\ ac \\ bc \\ abc \end{bmatrix} \tag{3.8}$$

If one writes what happens in detail, one gets:

Table 3.1. Yates algorithm

Response	1st time	2nd time	3rd time	Contrasts
(1)	$(1)+a$	$(1)+a+b+ab$	$(1)+a+b+ab+c+ac+bc+abc$	$[I]$
a	$b+ab$	$c+ac+bc+abc$	$-(1)+a-b+ab-c+ac-bc+abc$	$[A]$
b	$c+ac$	$-(1)+a-b+ab$	$-(1)-a+b+ab-c-ac+bc+abc$	$[B]$
ab	$bc+abc$	$-c+ac-bc+abc$	$(1)-a-b+ab+c-ac-bc+abc$	$[AB]$
c	$-(1)+a$	$-(1)-a+b+ab$	$-(1)-a-b-ab+c+ac+ab+abc$	$[C]$
ac	$-b+ab$	$-c-ac+bc+abc$	$(1)-a+b-ab-c+ac-bc+abc$	$[AC]$
bc	$-c+ac$	$(1)-a-b+ab$	$(1)+a-b-ab-c-ac+bc+abc$	$[BC]$
abc	$-bc+abc$	$c-ac-bc+abc$	$-(1)+a+b-ab+c-ac-bc+abc$	$[ABC]$

Parameter estimates are, with k =3

$$\hat{\mu} = \frac{[I]}{2^k.z}, \hat{A}_1 = \frac{[A]}{2^k.z}, \hat{B}_1 = \frac{[B]}{2^k.z}, \ldots\ldots\ldots, \widehat{ABC_{111}} = \frac{[ABC]}{2^k.z} \tag{3.9}$$

Correspondingly, the effect estimates are:

$$\widehat{A} = 2\widehat{A_1} \quad , \quad \widehat{B} = 2\widehat{B_1} \quad ,\ldots\ldots\ldots\ldots , \ \widehat{ABC} = 2\widehat{ABC_{111}} \tag{3.10}$$

$$SSQ_A = \frac{[A]^2}{2^k.z}, \quad SSQ_B = \frac{[B]^2}{2^k.z}, \ SSQ_{ABC} = \frac{[ABC]^2}{2^k.z} \tag{3.11}$$

where *SSQ* is sum of squares, The variances of the contrasts are found, with [*A*] as example:

$$Var\{[A]\} = Var\{-(1) + a - b + ab - c + ac - bc + abc\} = 2^k.z.\sigma^2 \tag{3.12}$$

where *k*=3 here.

The result is seen by noting that there are 2^k terms, which all have the same variance, which for example is

$$Var\{ab\} = Var\left\{z\sum_{y=1}^{r} Y110v\right\} = z.\sigma^2 \tag{3.13}$$

Further, it is now found, that

$$Var\left\{\widehat{A_1}\right\} = Var\left\{[A]/\left(2^k.r\right)\right\} = \sigma^2/\left(2^k.z\right) \tag{3.14}$$

$$Var\left\{\widehat{A}\right\} = Var\left\{2\widehat{A_1}\right\} = \sigma^2/\left(2^{k-2}.z\right) \tag{3.15}$$

3.3. Basic Steps in DOE Methodology Designed for Optimization

The basis of this approach is the assumption of a simplified linear model for the optimization parameter η given by $\eta=\beta_0+\beta_1x_1+\beta_2x_2$…….. where x_1, x_2 , ... etc. are the factors on which η depends and β_0, β_1, β_2, β_3 ……etc represent the "true" values of the corresponding unknowns. From the results of an experiment comprising a finite number of trials, one can arrive at sample estimates of coefficients, β, which are then usually fitted into a linear regression equation of type $y=b_0+ b_1x_1+ b_2x_2+$…….. where y is the response function and the bs are the "estimated" values of βs. In simple terms, each coefficient

represents the influence of corresponding factor on the quality of the weld expressed by optimization parameter.

The main algorithm that is used in determining the optimized parameters is represented in Figure 3.3 and this main obtains four phases.

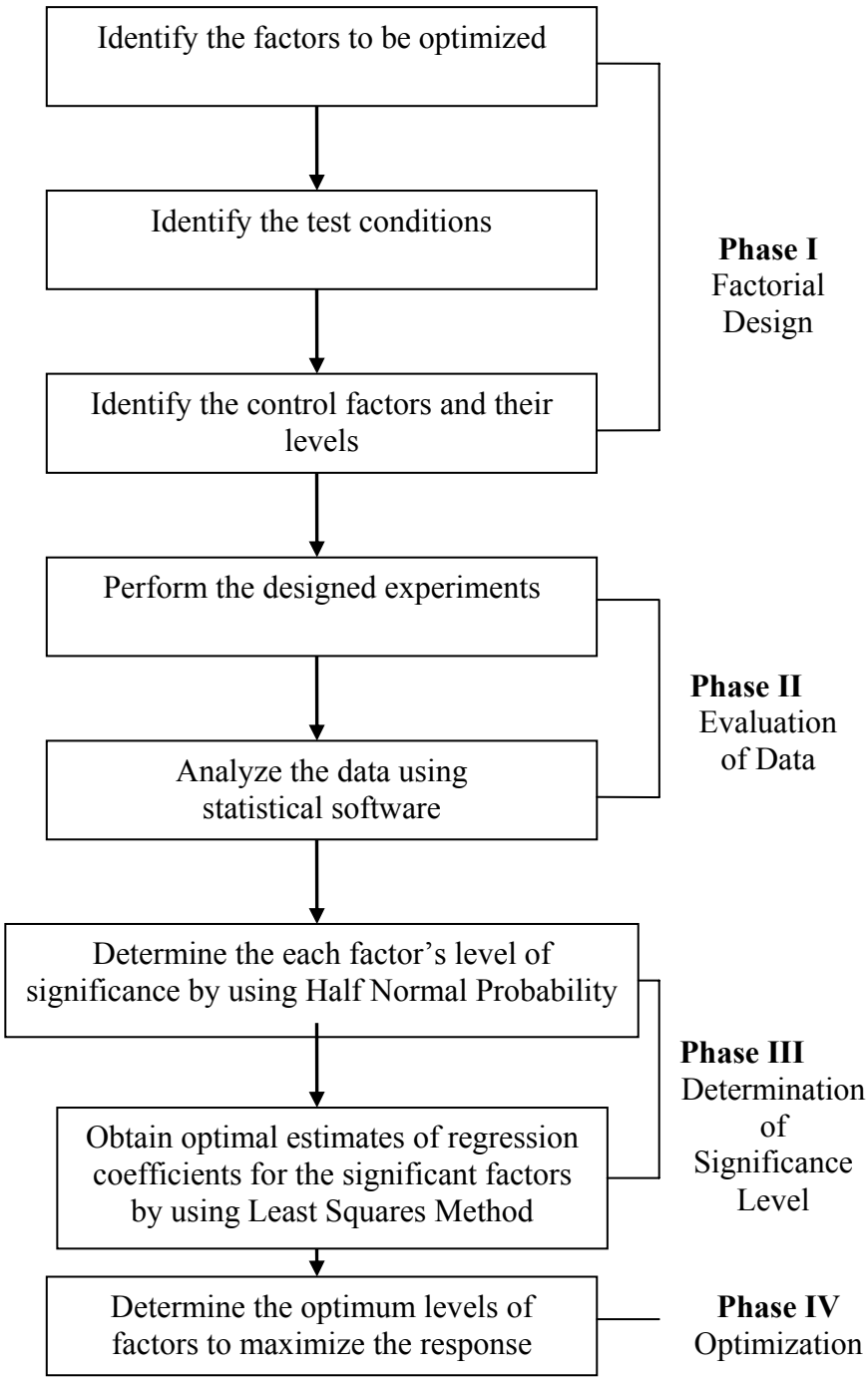

Figure 3.3. DOE algorithm for optimization process

3.3.1. Phase I

The first step in factorial design is to select the local region of the factorial space to be explored. This comprises two parts: choice of basic or zero levels and selection of intervals. The former are usually obtained from published literature as the best factorial combination so far known, while the latter are related to experimental points chosen symmetrically higher and lower than the basic level. The upper and lower levels thus obtained are usually transformed for convenience into coded variables +1 and -1 respectively [39].

3.3.2. Phase II

In the phase II the experiments are done and test results are recorded and evaluated carefully. When the data are finally collected, they must be analyzed in a way that will provide meaningful conclusions. Planning the analysis of the data is part of the initial process of setting up the research program. Knowing how the data can be correctly analyzed and interpreted will affect how the data are collected and the numbers of observations required [46].

3.3.3. Phase III

The statistical analysis involves two steps: first the adequacy of the model is tested. A suitable method is based on the half normal probability plot which can be used to confirm if the terms in the assumed linear function are statistically significant [47]. These plots provide a way to assess whether the data are normally distributed or not [48]. The second step is to obtain optimal estimates of regression coefficients for the significant factors which may be done using the method of least squares [38].

3.3.4. Phase IV

Once the regression equation is determined, settings for each factor can be determined to optimize the expected outcome of the process [39]. Positive coefficients for any factor indicate that increasing this variable would enhance the response, negative

coefficients the opposite. The optimum welding conditions within the range investigated can be found by selecting upper levels for factors with positive coefficients and lower ones for factors whose coefficients are negative. In cases where interaction effects are also established and mixed coefficients occur in the equation, the optimum levels for the corresponding factors are chosen so as to maximize the response [38].

3.4. Half Normal Probability

Graphical methods such as normal and half-normal probability plots are often used in determining which contrasts are significant in an orthogonal or independent set [49]. Quantitatively, the estimated effect of a given main effect or interaction and its rank relative to other main effects and interactions is given via least squares estimation (that is, forming effect estimates that minimize the sum of the squared differences between raw data and the fitted values from such estimates). Having such estimates in hand, one could then construct a list of the main effects and interactions ordered by the effect magnitude [49].

3.4.1. Interpretation of Half Normal Probability

Determining the subset of important factors is the most important task of the half normal probability plot of effects. The estimated effect of an unimportant factor will typically be on or close to a near-zero line, while the estimated effect of an important factor will typically be displaced well off the line [49].

The separation of factors into important-unimportant categories is thus done by answering the question: “Which points on the half-normal probability plot of effects are large and well-off the linear collection of points drawn in the vicinity of the origin?”

This line of unimportant factors typically encompasses the majority of the points on the plot. The procedure consists, therefore, of the following:

- Identifying the line of near-zero (unimportant) factors; then
- Declaring the remaining off-line factors as important.

4. EXPERIMENTAL STUDY

In order to conduct the experiments, an experimental set-up is needed. Thus, thesis study started with design and manufacturing of continuous drive friction welding experimental set-up. While manufacturing such a set-up, previous studies and design examples were taken into consideration.

4.1. Design and Manufacturing of Experimental Set-Up

As mentioned in Chapter 3, there are two types of friction welding mechanisms: continuous drive and inertia drive. In this study, continuous drive friction welding mechanism was selected because of being more controllable than inertia friction welding which means having more variables to control during welding operation.

4.1.1. Modification of Lathe

The design of experimental set-up is mainly based on the modification of a lathe. However some parts of the lathe were changed.

Design of Rotational Part:

- Selection of AC electrical motor
- Bearings that are selected with the purpose of damping the axial load during welding operation
- Two lathe chucks which was designed for the maximum friction moment which can be 2-2,5 times larger than the computed on the basis of the installed power

Design of Stationary Part:

- Hydraulic Part

- Control Unit for Automation of Welding Cycle: The aim of designing a control unit is to enhance the repeatability which is significant from the perspective of results.
- Rubber foots for damping vibrations

4.1.2. Design of Rotational Part

Selection of Electrical Motor: The main criteria for the rotational part is to enable it to keep rotating while friction takes place. This is possible only when the minimum motor moment is at least equal or bigger than brake moment; otherwise it will stop and will not rotate.

$$M_{motor} \geq M_{brake} \tag{4.1}$$

From this equation it is very clear that minimum motor moment or maximum brake moment must be known. The equation which determines the M_{brake} is as follows;

$$M_{brake} \approx \frac{2}{3}\pi pfR^3 \tag{4.2}$$

where M_{motor} is motor moment, M_{brake} is brake moment, p is unit pressure, f is friction coefficient and R is radius.

The main issue in determining the maximum M_{brake} is to determine the specimen diameter which will be welded, and to determine pressure that will be applied while parts are rotating. Firstly, the diameter of the specimens was selected as 10 mm. Additionally, it is referred that heating pressure for medium and high carbon steel is from 41 to 103 MPa (6 to 15 ksi) and welding pressures are from 103 to 415 MPa (15 to 60 ksi) [4]. In the light of this information heating pressure was taken as 42 MPa. Lastly coefficient of friction was found by reading the coefficient from the Figure 4.1 which was drawn by Hazlett [51]. In the Figure 4.1 the friction coefficient varies with peripheral angular velocity.

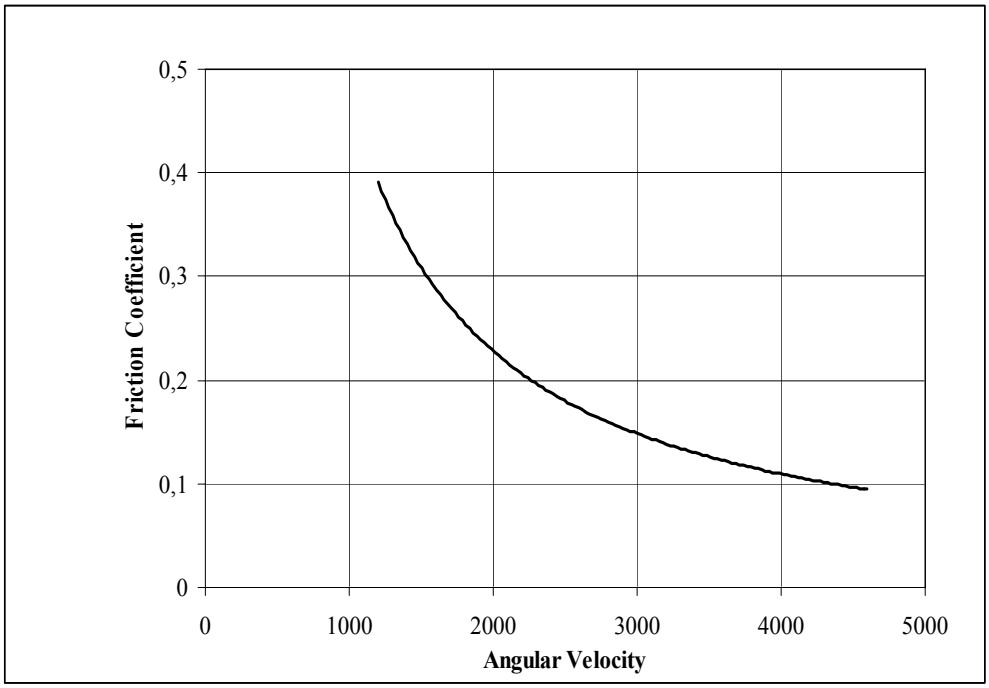

Figure 4.1. Change in friction coefficient with angular velocity [51]

If friction coefficient is marked as 0,32 for 1500 rpm (revolutions per minute) from the Figure 4.1 and accepted constant during whole process, then the M_{brake} becomes as in Equation 4.3.

$$M_{brake} = \frac{2}{3} \cdot (0,32) \cdot (42).\pi.(10)^3 = 28,149 \text{ Nm} \tag{4.3}$$

Then it is necessary to find the motor power. This can be done by

$$N_{motor} = \frac{M_{motor} \cdot n}{9550} \tag{4.4}$$

where N_{motor} is power, M_{motor} is moment of the motor and n is the number of rotation per minute.

If the moment and rotation per minute is inserted into the equation, then necessary power becomes 4,42 kW. To provide a chance to study bigger diameters in the future and as a result of relationship of $M_{motor} \geq M_{brake}$, a 7,5 kW AC motor was selected for the rotational part.

4.1.3. Design of Stationary Part

Design Hydraulic Part: For the stationary part the most significant issue is the design of the hydraulic part. In the hydraulic part a double-acting cylinder with piston diameter of 50 mm was used. In order to have 100 MPa upset pressure, the Equation 4.5 must be satisfied.

$$P_u * d^2 = P_{pump} * d^2{}_{piston} \tag{4.5}$$

where P_u is upset pressure, P_{pump} is gear pump pressure, d_p is piston diameter, d is specimen diameter. It is known that a standard gear pump can supply P=250 bar (≈25 MPa) maximum pressure. Then,

$100 * 10^2 = P_{pump} * 50^2$

P_{pump}= 4MPa= 40 bar which means that the 4 MPa capacity of 25 MPa capacity will be used.

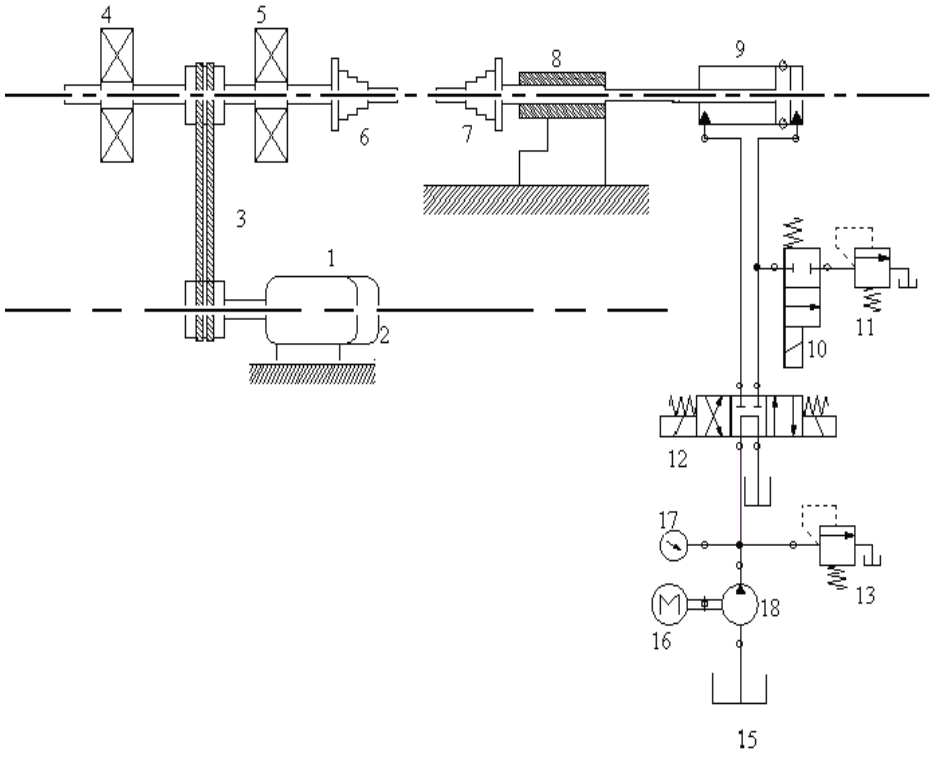

Figure 4.2. Schematic representation of experimental set-up

The schematic representation of experimental set-up with hydraulic part is shown in Figure 4.2. Additionally the parts of set-up are shown in Table 4.1 in detail.

Table 4.1. Contents of experimental set-up

Equipment	Specifications
1.Electrical Motor	7,5 kW, 1500 rpm
2.Electromagnetic Brake System	
3.Driving Belt	
4,5.Bearings	
6. Rotational Chuck	
7.Stationary Chuck	
8.Tailstock	
9. Double Acting Cylinder	d_p=250 bar
10.2/2 NC Electrical Control Valve with Spring Return	
11. Pressure Relief valve	
12.,13. 4/3 Tandem Type Double Electrical Control Valve	
14.Pressure Gauge	
15. Atmospheric Reservoir	
16.Electrical Motor	2,2 kW, 1500 rpm
17.Pressure Gauge	
18. Fixed Displacement Pump	Max. 250 bar

Table 4.2. Explanations of symbols

C0	Rotation Contactor
C1	Hydraulic Contactor
C2	Assistance Contactor

b0	Emergency Stop
b1	Rotation Start
b2	Hydraulic Start
b3	Welding Start
b4	Finish

Y1	Connected 2/2 Way Valve
Y2	Connected to 4/3 Way Directional Valve for forward motion of piston
Y3	Connected to 4/3 Way Directional Valve for backward motion of piston

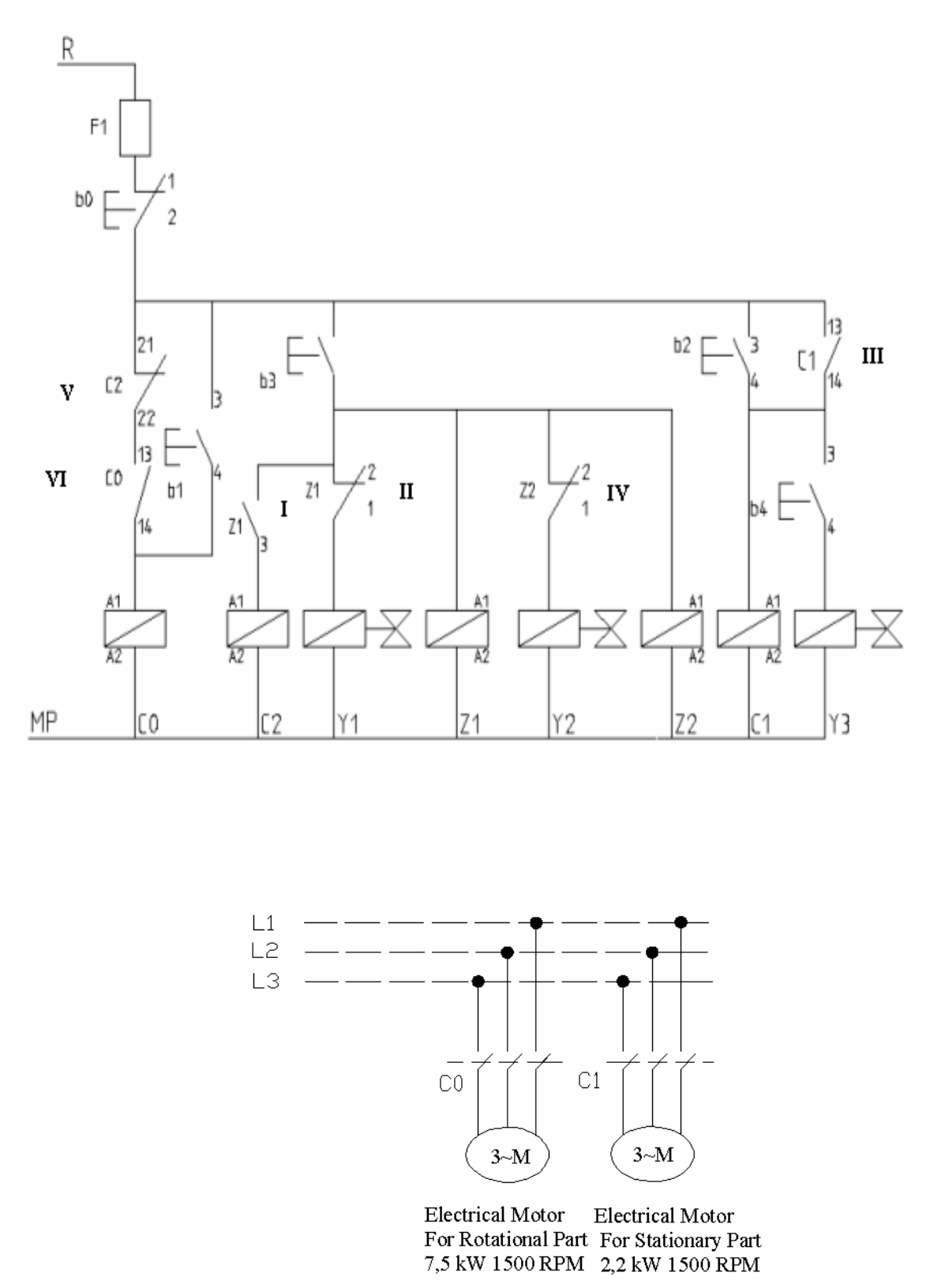

Figure 4.3. Analog control circuit of experimental set-up

Principle of Operation: The necessary symbols which are used in control circuit are shown in Table 4.2. With the assistance of this table, the basic working principle of control circuit can be clearly understood from Figure 4.3. Operation starts with pressing b1 button. By this, C0 contactor is activated with closing the contact of VI and enabling main motor to start rotating. After that hydraulic unit is started by pressing b2 button and activating C1 with closing contact of III that means hydraulic unit begins to work however hydraulic unit is not able to move piston. When b3 button is pressed, time relay Z1 and time relay Z2 is enabled power at the same time. Time relay Z1 activates main motor, 2/2 solenoid valve and 4/3 directional electrical control valve. In the mean time Z1 waits for friction phase and counts. When the friction time is up, it closes all the open contacts and opens all the closed contacts which are directly connected Z1. This enables to stop the rotation of main electrical motor by closing the contact of I and opening the contact of V thus influencing the electrical magnetic brake to cause to stop the rotation. It does not only influence the motor but also the 2/2 solenoid by closing the open way at the end of Z1 time. Thus friction time and friction pressure are controlled accurately. However upset phase or welding phase is started and Z2 is still continuing to count. At the end upset time, Z2 opens the closed contact IV and activates the 4/3 by changing its position to from A to B. Thus welding process is completed. At the end, pressing b4 changes 4/3 directional valve's position from B to C and provides the piston to come back. It is very important in circuit that Z1 is responsible from the friction time and Z2 is responsible from the friction time and upset time.

In summary, when b1 is pressed main motor starts to rotate and when b2 is pressed hydraulic starts to work. With b3, Z1 time relay and Z2 time relay are activated. Z1 provides to change 4/3 directional valve position from B to A, to open the way of 2/2 solenoid valve and controlling the friction pressure of system from 11 th pressure relief valve. At the end of Z1, rotation is suddenly stopped 2/2 solenoid valve closes the flow and pressure is controlled by the 13 th pressure relief valve which is arranged for upset pressure. At the end of the period Z2, welding operation is finished and 4/3 way valve changes its position to C by pressing b4 with resulting in backward motion of piston.

The experimental set-up on which analog control circuit was placed is shown in Figure 4.4.

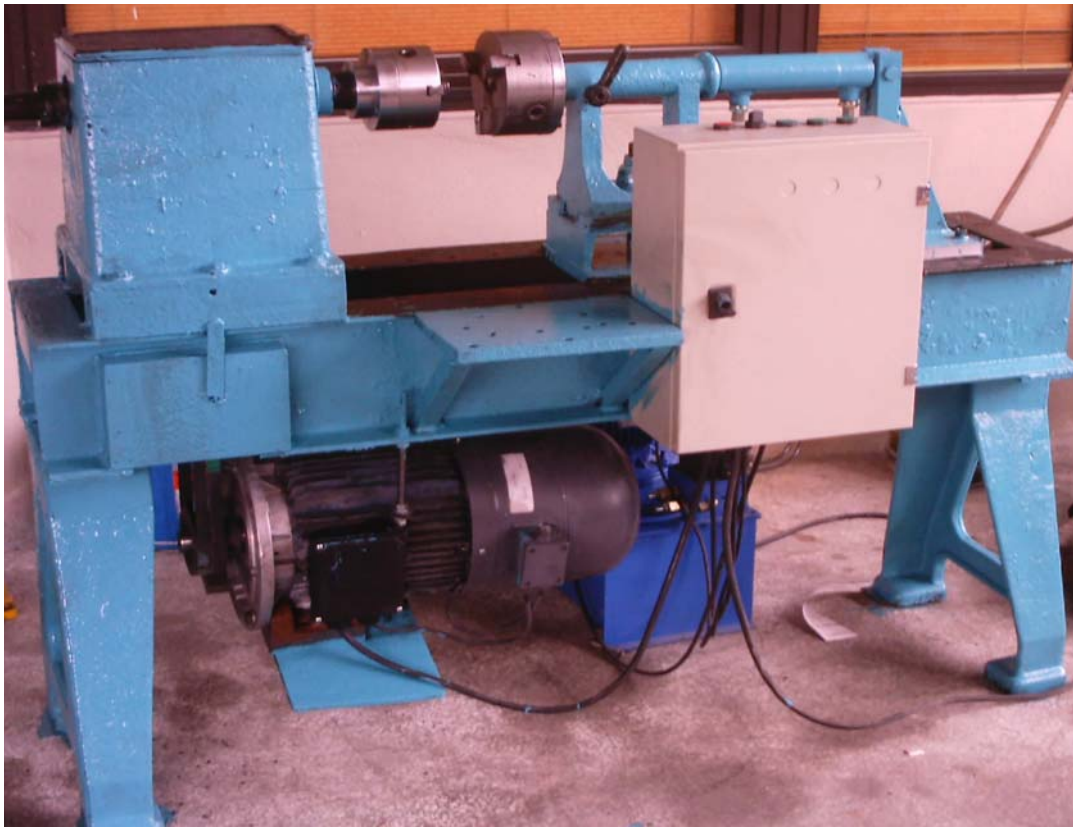

Figure 4.4. Experimental set-up built for the friction welding operation

Damping of Vibrations: Friction generates vibrations which must be dampened by the design of the machine and the choice of the process variables. This, in turn has direct influence on the weld quality and the life of the machine. In the light of this information rubber foots were placed on the set-up which is seen Figure 4.5.

Figure 4.5. Damper for reducing vibrations

4.2. Experimental Methodology

To begin to the experiments, it is necessary to determine the experimental parameters. For this purpose, parameter selection was carried out. The experiments were classified for two groups: hot forged AISI 1050–AISI 304 which is referred as "F" group and investment cast AISI 1050-AISI 304 which is referred as "C" group. Then, 2^3 factorial design was done and parameters optimization was provided to maximize the tensile strength. The microstructure, microhardness and the tensile test results of forged AISI 1050-AISI 304 (F group) were compared with those of investment cast AISI 1050-AISI 304 (C group).

The methodology that was followed in the present study is shown in Figure 4.6.

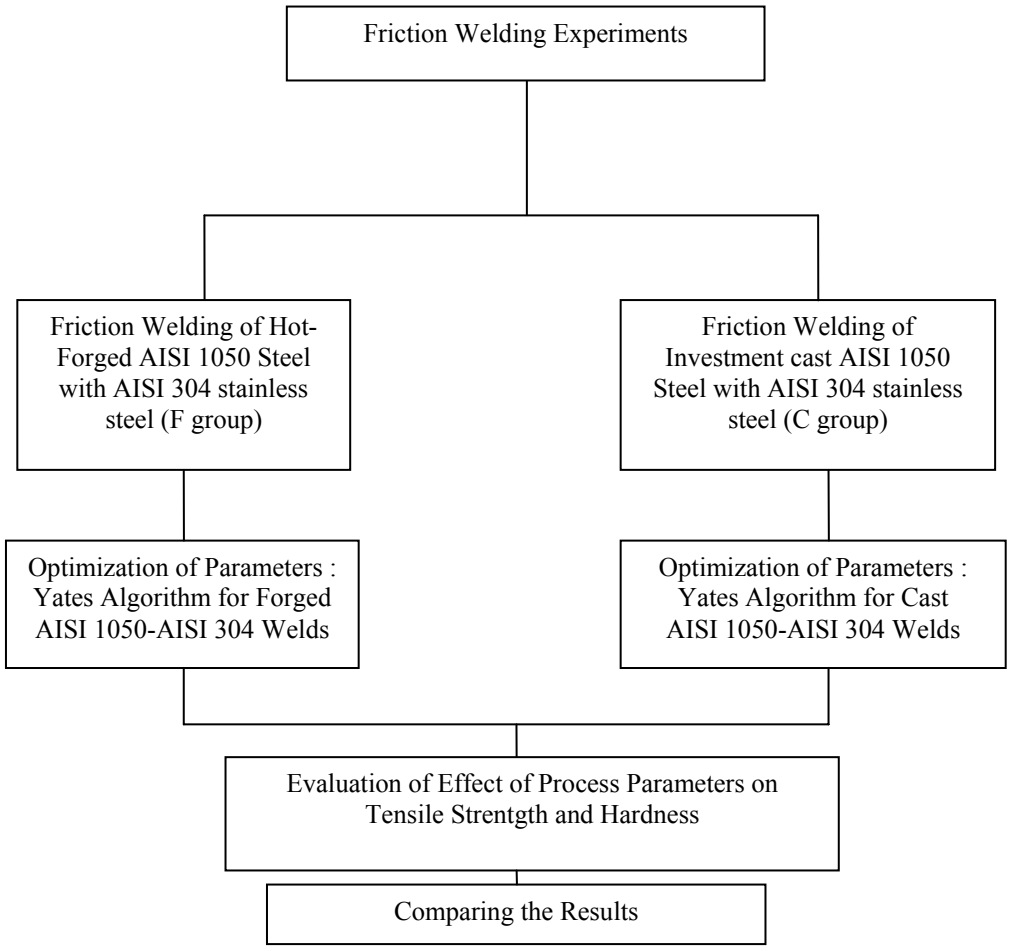

Figure 4.6. Experimental procedure

4.3. Statistical Approach

Statistical approach started with selecting the suitable process parameters with high and low levels +1 and -1 respectively. These levels were selected as 12 bar for low level and 17 bar for high level in friction pressure, 10 sec for low level and 14 sec for high level in friction time, and 25 bar for low level and 40 bar for high level in forge pressure. After that 2^3 factorial design was carried out in order to optimize the process parameters. Design matrix for factorial design is shown Table 4.3. The mechanical properties were subjected to statistical analysis to determine the influence of effects of the parameters and their interactive effects on the properties. ANOVA (analysis of variance) technique and half normal plot was used to study the significance of coefficients and regression equations were derived from this analysis.

Table 4.3.Process parameters

Trial Run	Friction Time (sec)	Friction Pressure (Bar)	Forging Pressure (Bar)
F1-C1	10	12	40
F2-C2	14	17	25
F3-C3	14	17	40
F4-C4	14	12	40
F5-C5	10	17	25
F6-C6	10	12	25
F7-C7	10	17	40
F8-C8	14	12	25

The regression equations enabled to understand the influence of the friction welding parameters on mechanical properties [52].

4.4. Materials Used

4.4.1. Test Materials and Specimen Dimensions

The materials for the present work were commercially available medium carbon steel AISI 1050 and austenitic stainless steel AISI 304 and the compositions of these materials are shown in Table 4.4 [53].

Table 4.4. Chemical compositions of materials [53]

	%						
Material	C	Si	Mn	P	S	Cr	Ni
AISI 304	< 0,08	< 1,00	< 2,0	< 0,045	< 0,030	18-20	8-10,50
AISI 1050	0,48-0,50	-	0,60-0,90	< 0,04	< 0,050	-	-

Forged AISI 1050 and investment cast AISI 1050 steel were manufactured bigger than the real specimen dimensions, and later they were machined to the dimensions shown in Figure 4.7, with 60 mm length and 10 mm diameter. No special preparation was needed for the welding surfaces before the friction welding experiments.

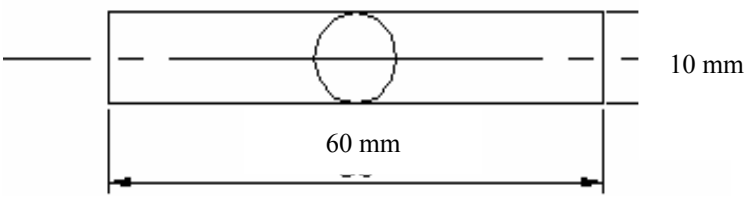

Figure 4.7. Welding specimen dimensions in mm

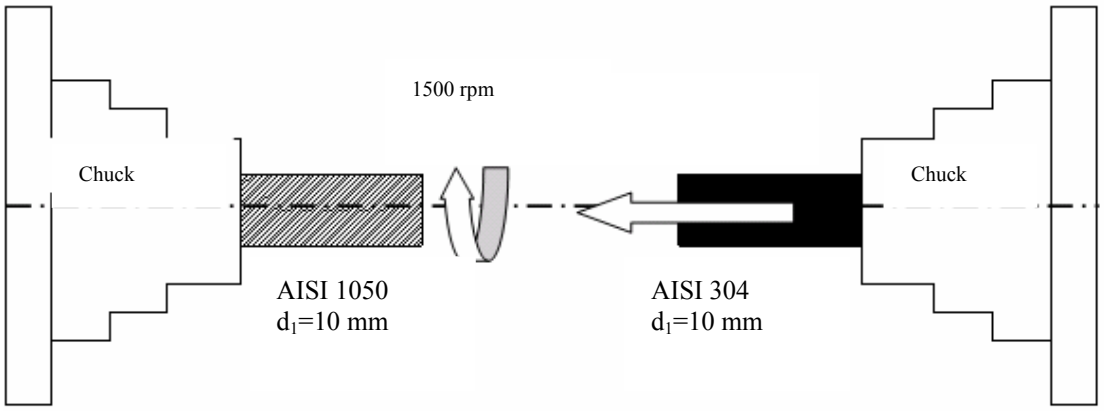

Figure 4.8. Schematic view of experiments

During the experiments AISI 1050 steel was rotated and AISI 304 was pushed against medium carbon steel and the schematic view of this condition is represented in Figure 4.8.

4.4.2. Preparation of Specimens

In order to evaluate the effect of forging and casting on the tensile strength and hardness of friction welded parts, AISI 1050 steel specimens were a investment cast and hot forged before welding operations. Hence manufacturing conditions become as follows:

Hot Forging of AISI 1050 Steel: Specimens were kept in a furnace and forged with a cross-sectional reduction of 30%.

Investment Casting of AISI 1050 Steel: Wax patterns were produced by injection molding. The mould in which wax patterns were produced by injection molding in the form of cylinder is shown in Figure 4.9. Multiple patterns were assembled and a shell was produced by immersing the assembly in a liquid ceramic slurry and then into a bed of extremely fine sand. The ceramic was dried; the wax is melted out; fired to burn all wax. The ceramic was dried; the wax was melted out; fired to burn all wax. After metal solidified, the ceramic shell was broken off by vibration or water blasting. All these were made by SERPA Investment Company in Tuzla.

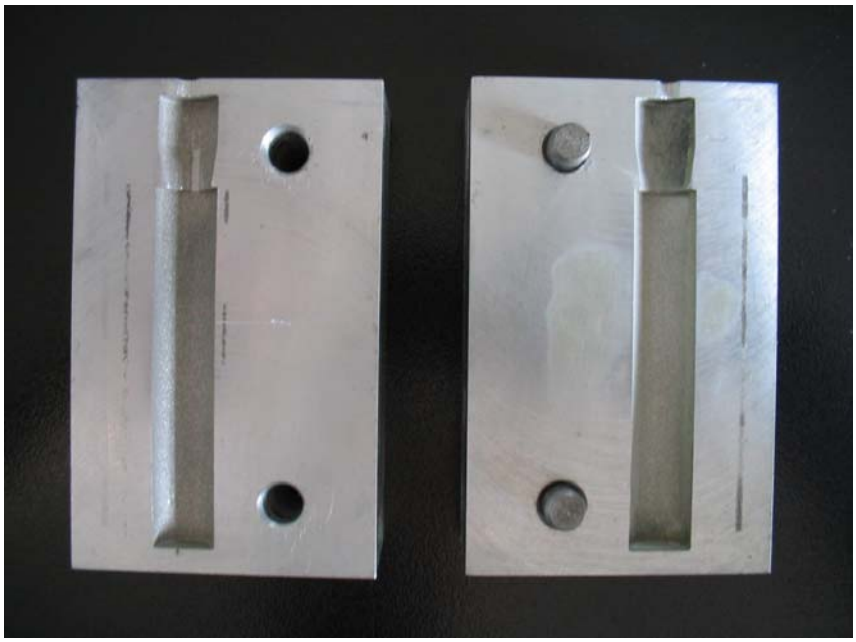

Figure 4.9. The mould made in SERPA Investment Casting Company

4.5. Mechanical Tests

4.5.1. Tensile Testing

After welding, tensile testing was carried out to evaluate the mechanical properties of joints. Tensile testing was done according to DIN 50125. The dimensions of tensile specimen are shown in Figure 4.10. Tensile tests were performed at room temperature using a Testometric type testing machine with crosshead speed of 17 mm/min.

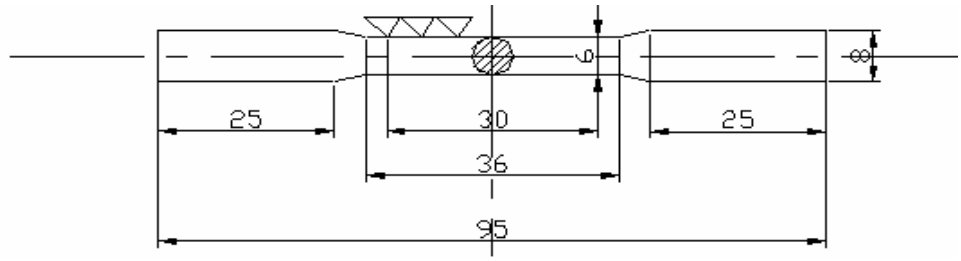

Figure 4.10. Dimensions of tensile test specimen according to DIN 50125 [54]

4.5.2. Hardness Tests

The microhardness was examined in the metallurgical microscope, ZWICK type which used 100 gr. load for the investigation of microhardness. The directions of the weld interface where hardness is investigated are given in Figure 4.11.

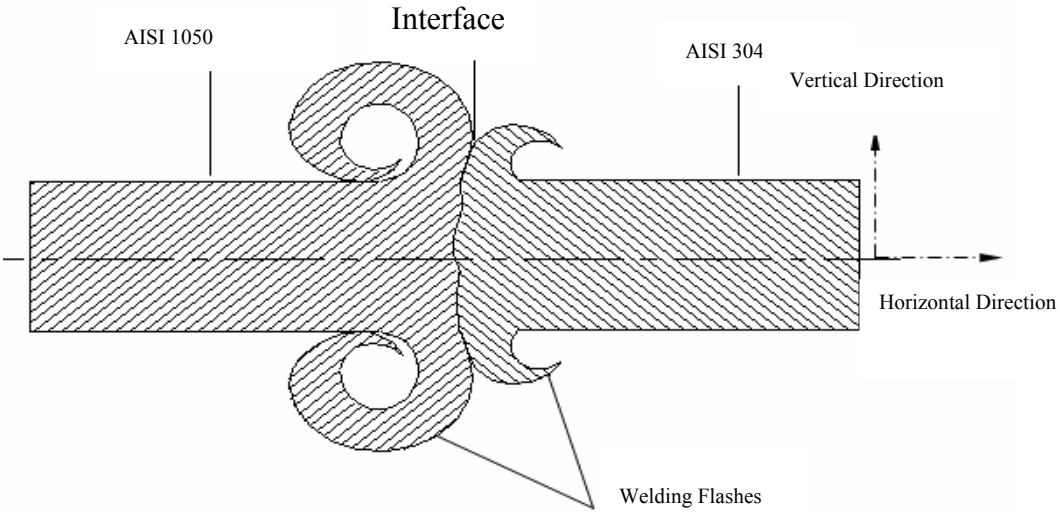

Figure 4.11. Horizontal plane in friction welded specimens

4.6. Metallographic Examination

The preparation of metallographic specimens consists of first selecting a sample of convenient size which will be representative of the material to be investigated. A specimen was selected by cutting a small section of metal from the part to be investigated. It was cut by-cut off disk perpendicular and parallel to the interface by Metkon Cutting Machine. Then mounted in a holder, which was a thick, plastic disk. The plastic was added as a power or liquid in order to conform to the shape of the specimen. Then the plastic was cured to form a hard mold about the specimen.

Grinding operation was carried out by rubbing the specimen on a paper coated with an abrasive in. This abrasive removed the surface layers of the metal. It also leaves a set of scratches and layer of deformed metal. In the next stage an abrasive having a finer particle size was used. It removed the scratches and deformed layer of the previous abrasive and leaves a finer set of scratches and a thinner deformed layer. All grinding operations were done in Metkon Gripo 1 with 60-120-180-220-320-400-600-800-1200 grinding papers.

In order to show the microstructure of a metal or alloy it was necessary to prepare a flat and polished surface, free of scratches. For this purpose, specimens were polished with first Al_2O_3 with 80-100μm surface quality, secondly, Cr_2O_3 with 20 μm surface quality and lastly with Alumina 0,05 μm surface quality. Then the features of the microstructure were developed by etching with a chemical reagent 2% Nital and Picral.

All metallographic examination was done with two types of microscope: Leitz and Olympus PMA 3.

5. RESULTS AND DISCUSSION

5.1. Tensile Testing and Optimization of Process Variables

DIN 50125 was selected as standard for the tensile testing and parameter optimization was employed according to the results of this testing procedure.

5.1.1. Parameter Optimization in Forged AISI 1050–AISI 304 Material Pair

Tensile testing results, percent elongation, reduction in area for forged AISI 1050-AISI 304 material combination (F group) are shown in Table 5.1. Each experimental group for three process parameters (A: friction time, B: friction pressure, C: forge pressure) is represented as F1,F2,F3…etc.

Table 5.1. Tensile testing results of F group

Run	Parameter (A-B-C)	Tensile Strength (N/mm^2)			Percent Elongation		Reduction in Area	
		Trial 1	Trial 2	Av.	Trial 1	Trial 2	Trial 1	Trial 2
F1	10-12-40	738	761	750	16	19	44	48
F2	14-17-25	773	771	772	17	22	48	41
F3	14-17-40	763	743	753	15	14	48	39
F4	14-12-40	739	767	753	17	16	49	47
F5	10-17-25	768	762	765	19	18	44	43
F6	10-12-25	765	745	755	15	21	39	39
F7	10-17-40	753	778	766	16	16	49	47
F8	14-12-25	758	774	766	14	14	43	52

The tensile testing results showed that some of the specimens have almost the same strength though they were manufactured under different conditions. This is because of the balance of process parameters amongst themselves.

Table 5.2. ANOVA table for tensile strength of F group

Source	Sum of Squares	Mean Value	F Value	Prob > F
Model	298	149	4,28	0,0825
B	132	132	3,80	0,1088
C	166	166	4,77	0,0808
Residual	174	35		
Cor Total	471			

Std. Dev.	5,90	R-Squared	0,63
Mean	760	Adj R-Squared	0,48
C.V.	0,78	Pred R-Squared	0,05
PRESS	445	Adeq Precision	4,77

The analysis of variance table (ANOVA) table is shown in Table 5.2. From the ANOVA table it is very clear that this model is significant. There is only a 8,25% chance that this model can fail due to noise. Factor B is significant at 10,88% and factor C is significant at 8,08%. From the R-Squared value it can be said that the model accounts for approximately 63% of the variability in the model.

Half Normal Plot for Significance of Parameters: Half Normal Plot was used to determine the significance of each factor on the optimization parameter and to understand the interaction effects. Regression coefficients were found by the method of least squares. The equations were used in the optimization process to predict the necessary tensile strength under determined welding conditions. To determine the significant factors and to predict the equation, Design Expert 6.0 was employed.

The basis of the half normal plot is to draw a straight line through the origin. The points that lie on this line are negligible and all the remaining points are determined as significant factors. In the light of the information in Table 5.2, half normal plot for forged 1050-AISI 304 (F group) is shown in Figure 5.1.

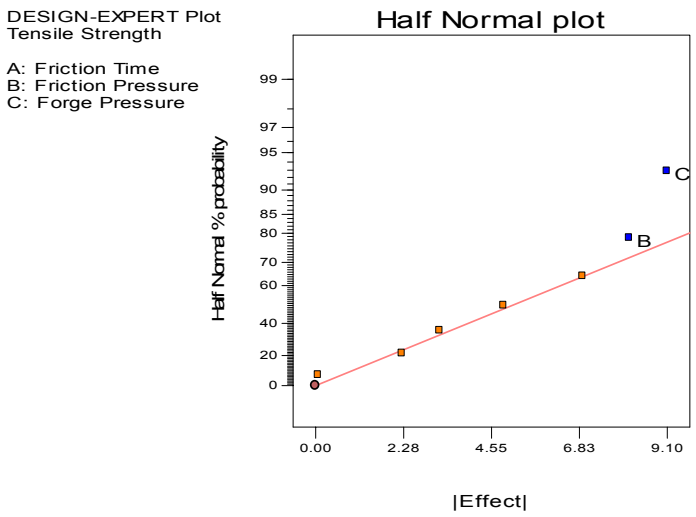

Figure 5.1. Half normal plot for F group

Final Equation in Terms of Coded Factors : If a half normal plot analysis is done according to rules and a straight line is drawn through the origin, it is very obvious that B and C are most important amongst others. Therefore all the other factors can be dropped from the model. Thus, the regression equation is predicted by the least squares method as below:

$$T.S. = 759.91 + 4.06B - 4.55C \tag{5.1}$$

Various plots are considered to see if any of the assumption are violated.

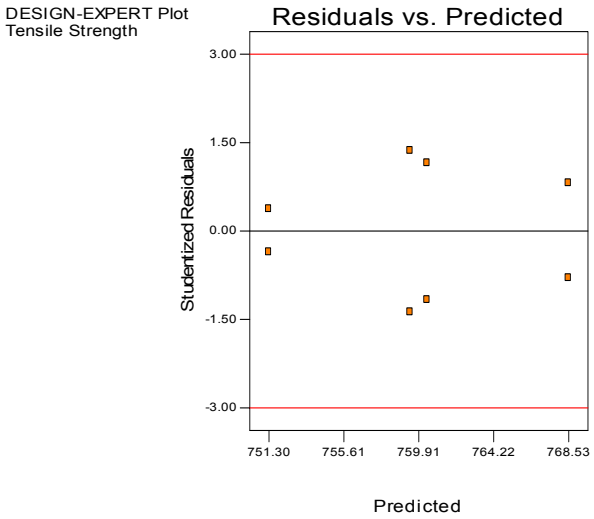

Figure 5.2. Residual and predicted plot

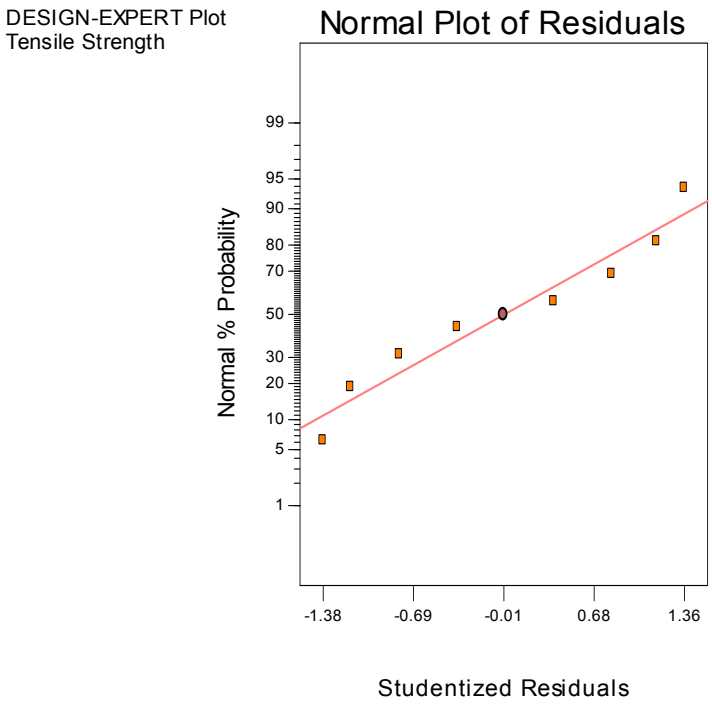

Figure 5.3. Normal plot of residuals

Figure 5.2 and Figure 5.3 show that residuals do not display any abnormality and also no outliers can be found.

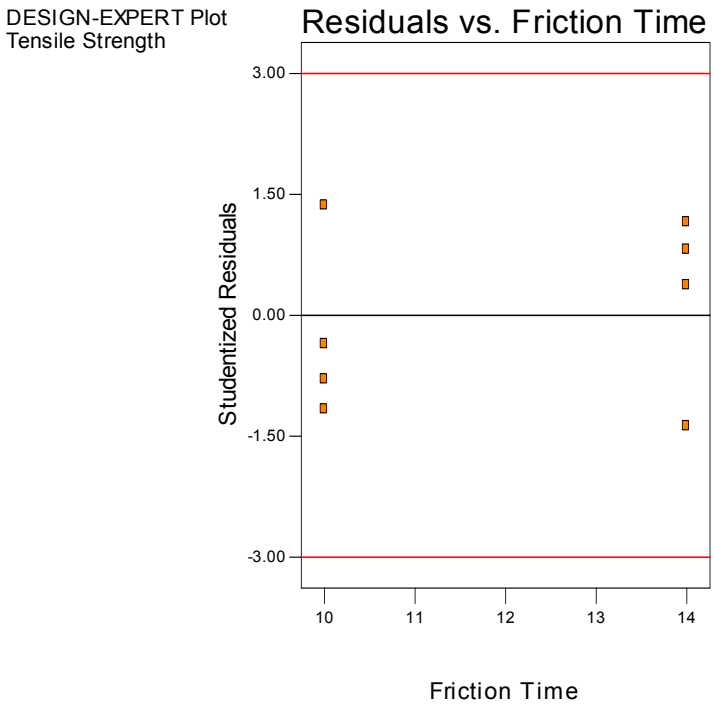

Figure 5.4. Residuals change with friction time

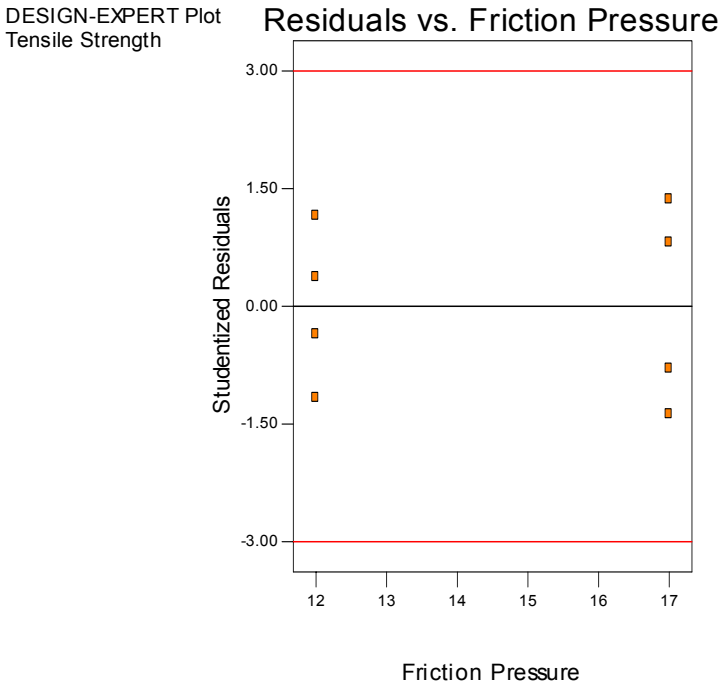

Figure 5.5. Residuals change with friction pressure

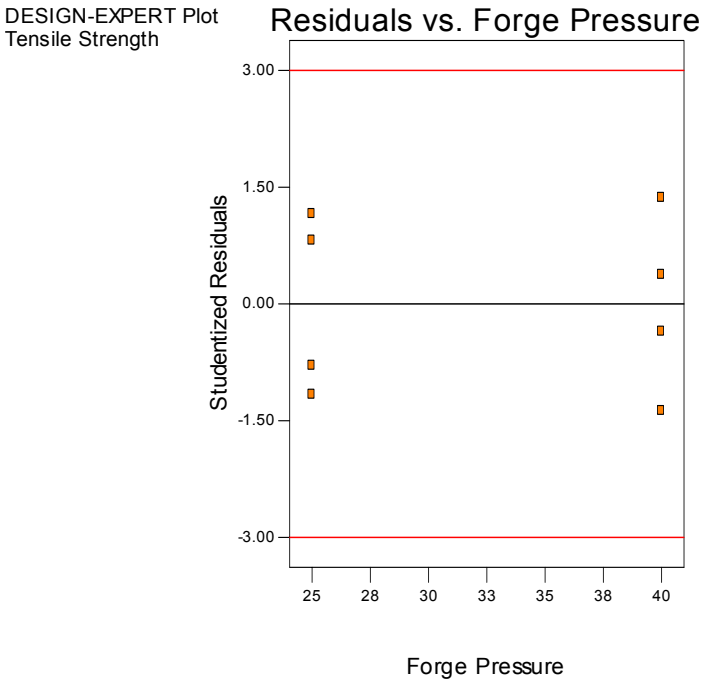

Figure 5.6. Residuals change with forge pressure

Figure 5.4-5.6 explain that because the points are in standard order, constant variance assumption is not violated.

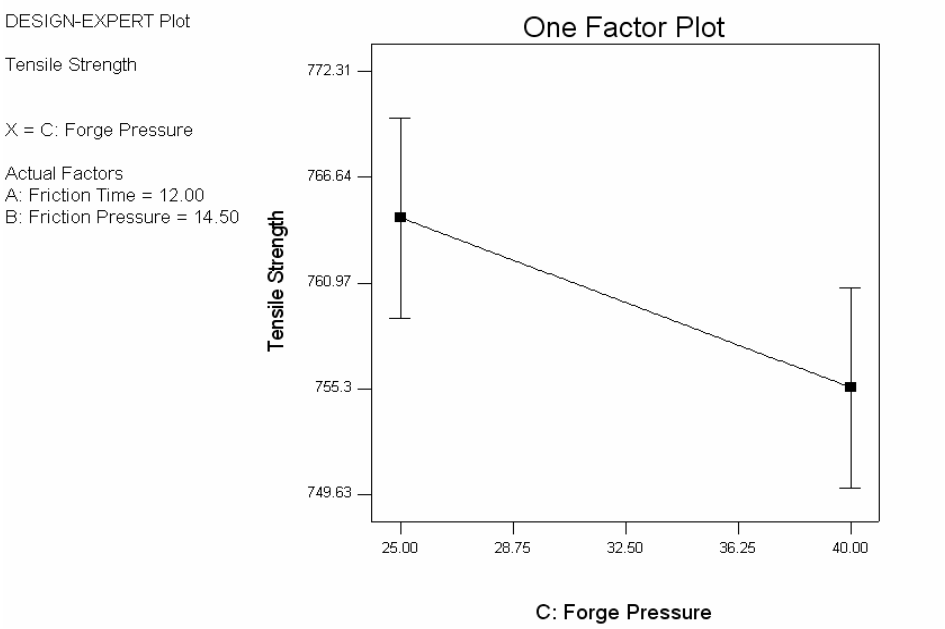

Figure 5.7. Change in tensile strength with forge pressure

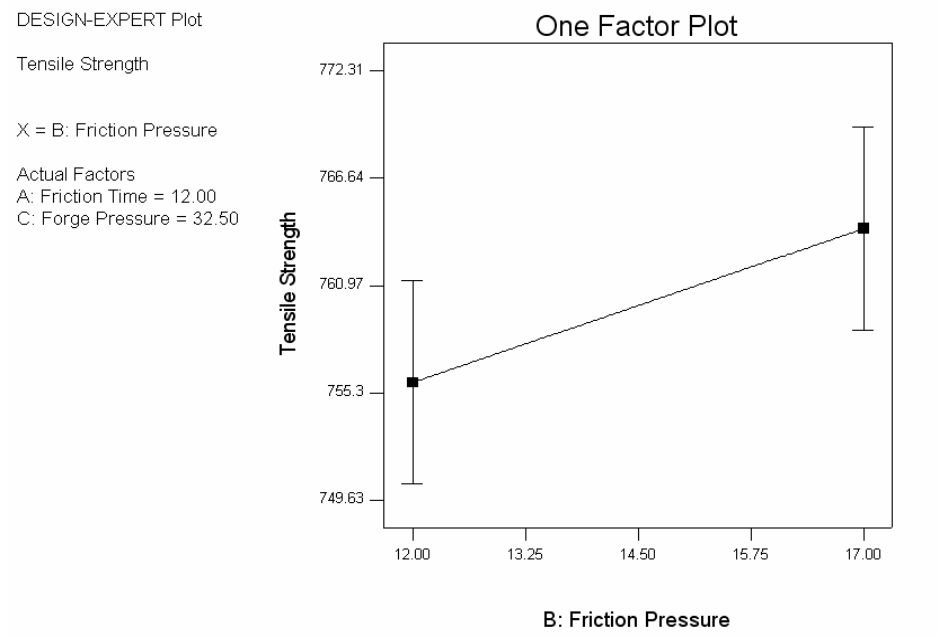

Figure 5.8. Change in tensile strength with friction pressure

Figure 5.7 demonstrates that tensile strength of F group decreases with increase in forge pressure. In opposite, it is very clear in Figure 5.8 that tensile strength is proportional to friction pressure.

Determination of Optimum Welding Conditions: It is very interesting for the friction welded forged AISI 1050-AISI 304 material pair that the equation in terms of coded factors displays friction pressure and forge pressure as the most significant factors. In addition, positive coefficients for any factor in the equation indicate that increase in this variable also increases the response and negative coefficients indicate that increase in this variable decreases the response which is shown in Figure 5.7 and Figure 5.8. Taking this into consideration, the optimum welding conditions within the range can be obtained by selecting upper levels for positive coefficients and lower levels for negative coefficients. For the forged AISI 1050-AISI 304 material combination optimum conditions can be found by Solver Editor in Microsoft Excel. Thus, optimum conditions in terms of coded factors become as in Table 5.3.

Table 5.3. Optimum welding parameters for F group

Material Combination	Friction Time (sec)	Friction Pressure (bar)	Forge Pressure (bar)	Rotational Speed (rpm)
Forged AISI 1050-AISI 304	10-14	17	25	1500

It is very obvious from Table 5.3 that higher level of friction pressure and lower level of forge pressure would be beneficial while remaining in the interval within the friction time. Hence the predicted maximum tensile strength becomes 768 N/mm^2 for the optimum process parameters in this material combination.

5.1.2. Parameter Optimization in Cast AISI 1050–AISI 304 Material Pair

The parameter optimization was based on the average of two trials. The tensile strength, percent elongation, and reduction in area of investment cast AISI 1050-AISI 304 material combination (C group) under the different process parameters (A: friction time, B: friction pressure, C: forge pressure) are given in Table 5.4.

Table 5.4. Tensile test results of C group

Run	Parameter (A-B-C)	Tensile Strength (N/mm^2)			Percent Elongation		Reduction in Area	
		Trial 1	Trial 2	Av.	Trial 1	Trial 2	Trial 1	Trial 2
C1	10-12-40	734	726	730	28	31	9	10
C2	14-17-25	742	731	736	22	16	11	9
C3	14-17-40	734	738	736	30	28	11,5	11
C4	14-12-40	740	746	743	26	14	11	8
C5	10-17-25	713	734	723	16	28	7	10
C6	10-12-25	732	780	756	28	23	13	13
C7	10-17-40	742	758	750	13	15	8	11
C8	14-12-25	729	763	746	26	22	11	16

Table 5.5. ANOVA table for tensile strength of C group

Source	Sum of Squares	Mean Value	F Value	Prob > F
Model	760	265	226	<0.0001
B	110	111	94	0,0006
BC	380	380	323	<0,0001
ABC	306	306	260	<0,0001
Residual	4,7	1,2		
Cor Total	80			

Std. Dev.	1,08	R-Squared	0,99
Mean	740	Adj R-Squared	0,98
C.V.	0,15	Pred R-Squared	0,97
PRESS	18,8	Adeq Precision	43,79

From the Table 5.5, it is seen that this model is significant. The reason of this is Prob>F ratio is only 0,0001 while 0,05 is enough for being significant. One more important thing is there is only 0,01% probability this model can fail.

Half Normal Plot for Significance of Parameters: If a straight line is drawn through the origin, it seems in Figure 5.9 that B, ABC and BC are the most important factors amongst others.

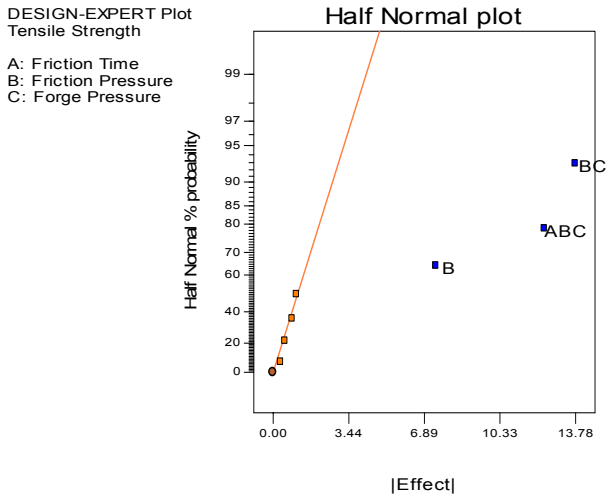

Figure 5.9. Half normal plot for C group

Final Equation in Terms of Coded Factors: After half normal investigation, the equation in terms of coded factors can be obtained. Regression analysis was done in order to have this equation and the result seems below:

$$T.S = 740.12 - 3.71B + 6.89BC - 6.18ABC \tag{5.2}$$

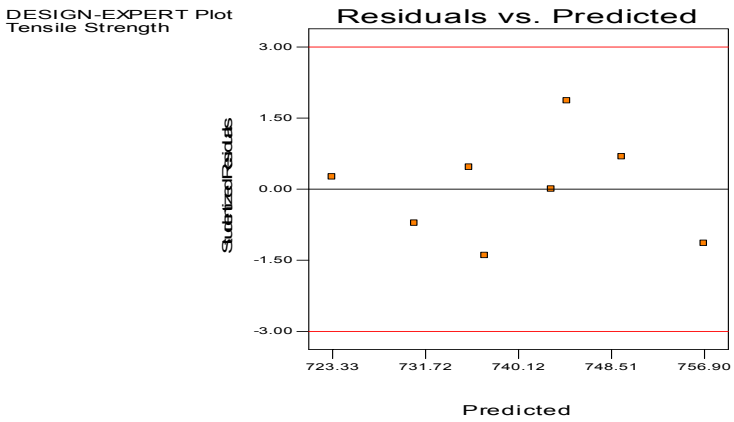

Figure 5.10. Residual and predicted plot

Figure 5.10 shows that an outlier doesn't exist, therefore ANOVA (analysis of variance) assumption is right.

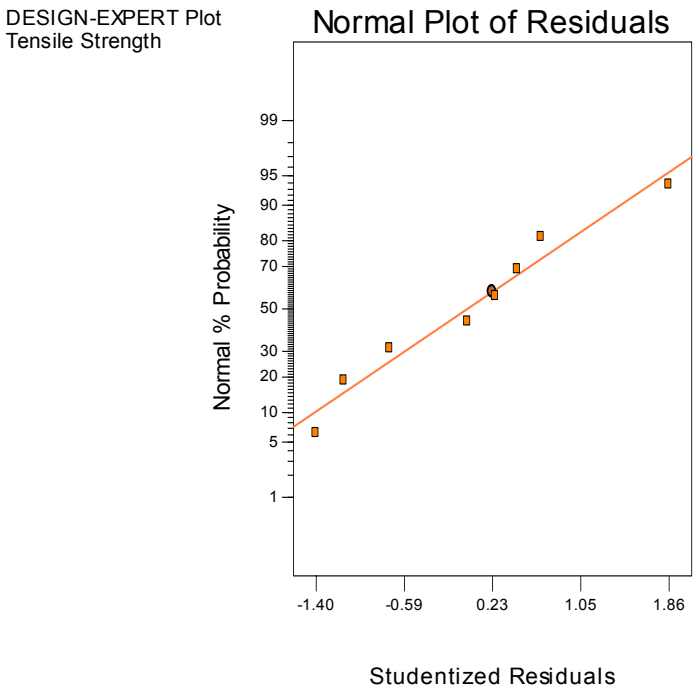

Figure 5.11. Normal plot of residuals

Residual plots do not display any abnormality, and there are no certain outliers. It is true to say that Figure 5.11 confirms the ANOVA table.

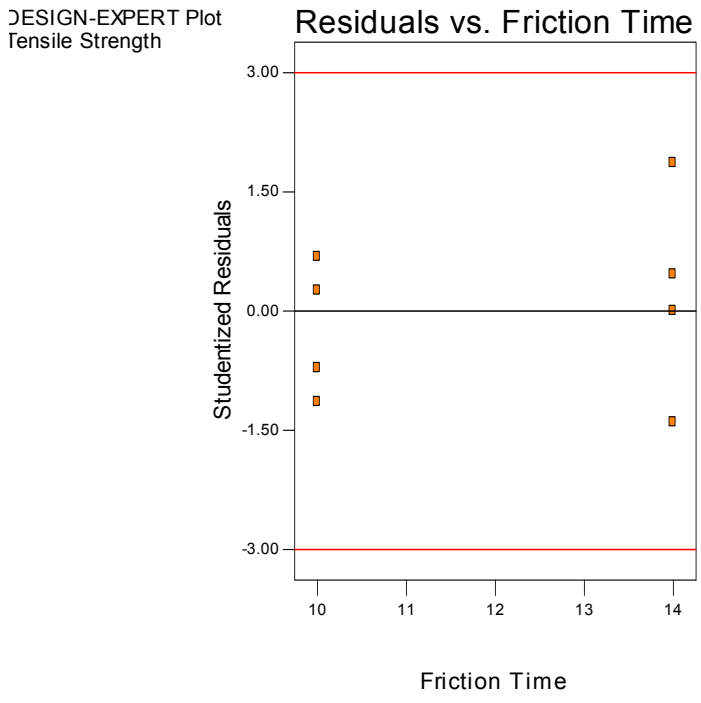

Figure 5.12. Residual and friction time plot

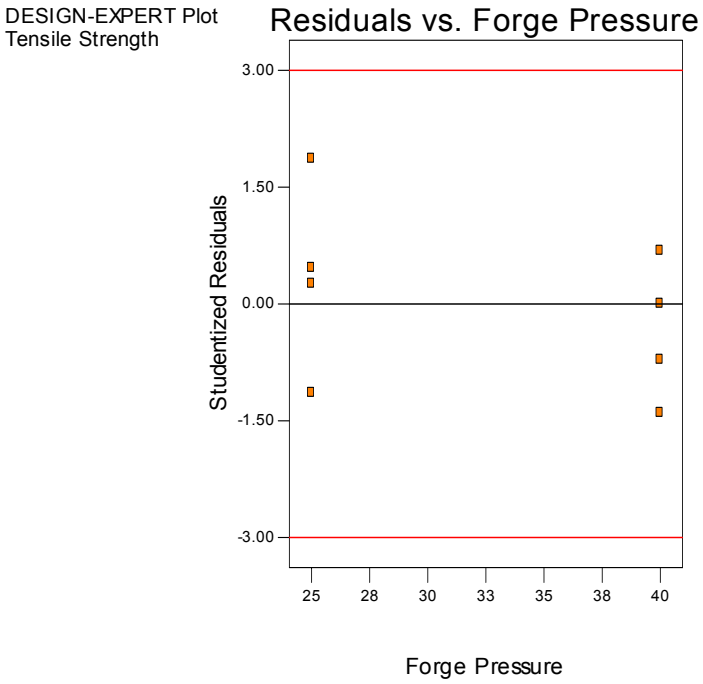

Figure 5.13. Residual and forge pressure plot

Figure 5.12 and 5.13 shows that there is some change in the variance in both the graphs, however this can be omitted in ANOVA assumption.

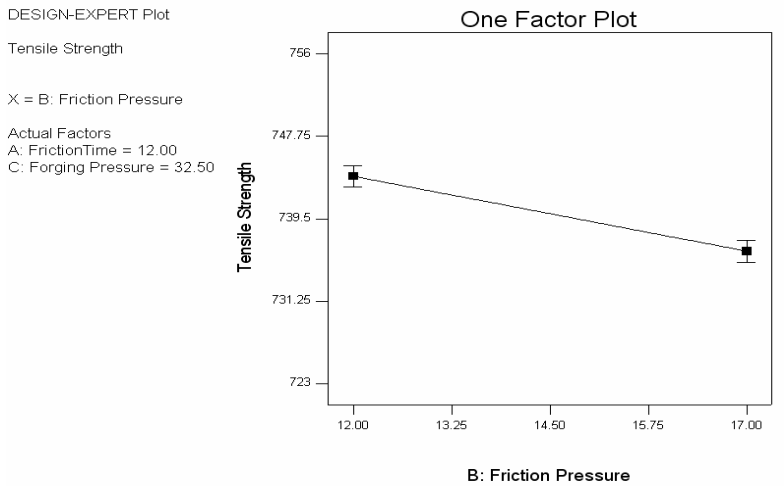

Figure 5.14. Change in tensile strength with friction pressure

Figure 5.14 gives idea about the correlation between friction pressure and tensile strength and it is true to say that an increase friction pressure leads decrease in tensile strength in C (investment cast AISI 1050-AISI 304) group.

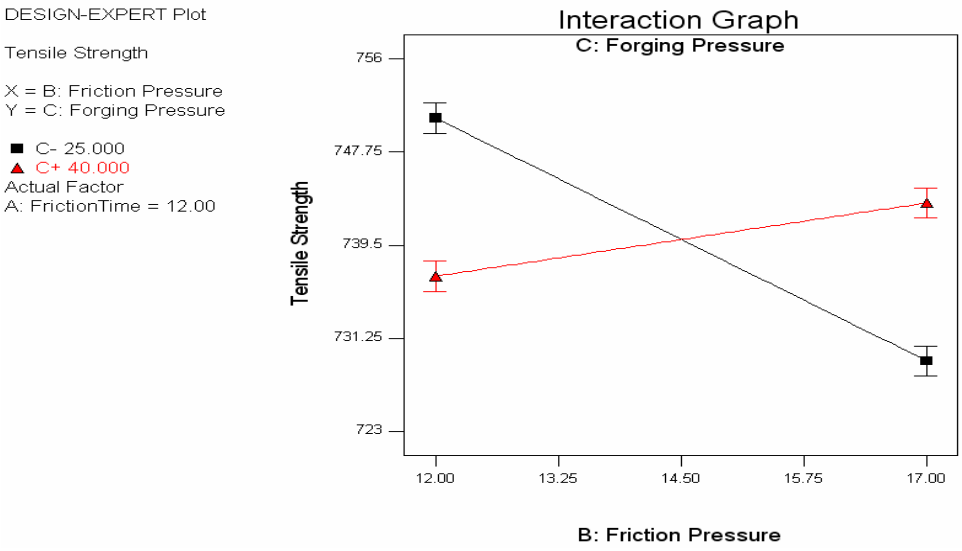

Figure 5.15. Change in tensile strength with friction pressure and forge pressure

Figure 5.15 indicates that BC interaction term leads to decrease in tensile strength where interaction term is self effective at low levels of forge pressure.

Determination of Optimum Welding Conditions: To obtain optimum welding conditions, the mathematical model was built and based on this model and the Solver Editor in the Microsoft Excel was run. The optimum welding conditions are given in Table 5.6.

Table 5.6. Optimized parameters for C group

Material Combination	Friction Time (sec)	Friction Pressure (bar)	Forge Pressure (bar)	Rotational Speed (rpm)
Cast AISI 1050-AISI 304	10	12	25	1500

The optimized parameters of C (investment cast AISI 1050-AISI 304) group are different from those of F (forged AISI 1050-AISI 304) group. Less friction pressure and friction time are needed in the case of C group compared to F group. As it is known friction time and friction pressure are effective parameters especially in the heating phase of process.

5.2. Hardness Test Results and Statistical Approach

The hardness tests across the horizontal plane were conducted. The width of heat affected zone and hardness value at the weld interface can be clearly seen in Figures 5.16-5.23.

5.2.1. Hardness Test Results of F Group

Microhardness Profiles across the Horizontal Plane of F Group: Hardness profiles of each group represent different characteristics based on the different friction welding parameters.

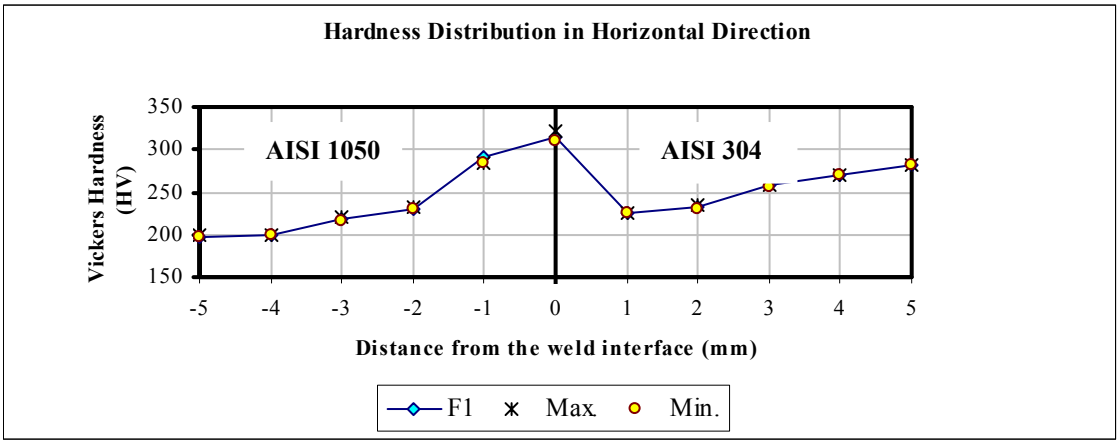

Figure 5.16. Change in hardness at and near the weld interface for F1

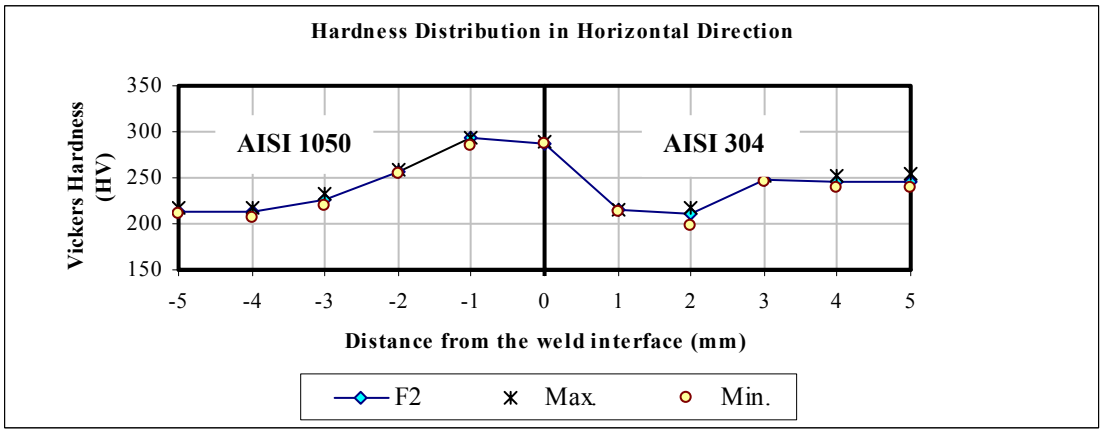

Figure 5.17. Change in hardness at and near the weld interface for F2

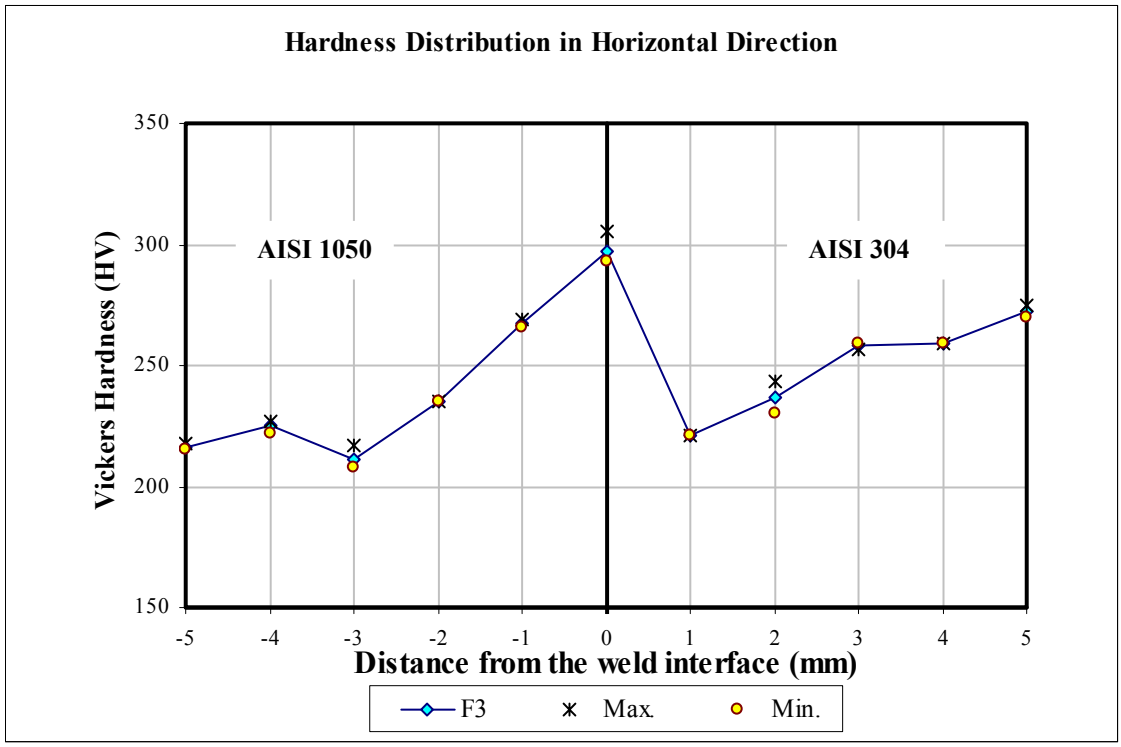

Figure 5.18. Change in hardness at and near the weld interface for F3

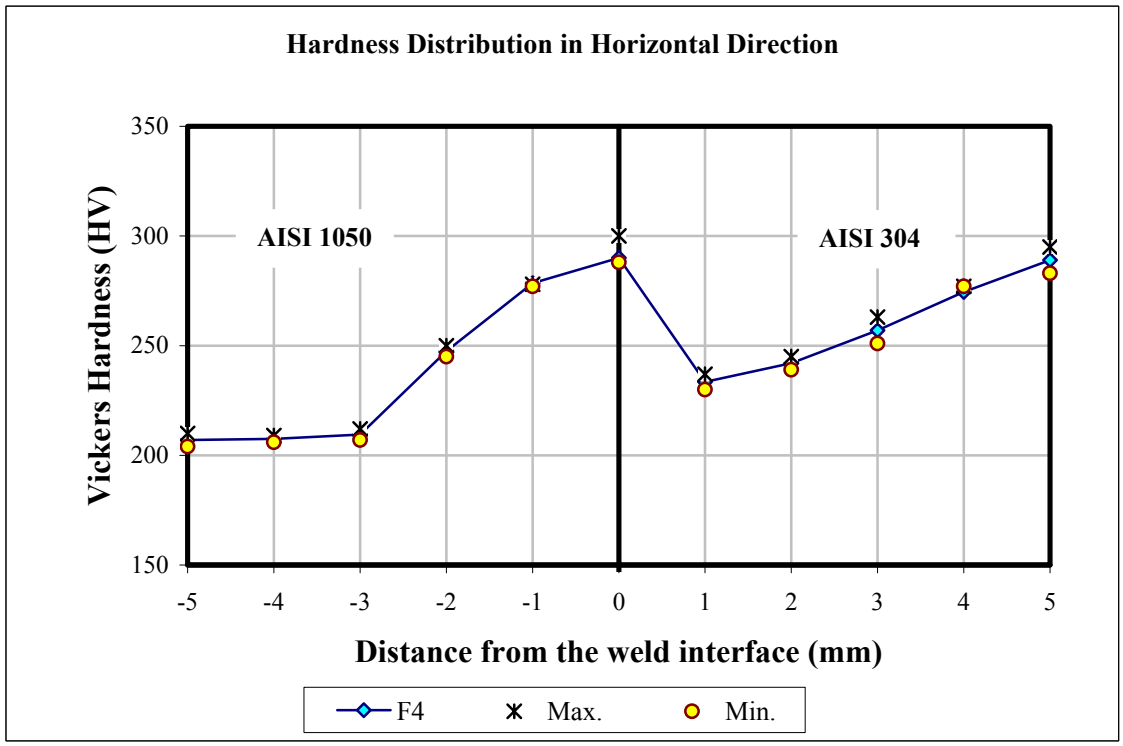

Figure 5.19. Change in hardness at and near the weld interface for F4

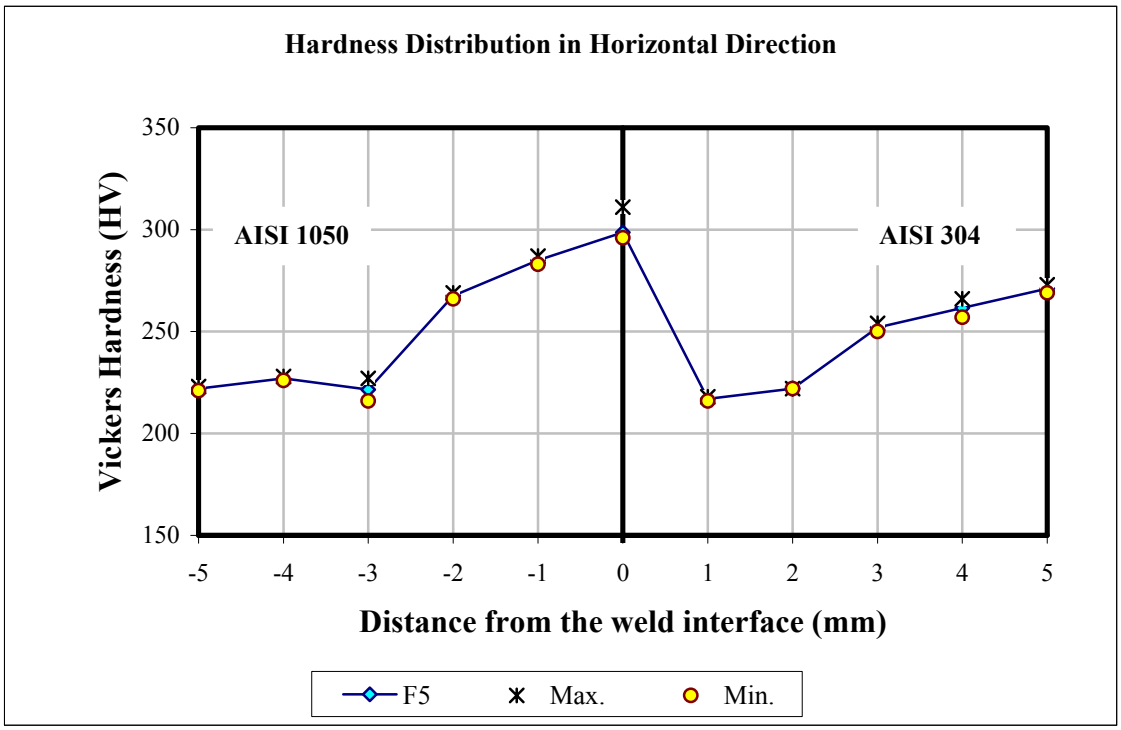

Figure 5.20. Change in hardness at and near the weld interface for F5

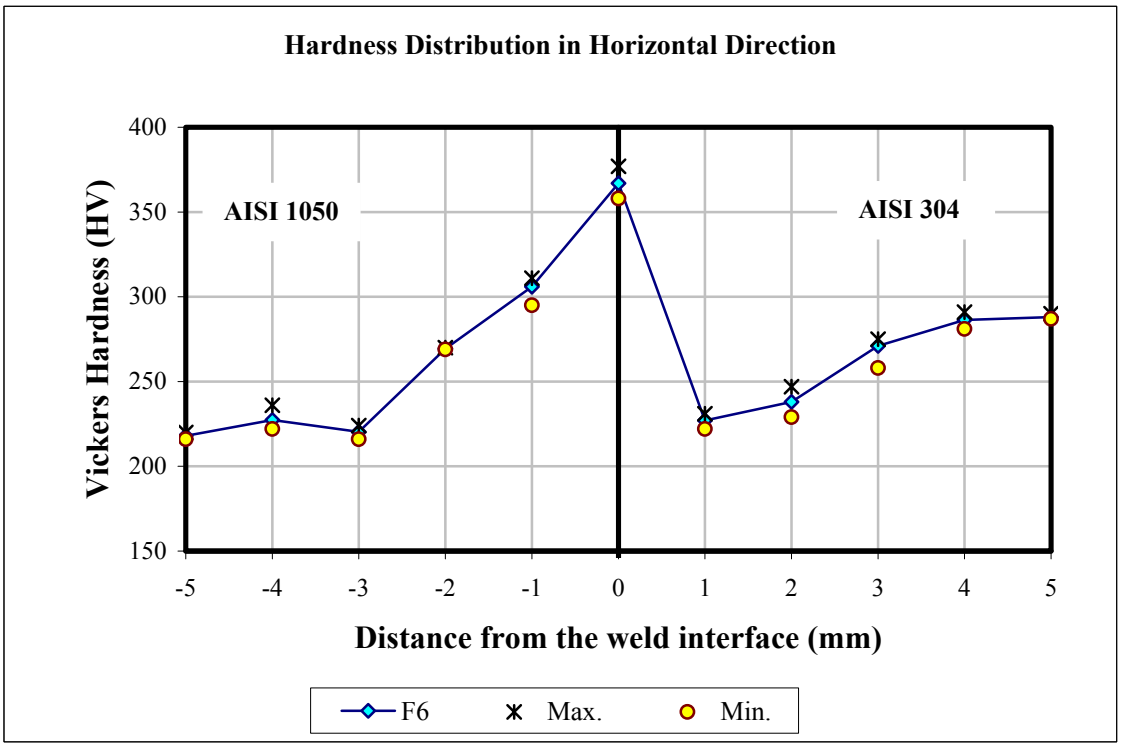

Figure 5.21. Change in hardness at and near the weld interface for F6

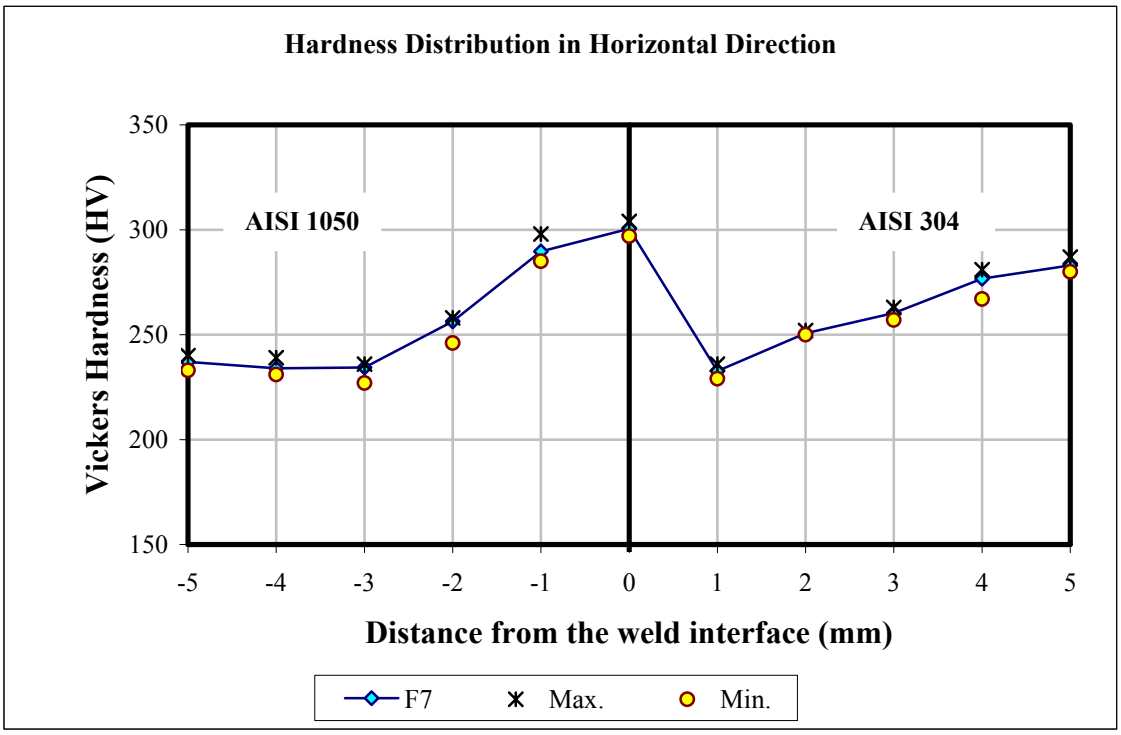

Figure 5.22. Change in hardness at and near the weld interface for F7

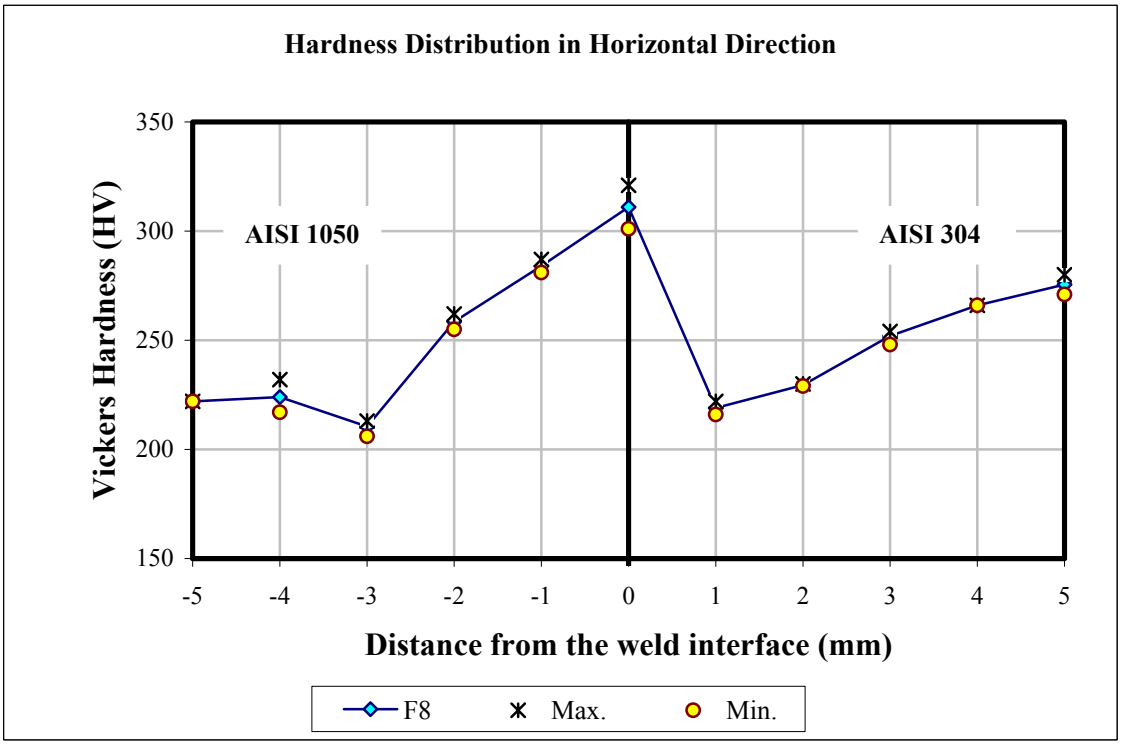

Figure 5.23. Change in hardness at and near the weld interface for F8

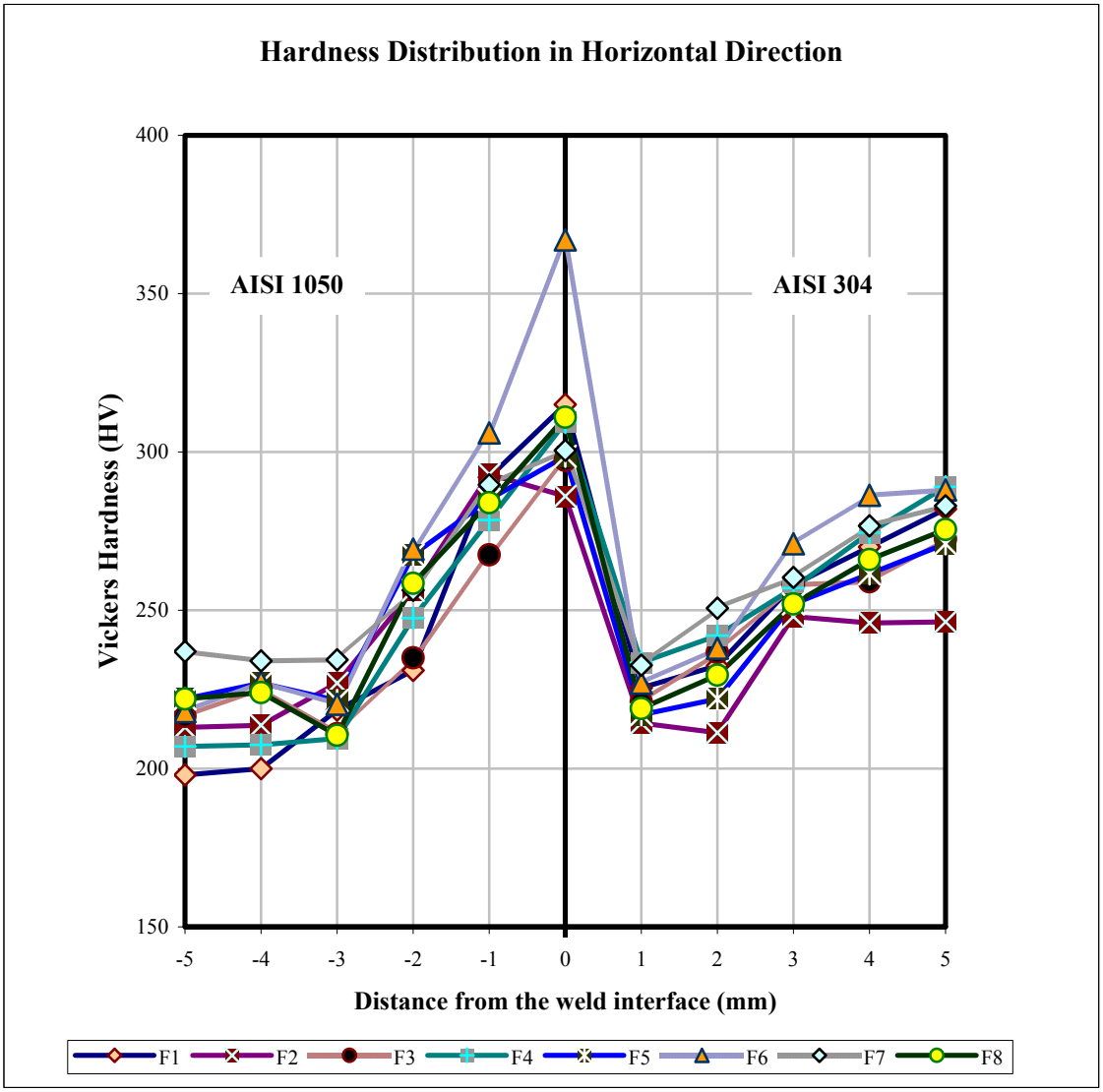

Figure 5.24. Change in hardness at and near the weld interface for F group

The microhardness profiles of F group in general increases from the base metal and reaches a maximum value at the interface. Moreover, the hardness gradient of each group is different in the HAZ of AISI 1050 steel.

Hardness Test Results in Vertical Direction for F Group: Hardness changes in vertical direction with 1,5 mm interval are given in Figures 5.25-5.32. It is understood from this figures that there is an increase in hardness of AISI 1050 steel and almost no change in hardness of AISI 304 steel. Because the heat generation is proportional to interface radius, the higher hardness values were obtained at the outer radius.

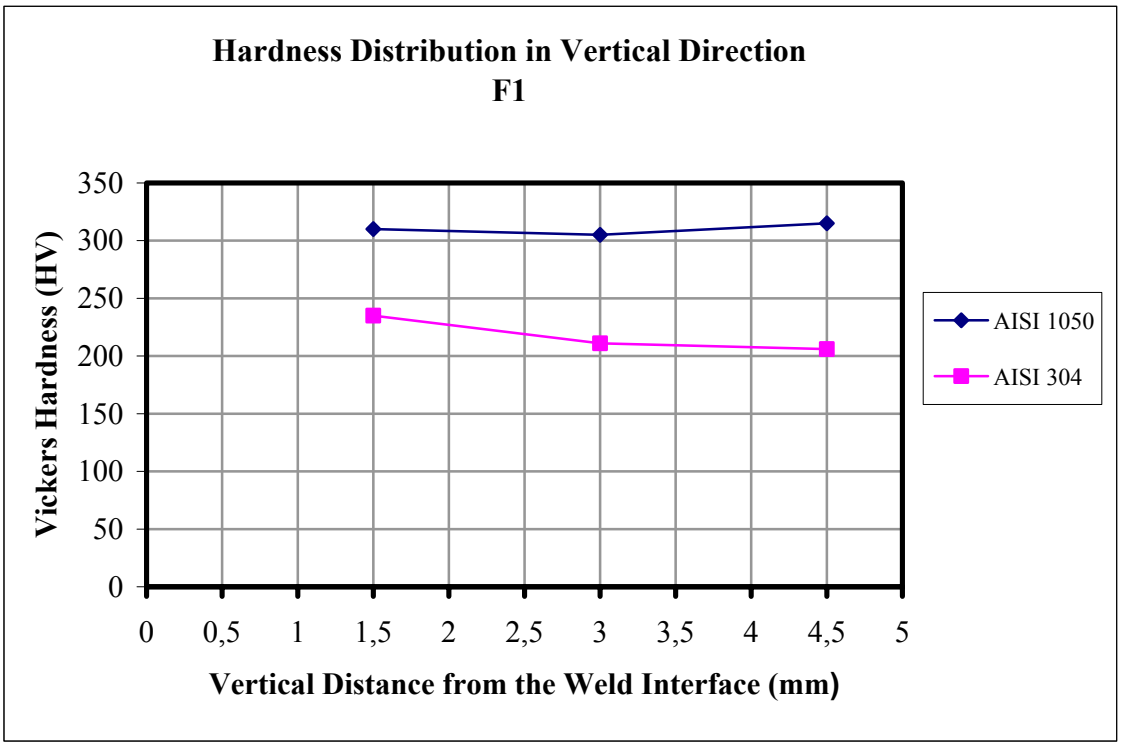

Figure 5.25. Microhardness profile in vertical direction for F1

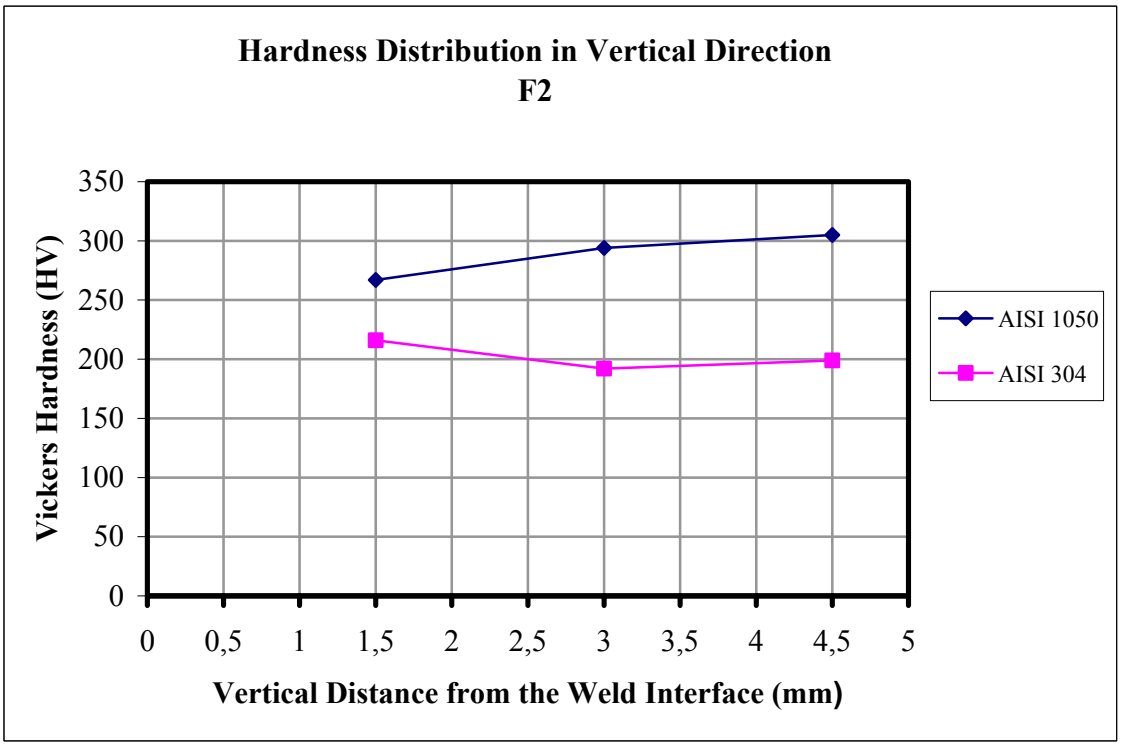

Figure 5.26. Microhardness profile in vertical direction for F2

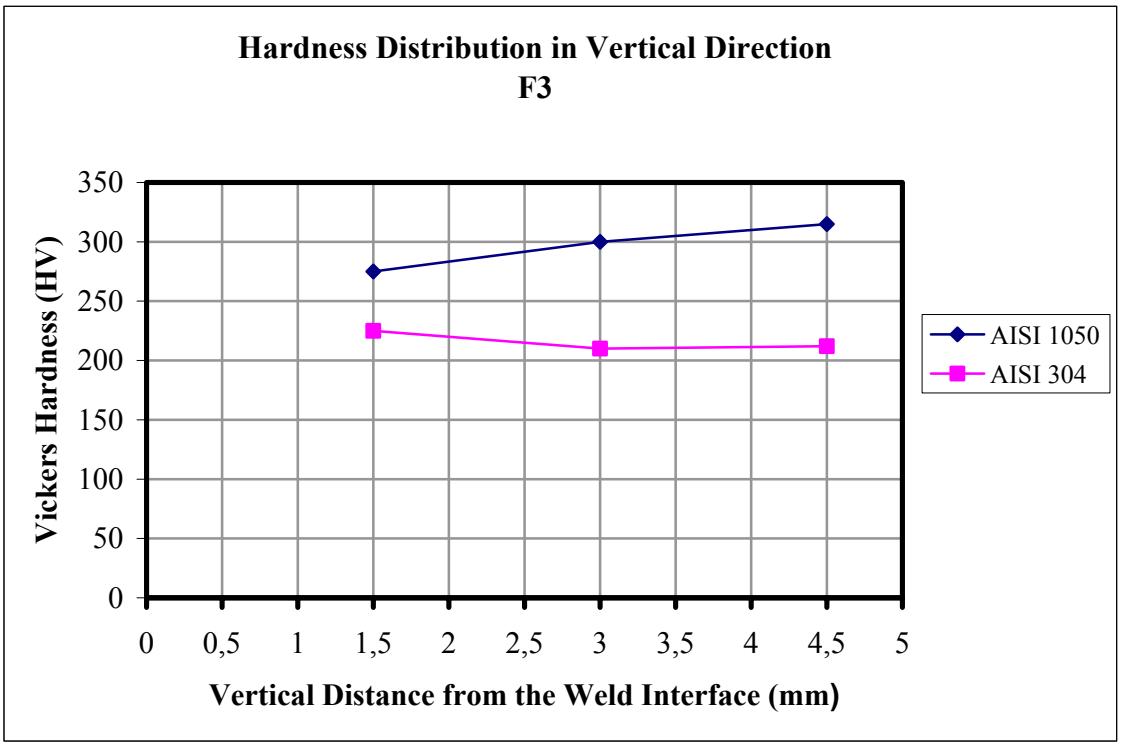

Figure 5.27. Microhardness profile in vertical direction for F3

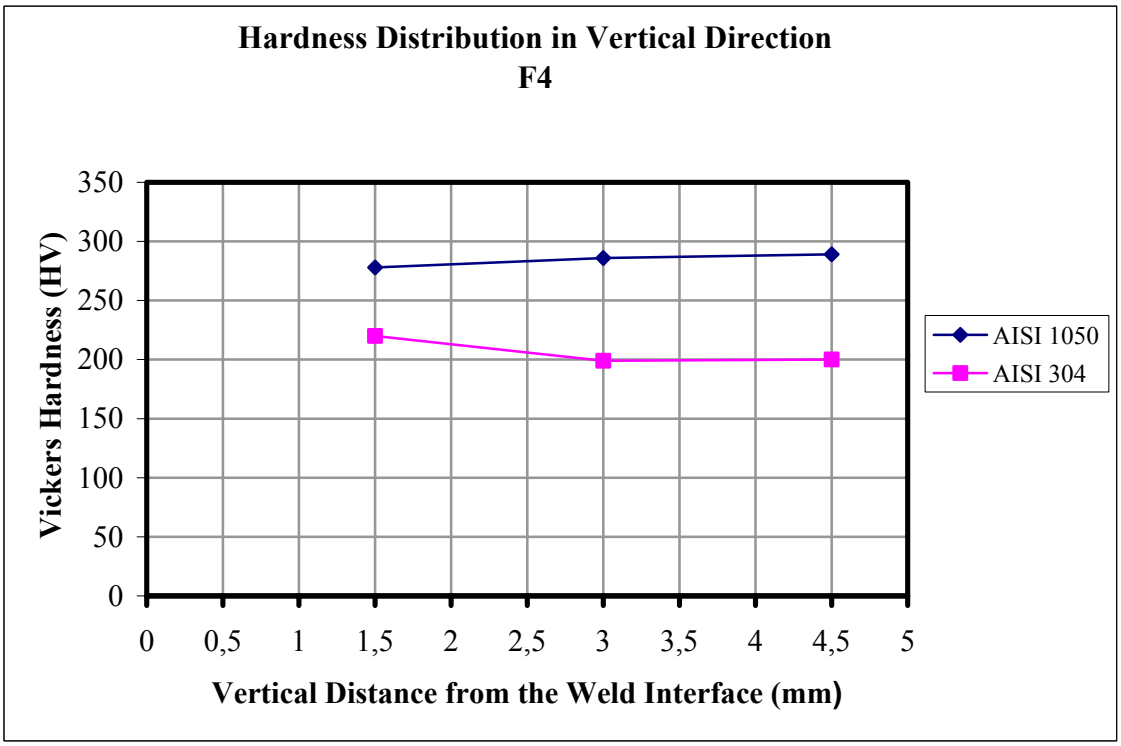

Figure 5.28. Microhardness profile in vertical direction for F4

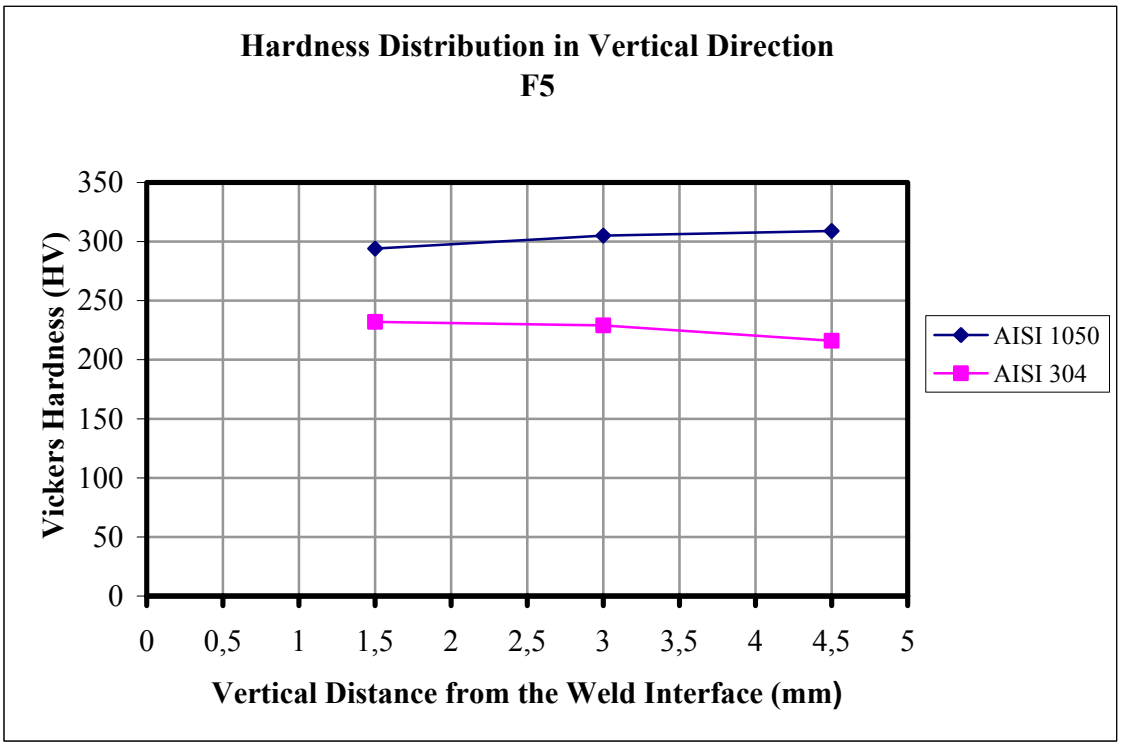

Figure 5.29. Microhardness profile in vertical direction for F5

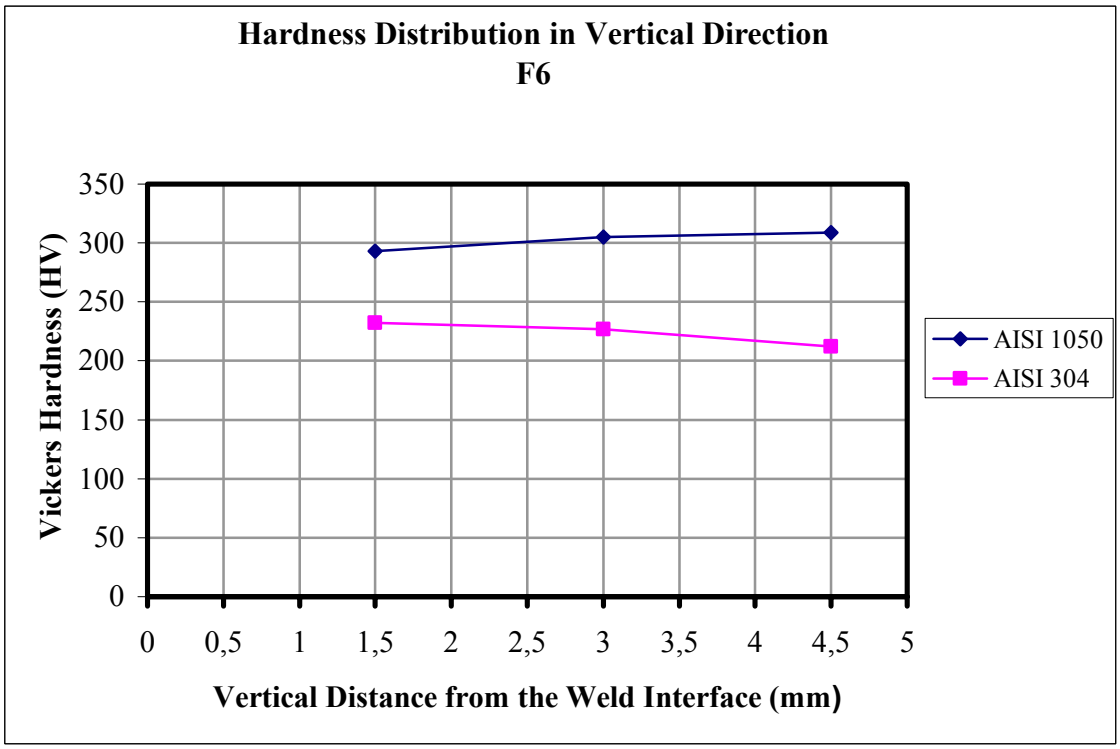

Figure 5.30. Microhardness profile in vertical direction for F6

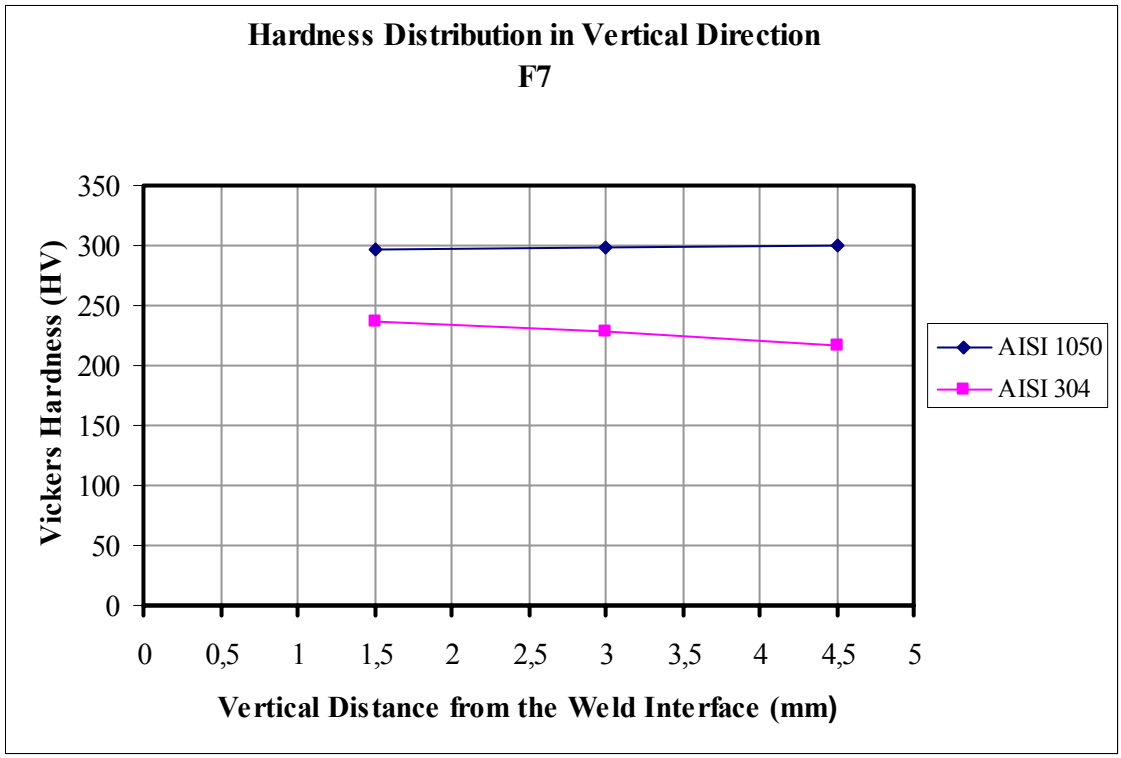

Figure 5.31. Microhardness profile in vertical direction for F7

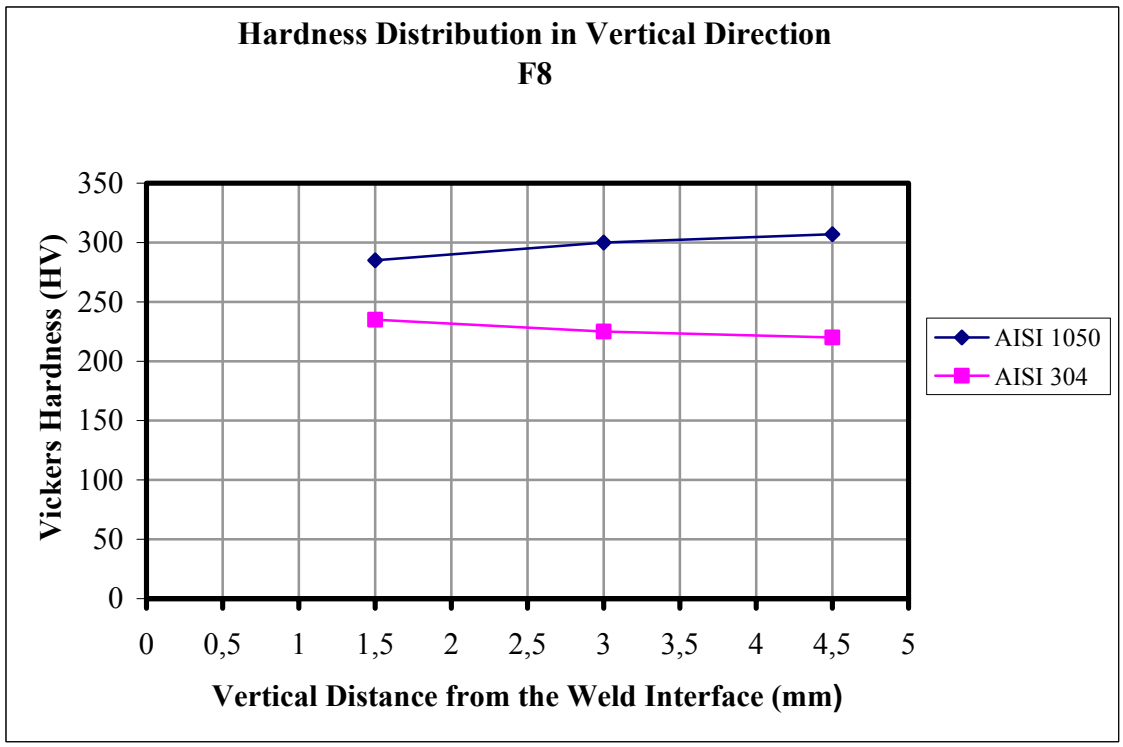

Figure 5.32. Microhardness profile in vertical direction for F8

5.2.2. Hardness Test Results of C Group

Hardness Test Results in Horizontal Direction for C Group: Variations of hardness of C group across the horizontal plane are represented in Figures 5.33-5.41. The hardness of interface is higher than the base because of the reason the distribution and generation of heat is maximum at this location.

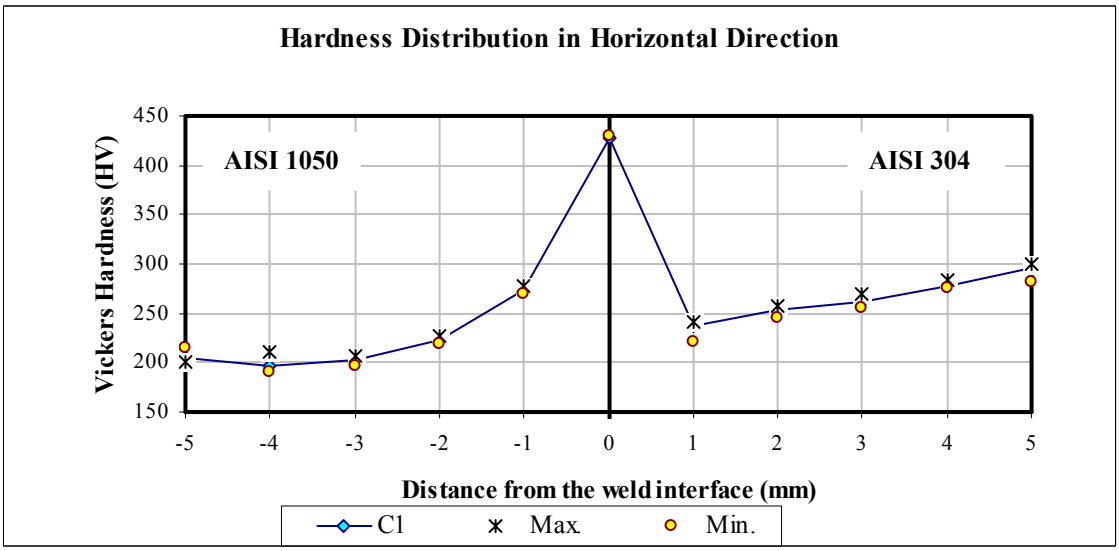

Figure 5.33. Change in hardness at and near the weld interface for C1

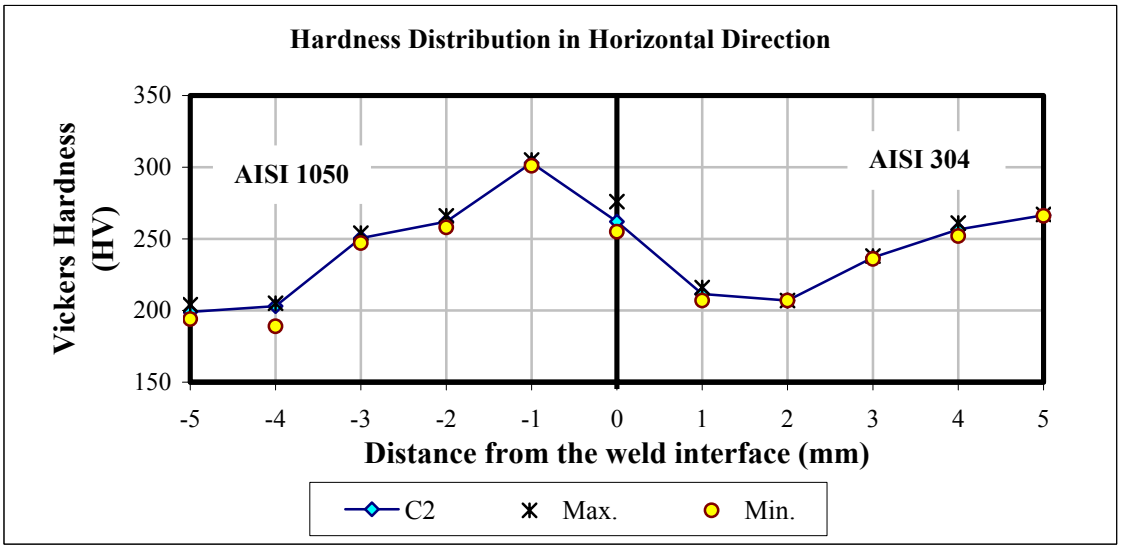

Figure 5.34. Change in hardness at and near the weld interface for C2

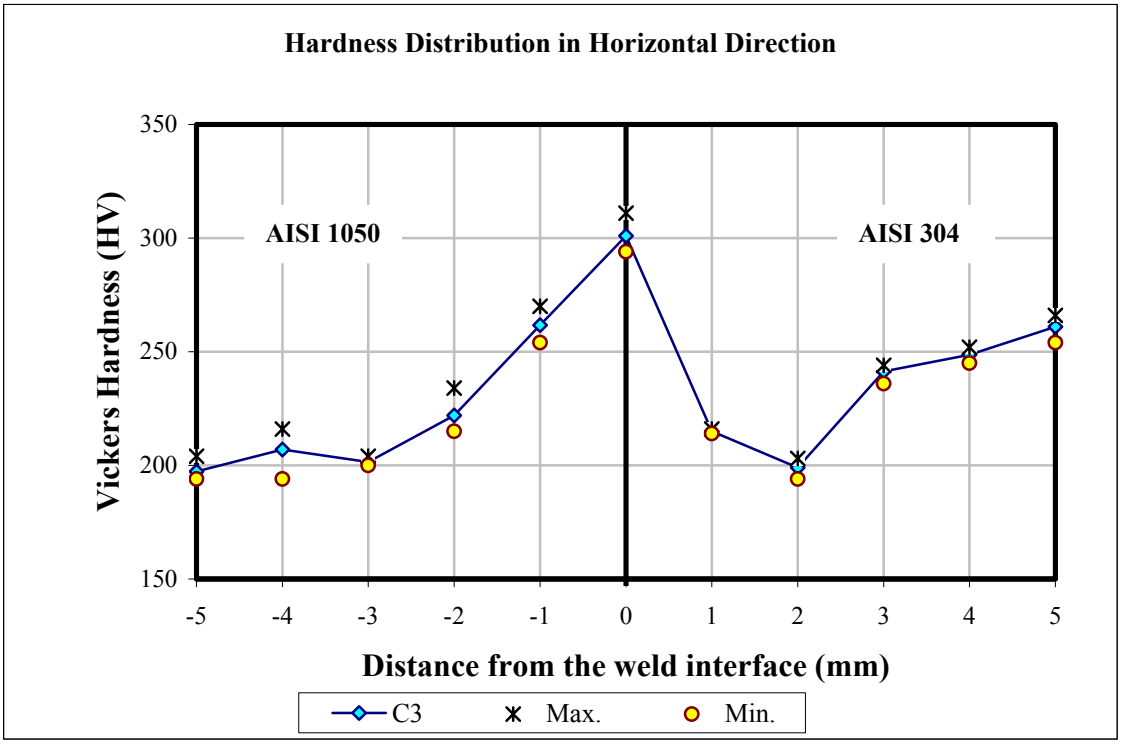

Figure 5.35. Change in hardness at and near the weld interface for C3

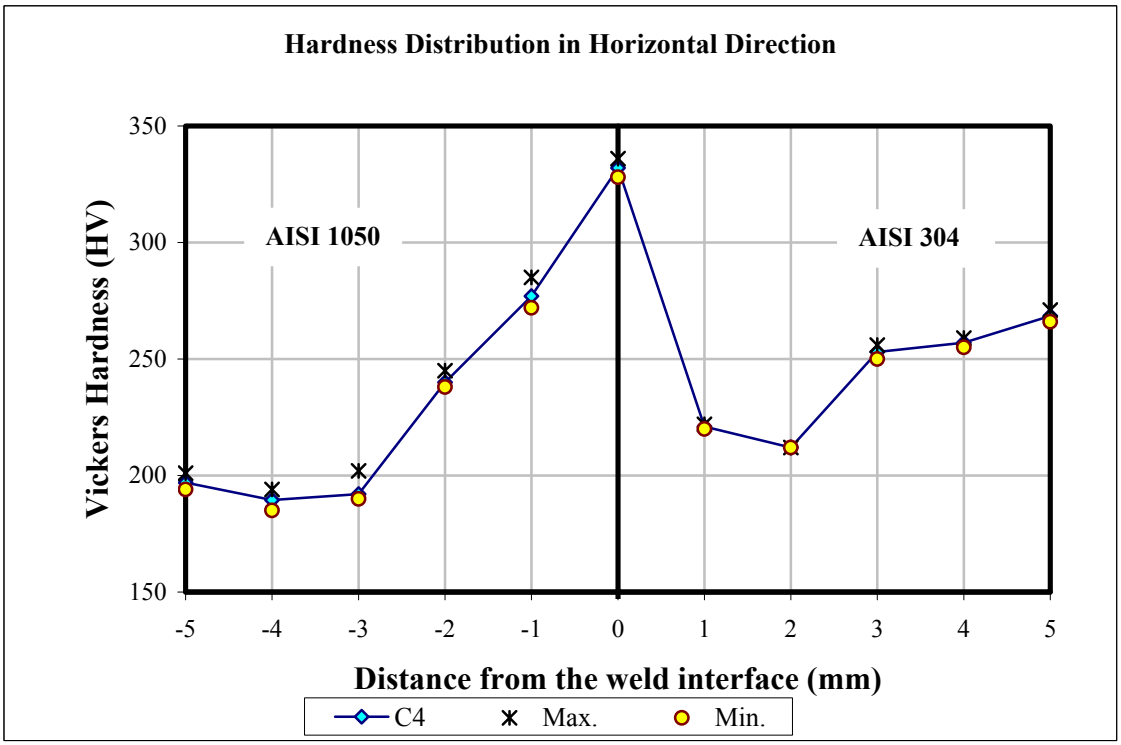

Figure 5.36. Change in hardness at and near the weld interface for C4

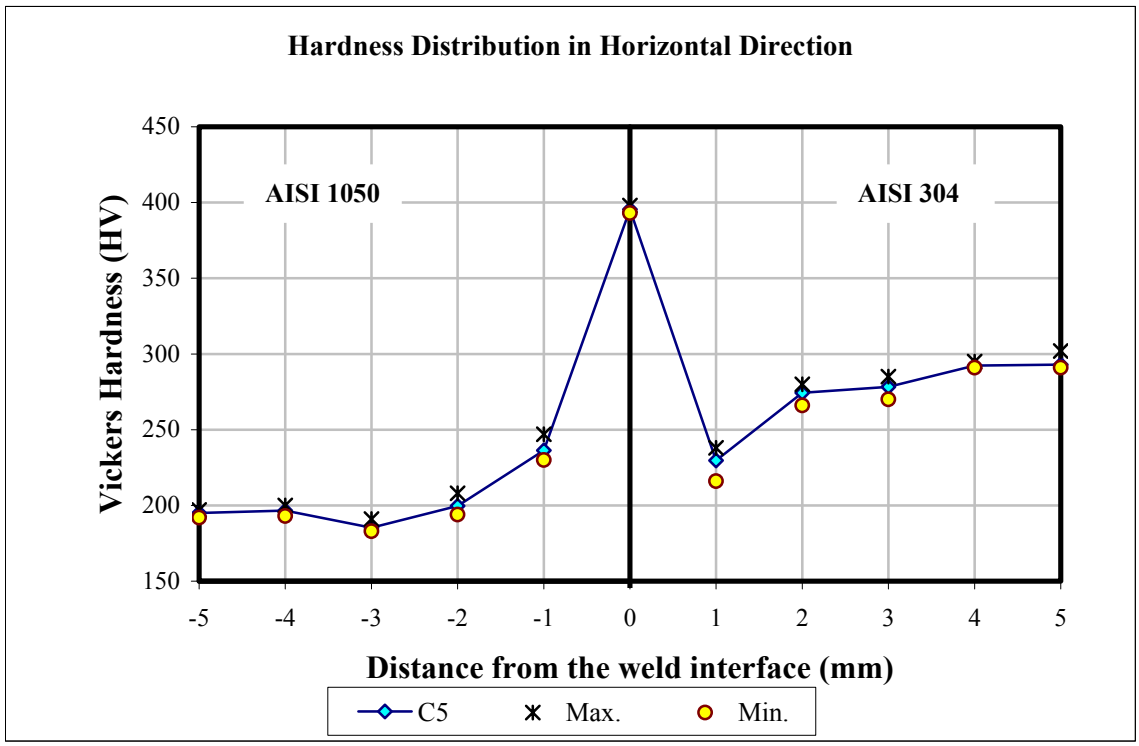

Figure 5.37. Change in hardness at and near the weld interface for C5

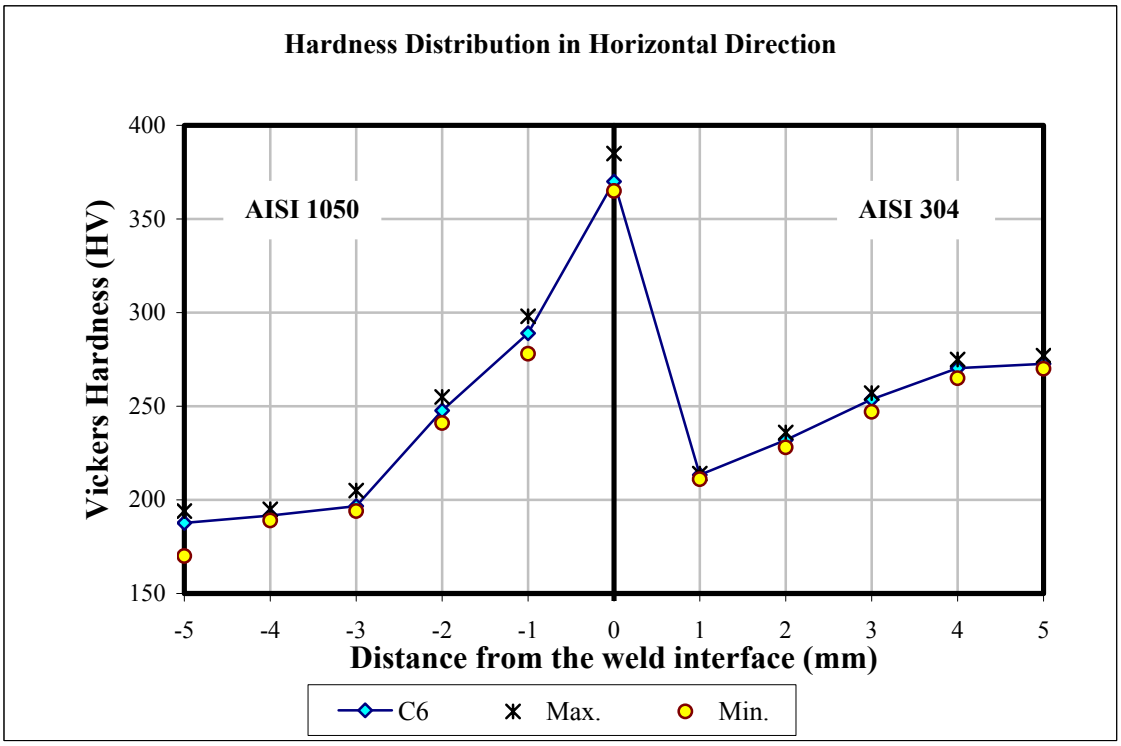

Figure 5.38. Change in hardness at and near the weld interface for C6

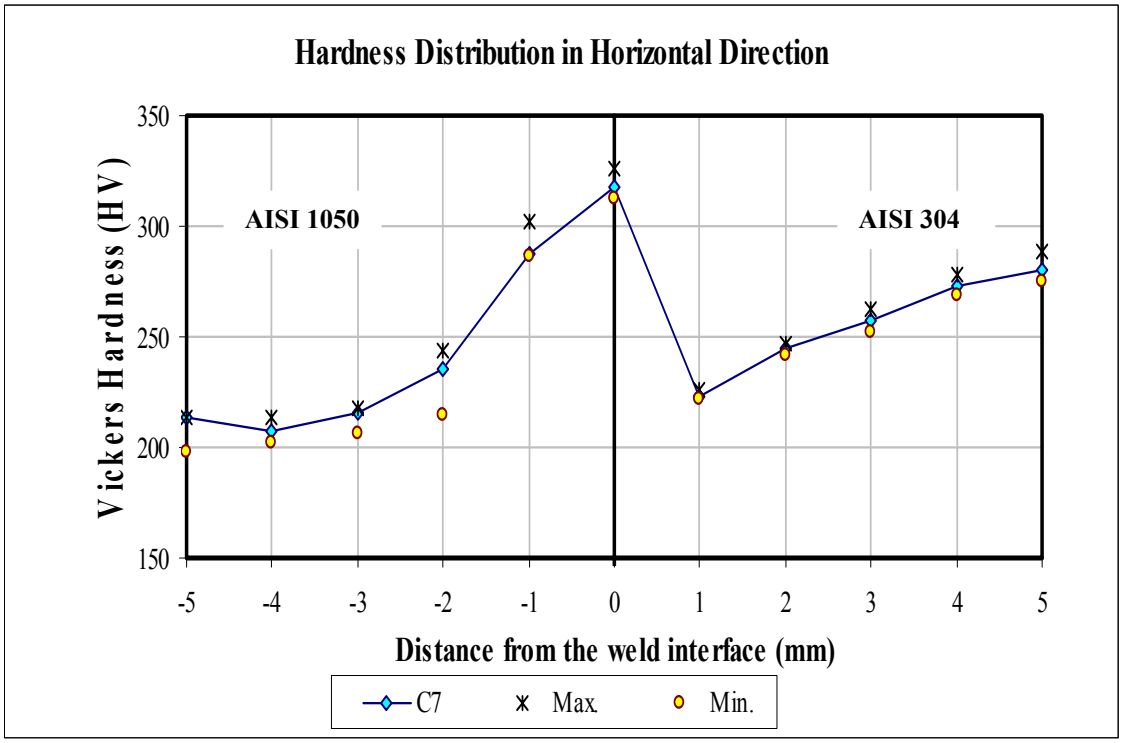

Figure 5.39. Change in hardness at and near the weld interface for C7

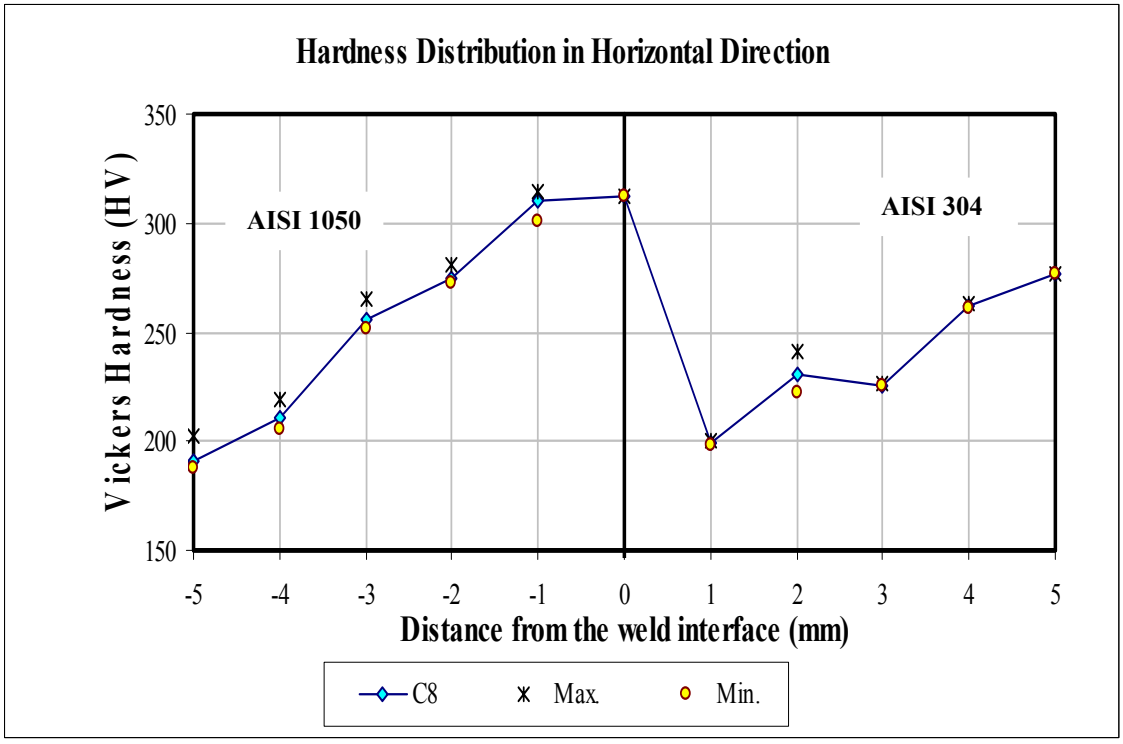

Figure 5.40. Change in hardness at and near the weld interface for C8

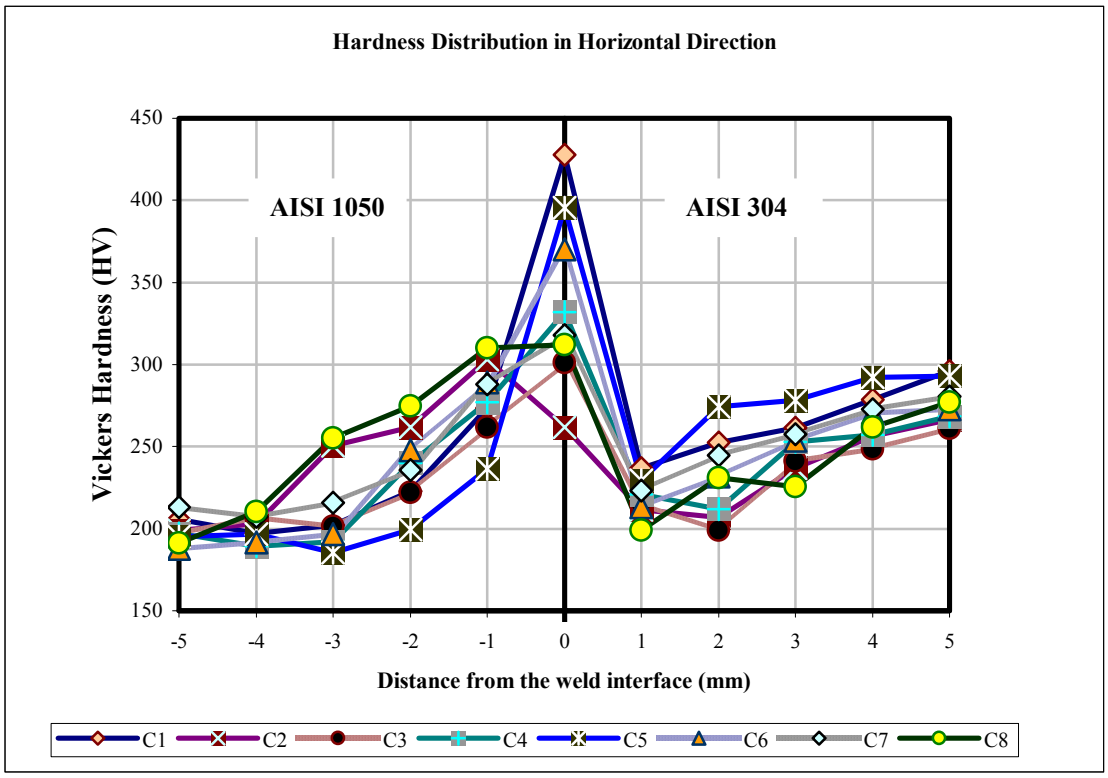

Figure 5.41. Change in hardness at and near the weld interface for C group

Hardness Test Results in Vertical Direction for C Group: The microhardness profile in vertical direction with interval of 1,5 mm are shown in Figures 5.42-5.48.

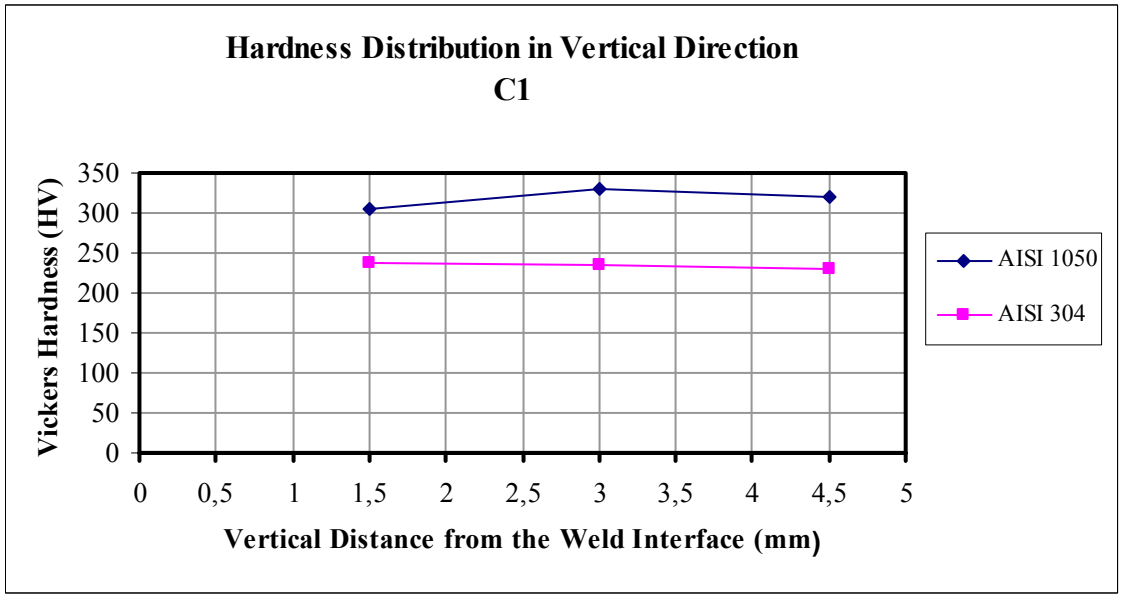

Figure 5.42. Microhardness profile in vertical direction for C1

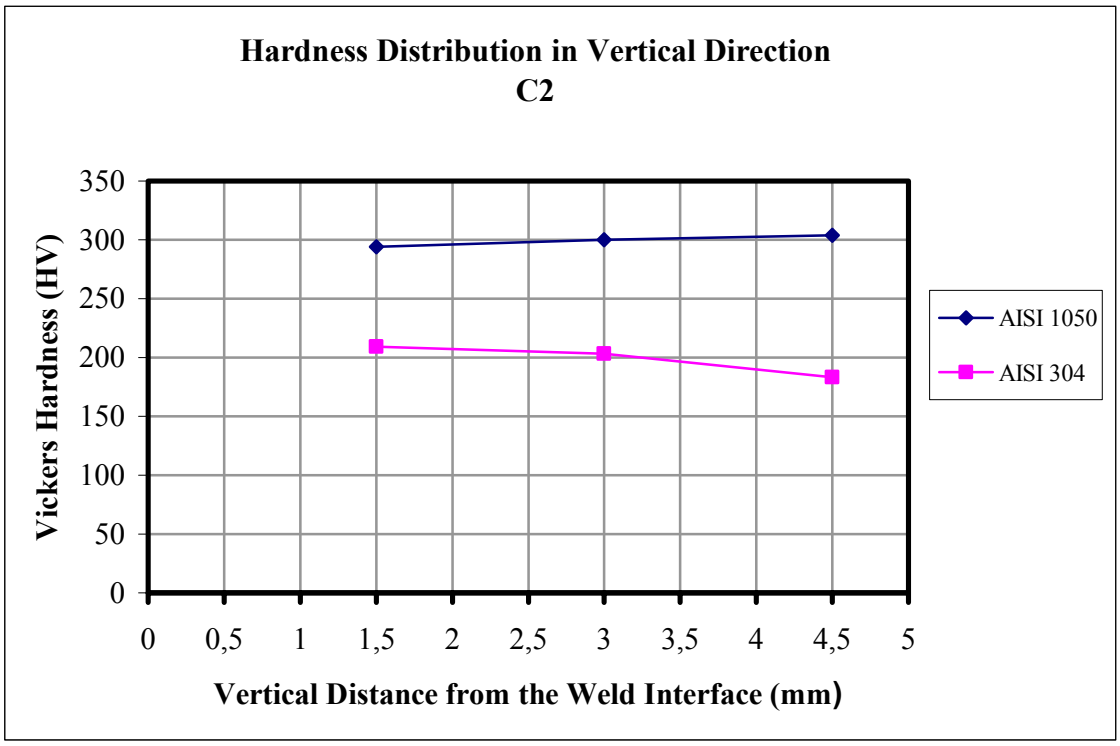

Figure 5.43. Microhardness profile in vertical direction for C2

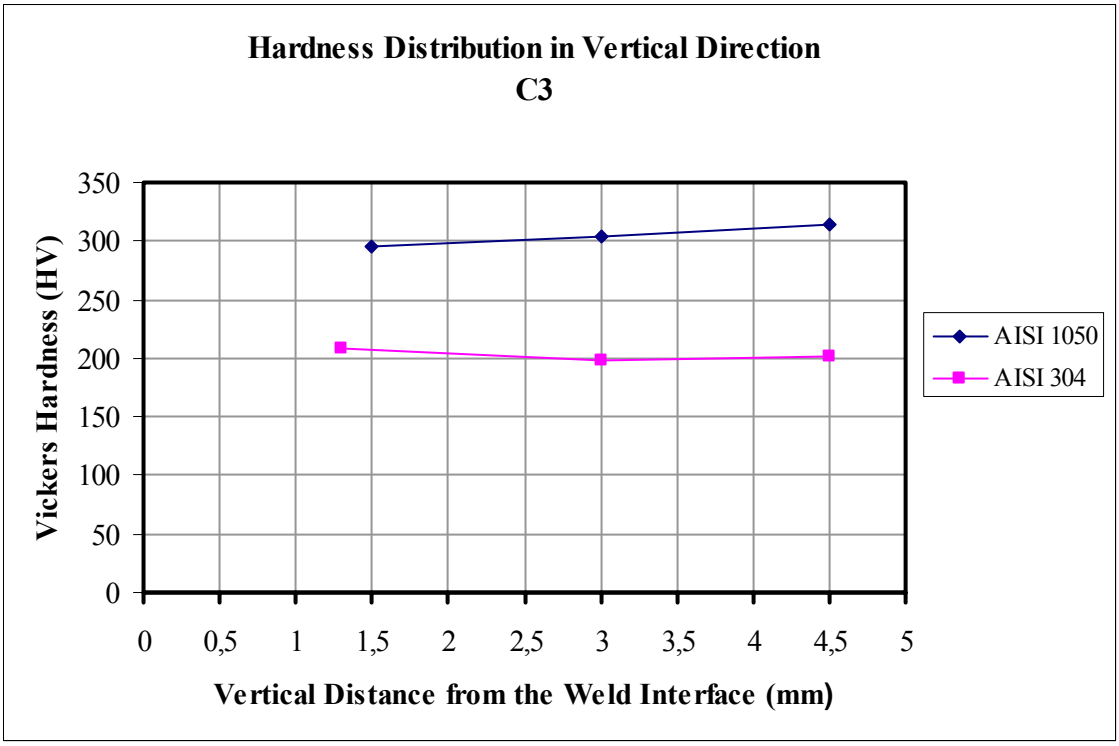

Figure 5.44. Microhardness profile in vertical direction for C3

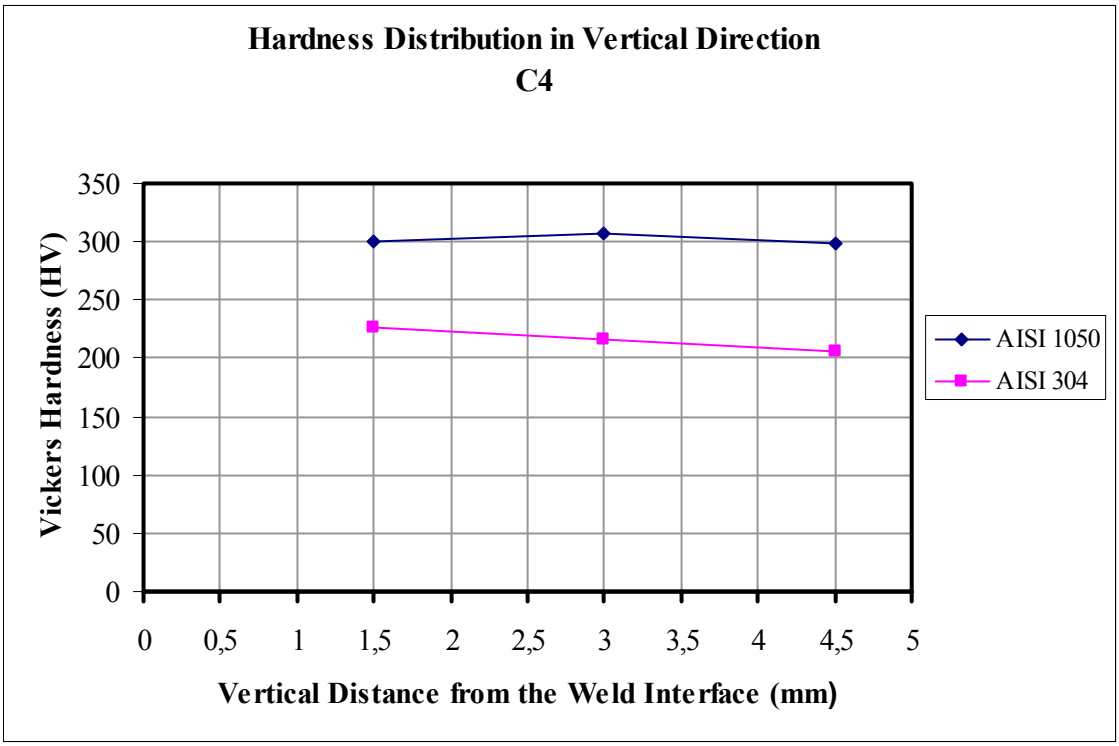

Figure 5.45. Microhardness profile in vertical direction for C4

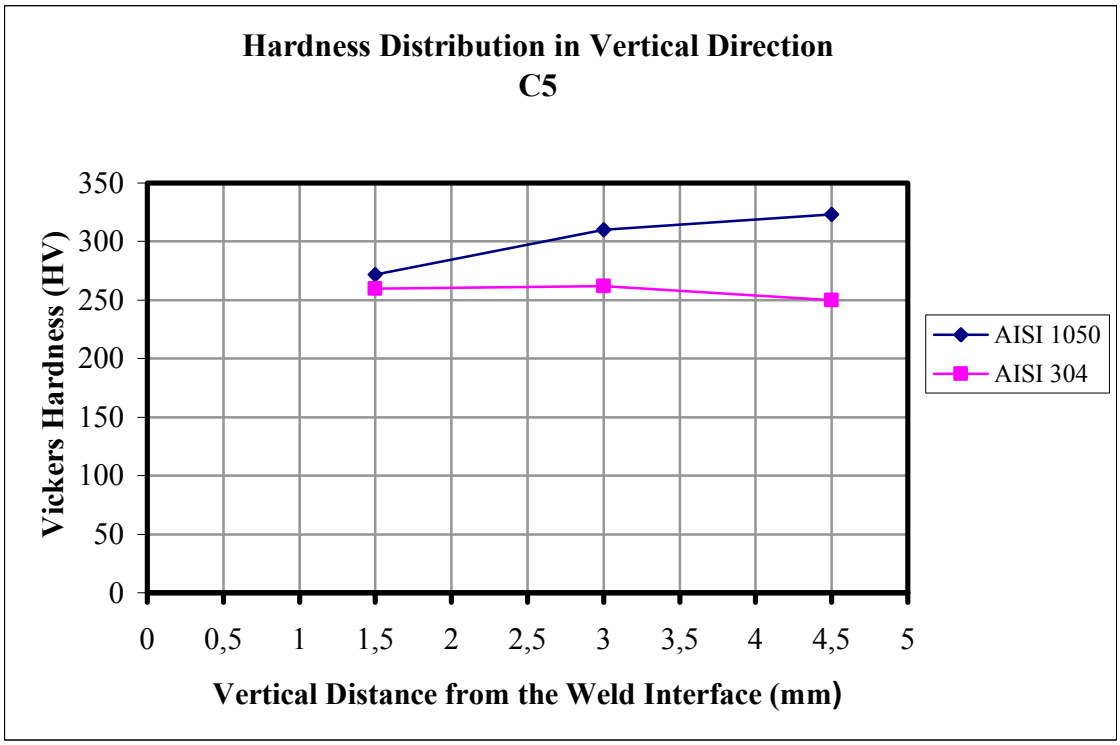

Figure 5.46. Microhardness profile in vertical direction for C5

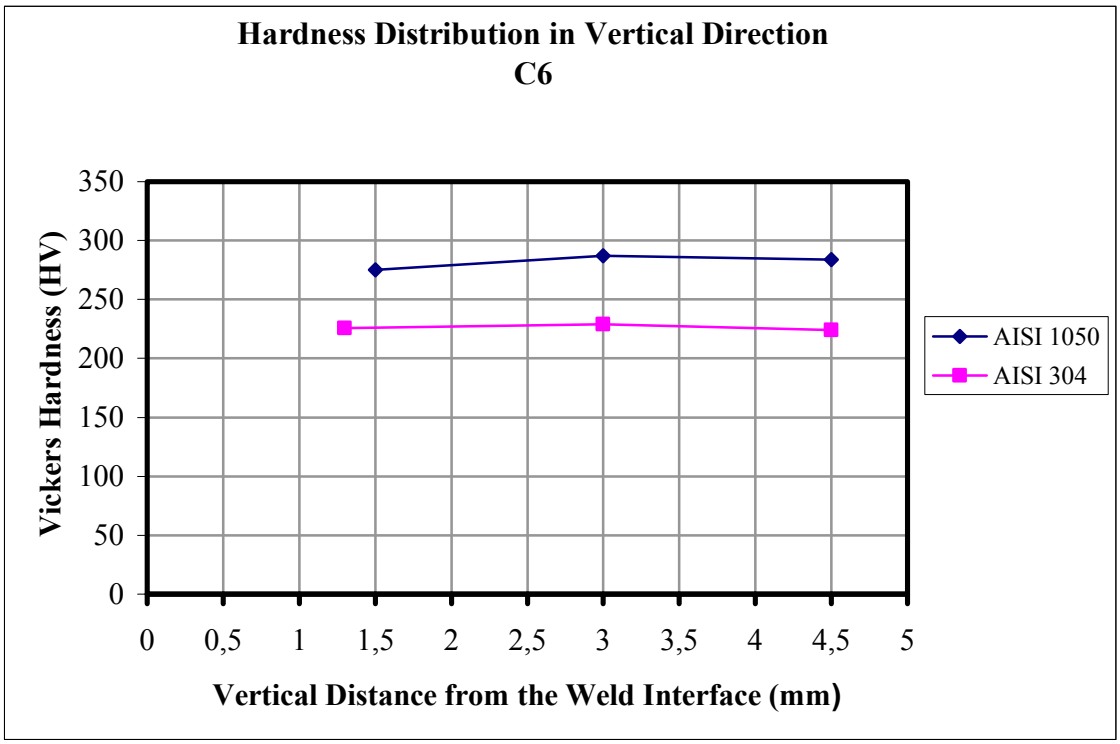

Figure 5.47. Microhardness profile in vertical direction for C6

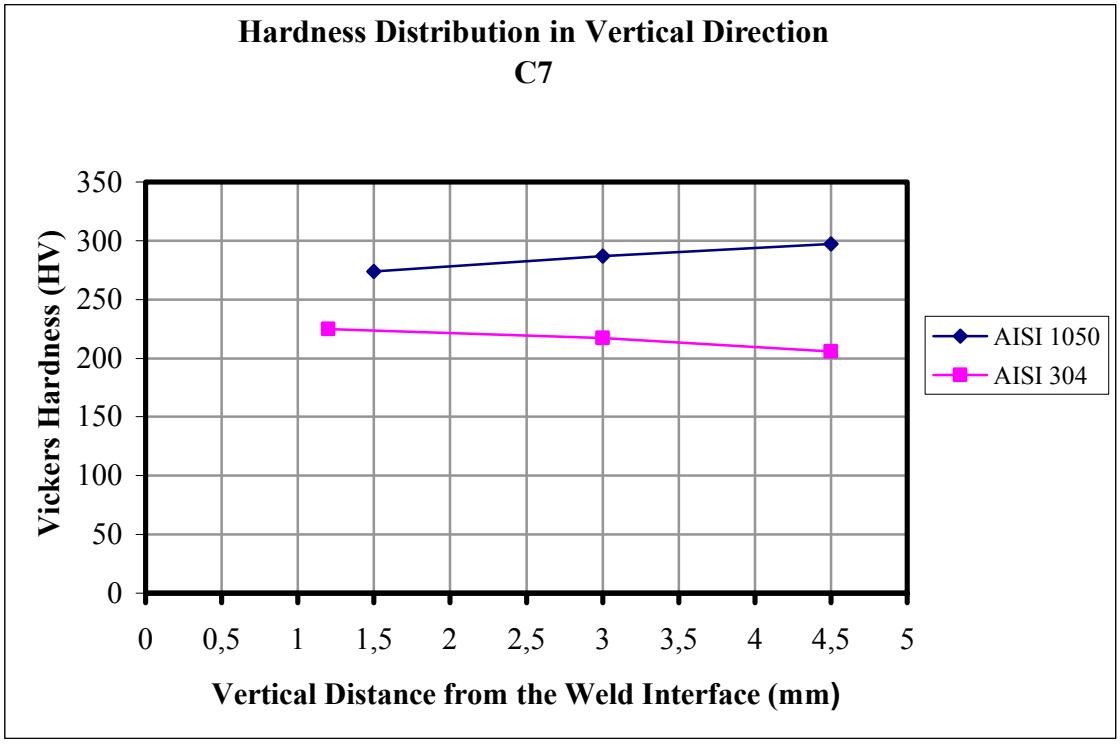

Figure 5.48. Microhardness profile in vertical direction for C7

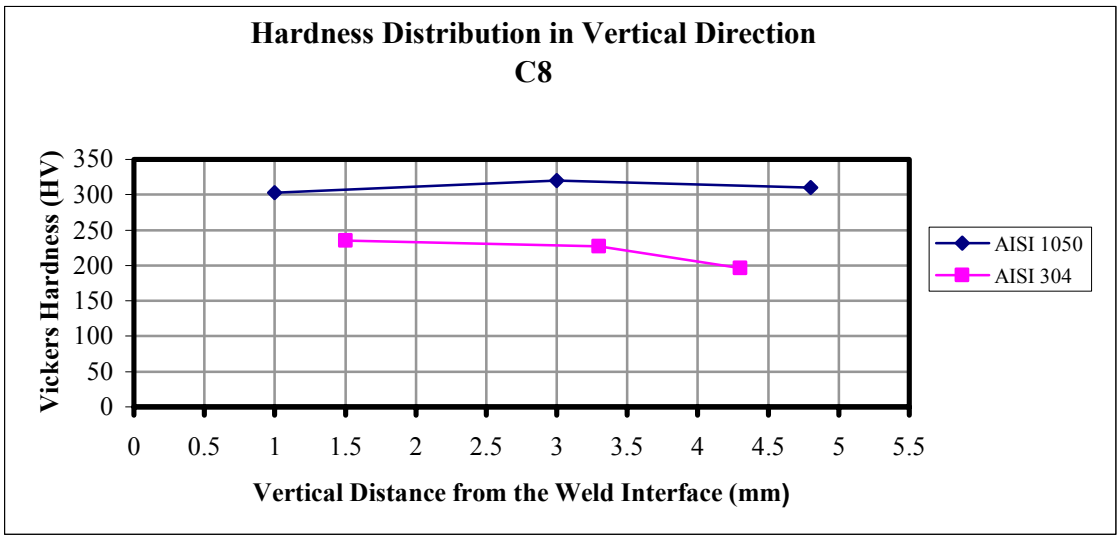

Figure 5.49. Microhardness profile in vertical direction for C8

5.2.3. Effective Process Parameters in Hardness of F Group

The maximum hardness values for the different process parameters are as shown in Table 5.7. If one can obtain 2^3 factorial design for determined maximum hardness values than it becomes easy to get the most interesting factors that affect the hardness.

Table 5.7. Maximum hardness values across the interface of F group

Run	Parameter (A-B-C)	Hardness HV
		Max.
F1	10-12-40	315
F2	14-17-25	286
F3	14-17-40	297
F4	14-12-40	290
F5	10-17-25	298
F6	10-12-25	367
F7	10-17-40	300
F8	14-12-25	311

Table 5.8. ANOVA table for microhardness for F group

Source	Sum of Squares	Mean Value	F Value	Prob > F
Model	39120	980	4,22	0,11
A	1156	1156	4,97	0,11
B	1279	1279	5,50	0,1
AB	542	542	2,33	0,22
BC	943	943	4,05	0,13
Residual	697	232		
Cor Total	4617			

Std. Dev.	15	R-Squared	0,84
Mean	308	Adj R-Squared	0,64
C.V.	5	Pred R-Squared	0,07
PRESS	4959	Adeq Precision	5,89

Table 5.8 shows that this model can fail with 11% probability. Factor AB and factor BC is significant at 22% and 13% level respectively. R-Squared value shows that the model accounts for 85% of the variability in the model

Half Normal Plot for Significance of Parameters: If a straight line is drawn through the origin, it is indicated in Figure 5.50 that AB, BC, A and B are the most important factors amongst others.

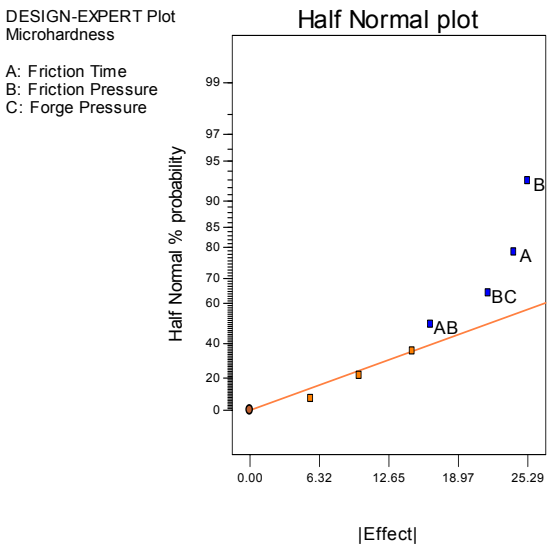

Figure 5.50. Half normal plot of microhardness of F group

Final Equation in Terms of Coded Factors: Half normal plot shows the most interesting factors that affect the response. The next step in determining the significant parameters is to obtain the mathematical equation which has been calculated by least squares method. The final equation in terms of coded factors is in Equation 5.3.

$$H.V. = 308.1 - 12.02A - 12.65B + 8.23AB + 10.85BC \qquad (5.3)$$

From the above equation it seems that factor A and factor B has negative effect on hardness however the interaction term AB and the interaction term BC has positive effect. Various plots must be investigated to see if any of the assumption are violated.

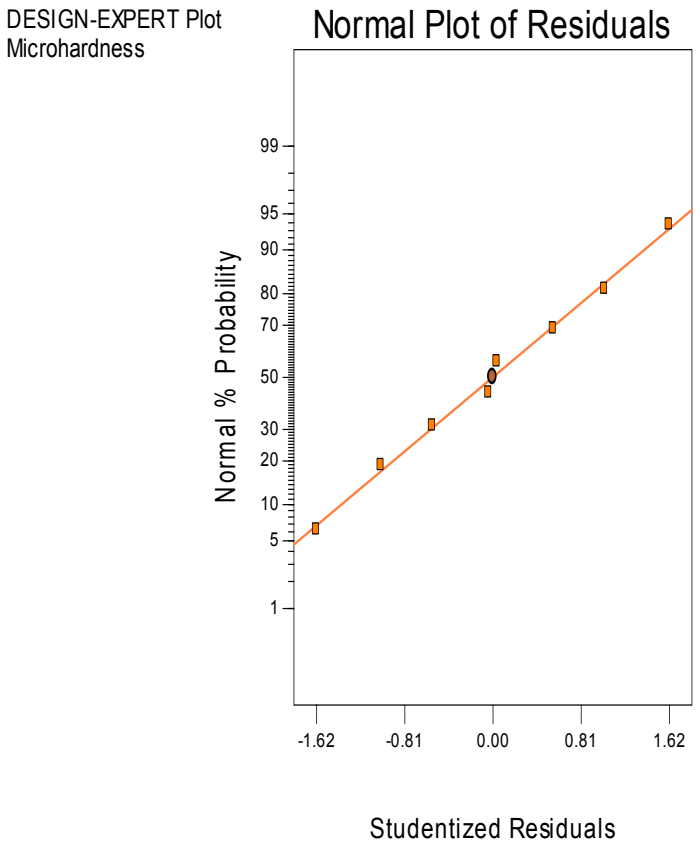

Figure 5.51. Normal plot of residuals

In Figure 5.51 residual plot doesn't display abnormality and evidence exhibiting the possible outliers. This proves that the ANOVA table assumption is right.

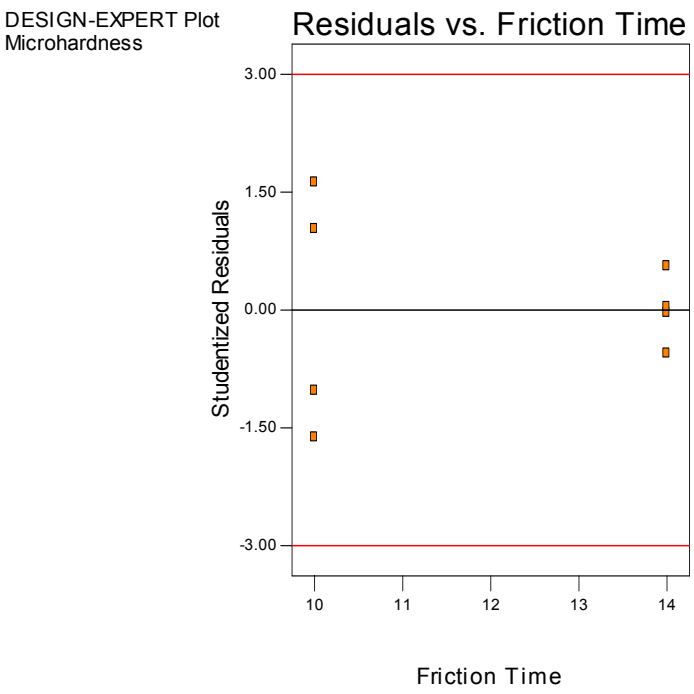

Figure 5.52. Residuals and friction time plot

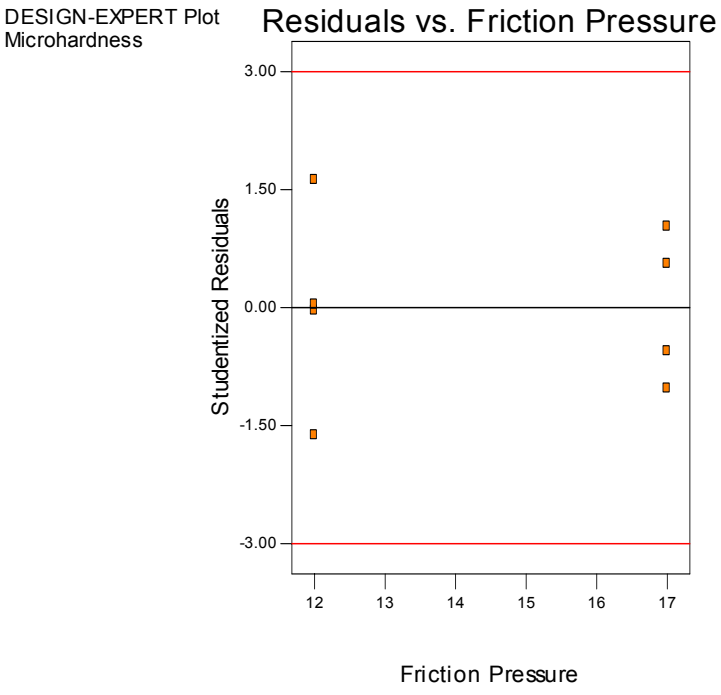

Figure 5.53. Residuals and friction pressure plot

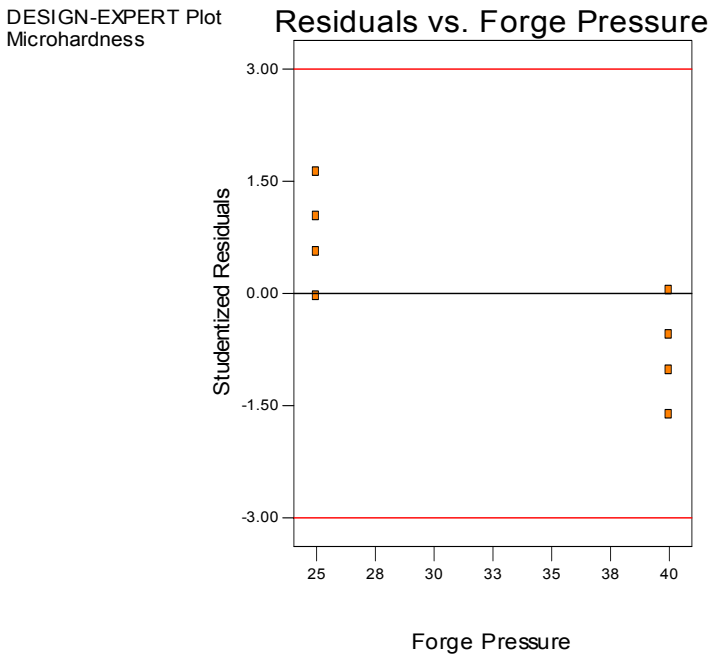

Figure 5.54. Residuals and forge pressure plot

Figure 552-5.54 show that constant variance assumption is not violated

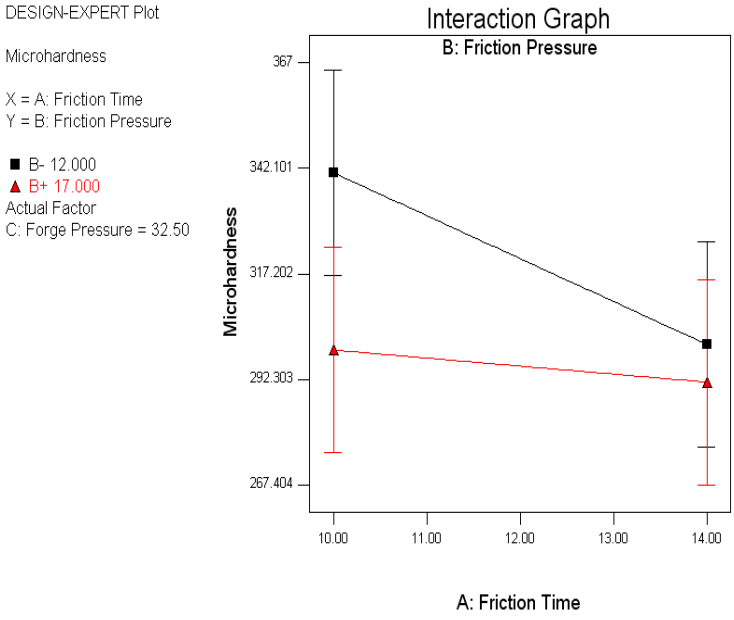

Figure 5.55. Change in hardness with friction pressure and friction time

Figure 5.55 indicates that AB interaction term leads to decrease in tensile strength where interaction term is self effective at low levels of friction pressure.

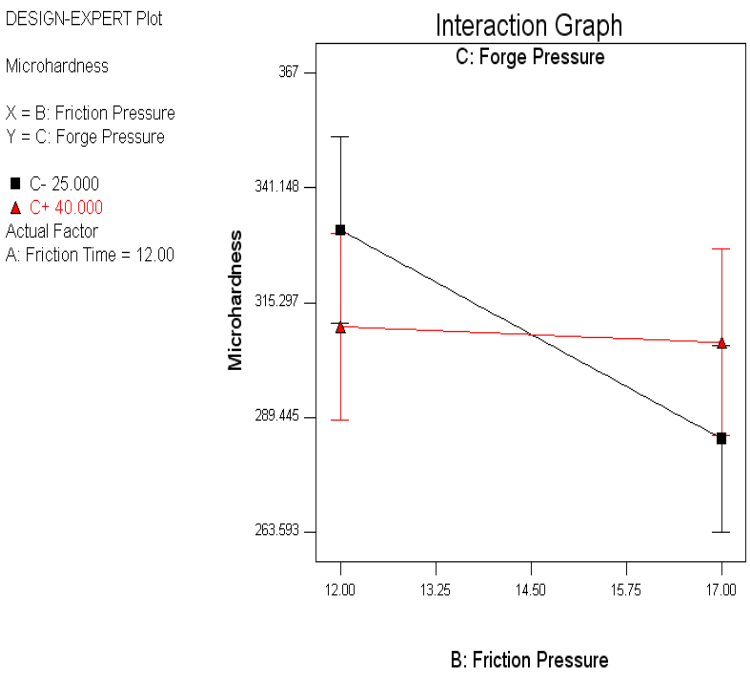

Figure 5.56. Change in hardness with friction pressure and forge pressure

Figure 5.56 indicates that BC interaction term leads to decrease in tensile strength where interaction term is self effective at low levels of forge pressure. However this decrease in tensile strength is less at high levels of forge pressure.

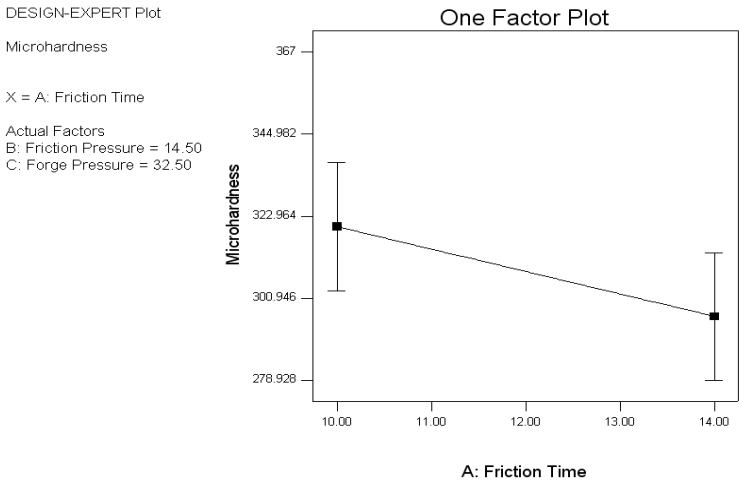

Figure 5.57. Change in hardness with friction time

Figure 5.57 shows that an increase in friction time leads to decrease in tensile strength.

5.2.4. Effective Process Parameters in Hardness of C Group

The determination of process parameters that affect hardness is based on the results shown in Table 5.9.

Table 5.9. Maximum hardness values across the interface of C group

Run	Parameter (A-B-C)	Hardness HV
		Max.
C1	10-12-40	413
C2	14-17-25	262
C3	14-17-40	301
C4	14-12-40	332
C5	10-17-25	395
C6	10-12-25	370
C7	10-17-40	318
C8	14-12-25	312

If 2^3 factorial design is performed for the C group then one can have the results as Table 5.10.

Table 5.10. ANOVA table for microhardness of C group

Source	Sum of Squares	Mean Value	F Value	Prob > F
Model	18074	3615	4,22	0,012
A	10422	10422	4,97	0,004
B	2859	2856	5,50	0,015
AC	1087	1087	2,33	0,039
BC	1281	1282	4,05	0,033
ABC	2424	2424	53,26	0,018
Residual	91			
Cor Total	18164			

Std. Dev.	6,75	R-Squared	0,99
Mean	338	Adj R-Squared	0,98
C.V.	2	Pred R-Squared	0,91
PRESS	1456	Adeq Precision	24,5

It is evidence from the Table 5.10 that this model is important and there is only 1,2% probability that this model can fail.

Half Normal Plot for Significance of Parameters: In general half normal plot displays the most important factors which are directly related to process parameters. If a straight line can be drawn from the origin it is obvious in Figure 5.58 that AC, BC, ABC, B, A are the outliers and also the important factors.

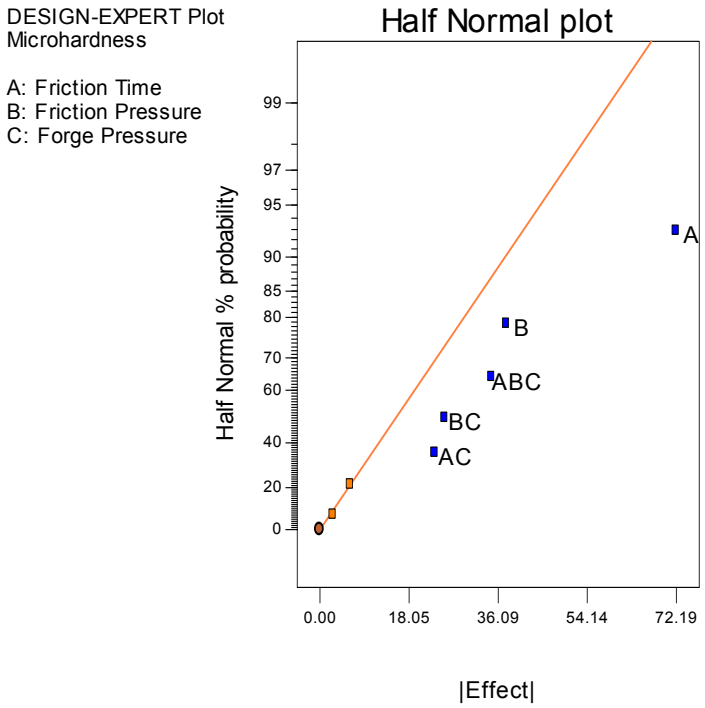

Figure 5.58. Half normal plot for microhardness of C group

Final Equation in Terms of Coded Factors: After determining the significance of factors it is now time to find the final equation which emphasizes the general behavior of hardness values for C group. At the end of least squares method the following equation is obtained.

$$H.V. = 337.84 - 36.09A - 18.91B + 11.66AC - 12.66BC + 17.41ABC \qquad (5.4)$$

From Equation 5.4 it is true that A and B has negative effect on the hardness. Various plots must be displayed to see if any of the assumption is violated.

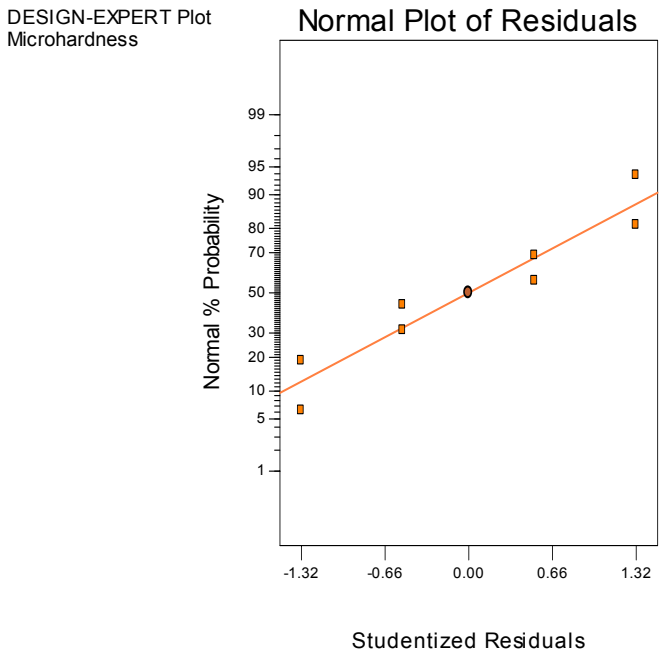

Figure 5.59. Normal plot of residuals graph

Figure 5.59 doesn't display of abnormality which can be generally showing the possible outliers.

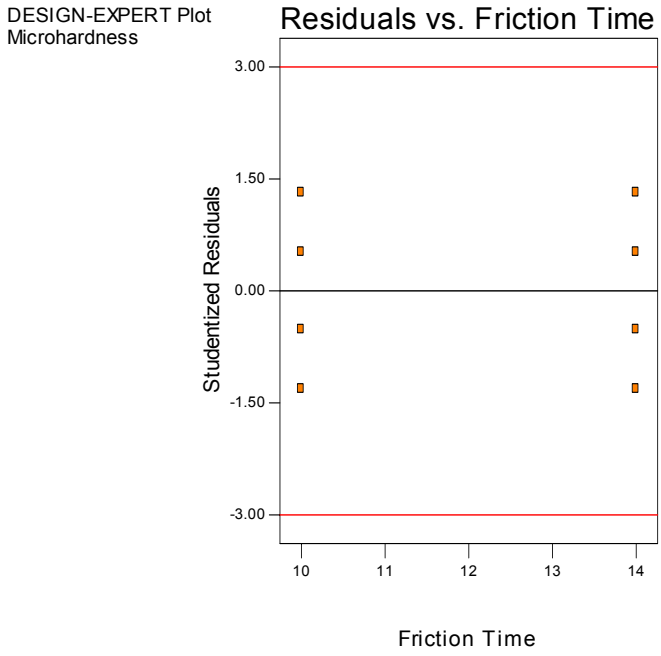

Figure 5.60. Residuals and friction time graph

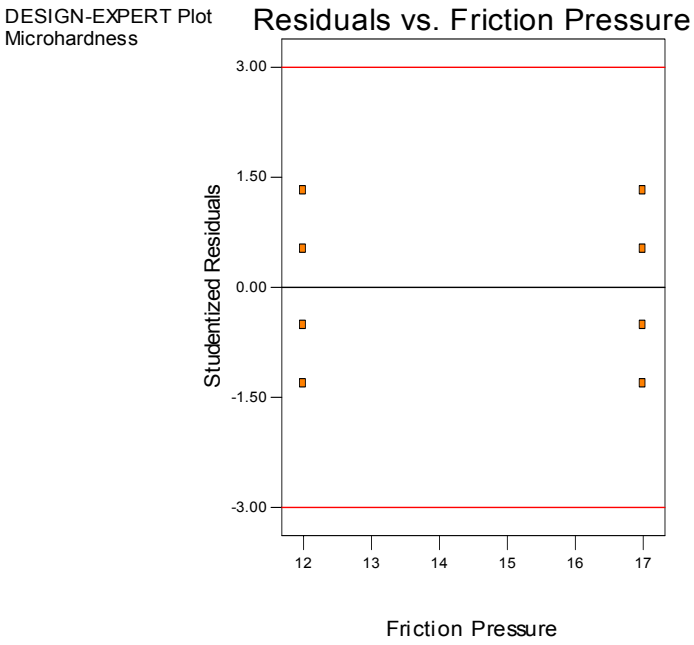

Figure 5.61. Residuals and friction pressure graph

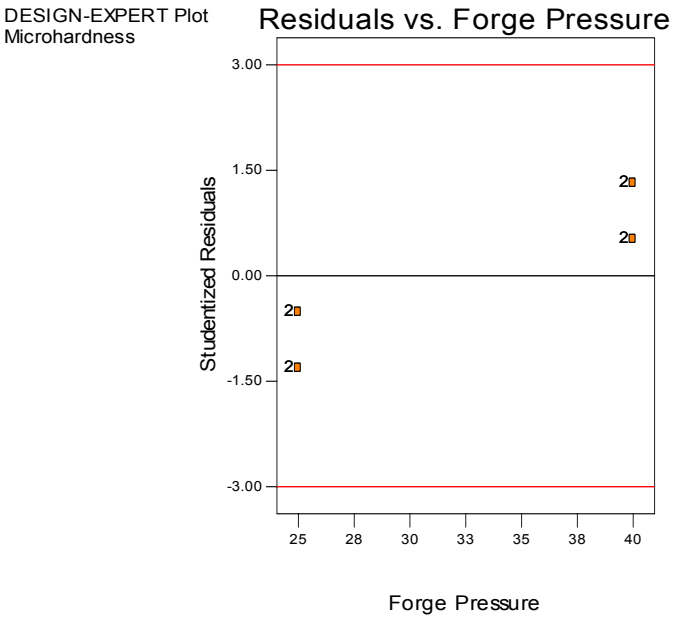

Figure 5.62. Residuals and forge pressure graph

It is very obvious from the Figure 5.60-5.62 that constant variance assumption is not violated.

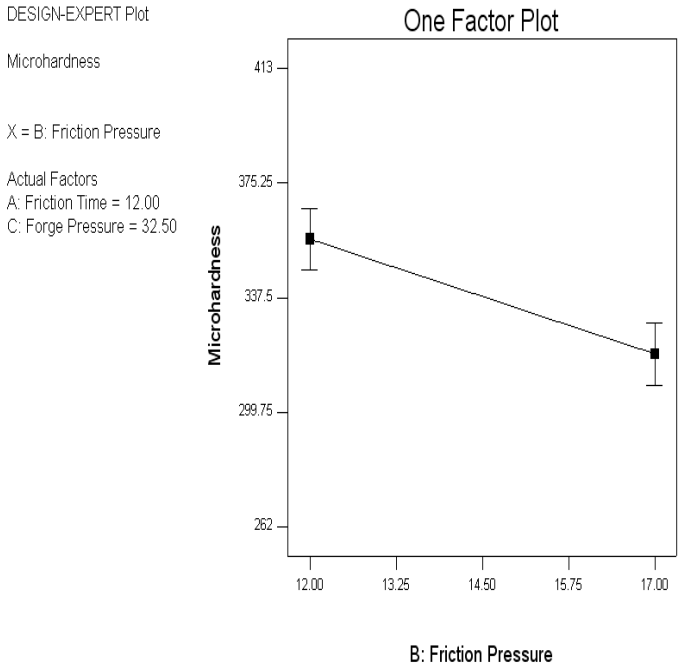

Figure 5.63. Change in microhardness with friction pressure

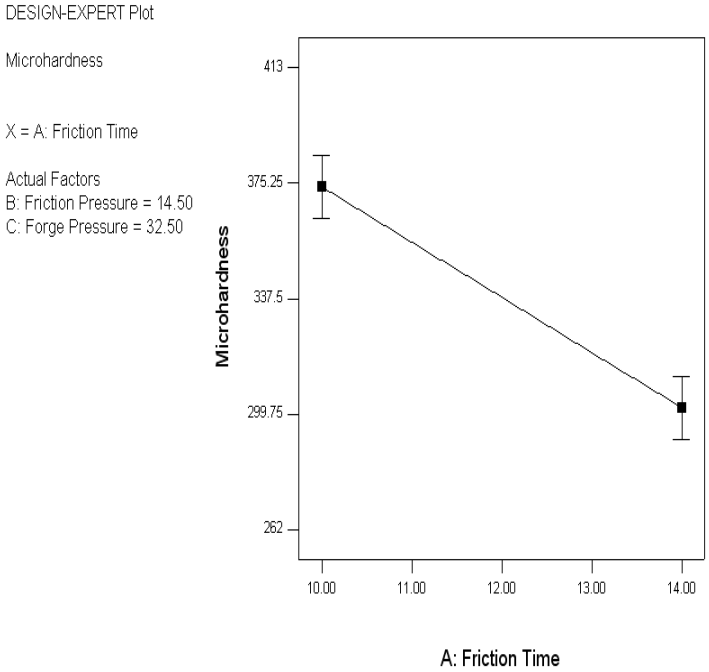

Figure 5.64. Change in microhardness with friction time

Figures 5.63 and 5.64 reveal that hardness tends to decrease with increase in friction time and friction pressure as a confirmation of Equation 5.4. The shorter friction time and smaller friction pressure within the given interval make the hardness bigger.

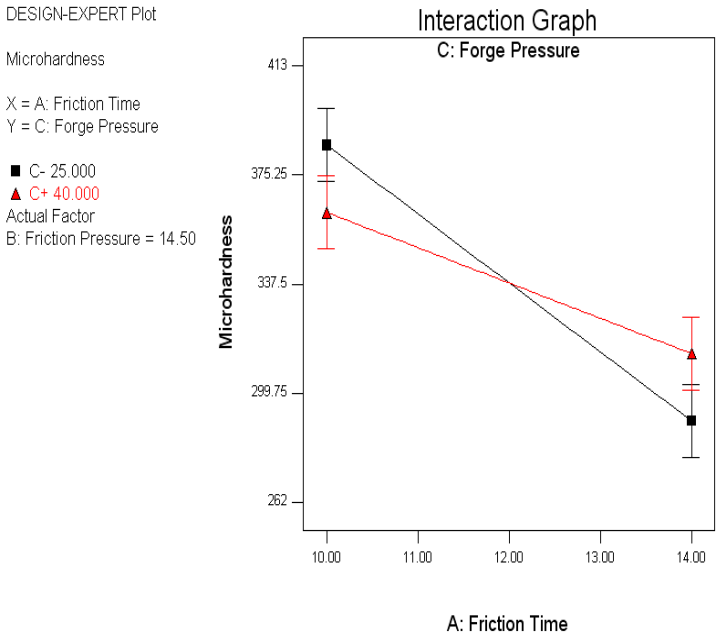

Figure 5.65. Change in hardness with friction time and forge pressure

Figure 5.56 reveals that AC interaction term leads to decrease in tensile strength where interaction term is self effective at low and high levels of forge pressure.

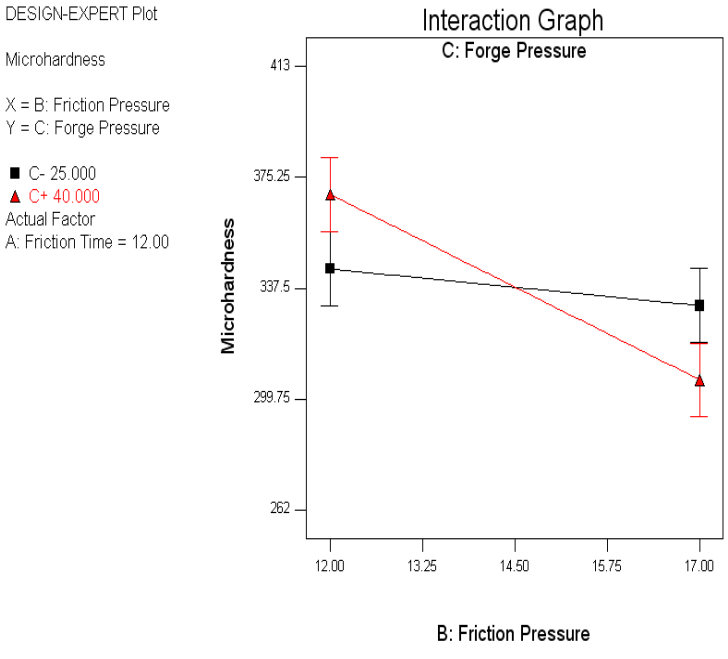

,

Figure 5.66. Change in hardness with friction pressure and forge pressure

BC interaction term leads to decrease in tensile strength where interaction term is self effective at low and high levels of forge pressure.

5.3. Macrographs of C and F Group

The size of burr under different process parameters are shown in Figure 5.67-5.74.

Figure 5.67. Macrographs of F1 and C1 (10-12-40)

Figure 5.68. Macrographs of F2 and C2 (14-17-25)

Figure 5.69. Macrographs of F3 and C3 (14-17-40)

Figure 5.70. Macrographs of F4 and C4 (14-12-40)

The size of burr increases with increase in forge pressure and friction time due to heat generation and plastic deformation phenomena.

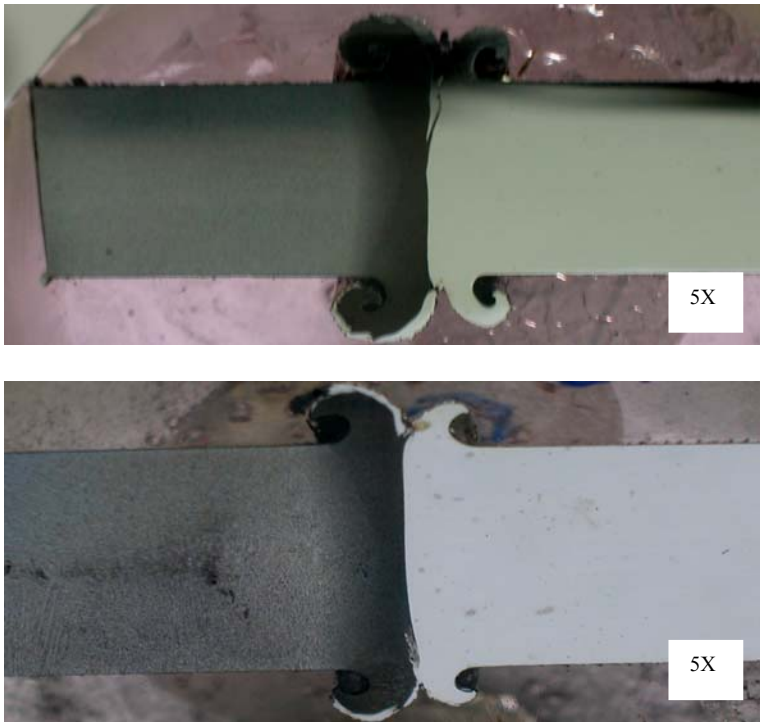

Figure 5.71. Macrographs of F5 and C5 (10-17-25)

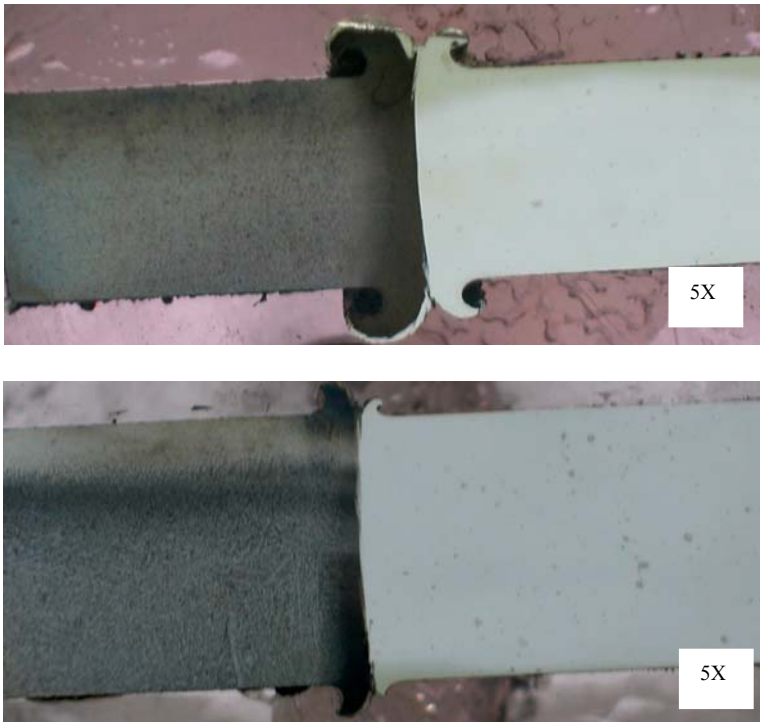

Figure 5.72. Macrographs of F6 and C6 (10-12-25)

Figure 5.73. Macrographs of F7 and C7 (10-17-40)

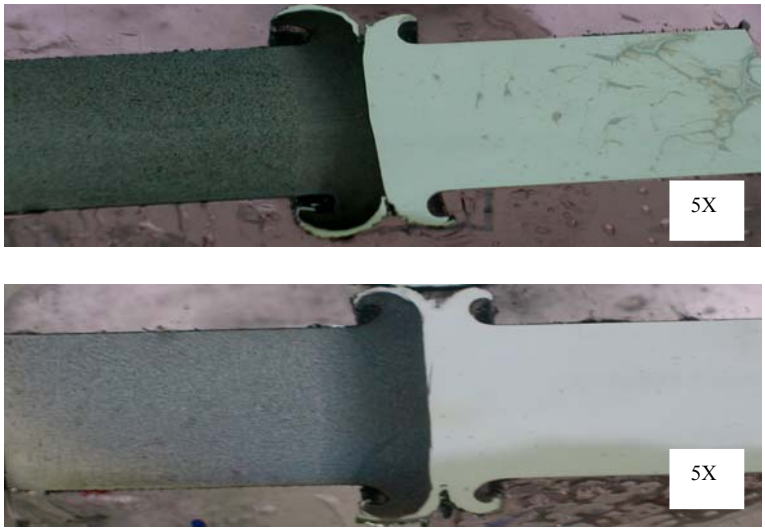

Figure 5.74. Macrographs of F8 and C8 (14-12-25)

F group (forged AISI 1050-AISI 304) specimens represent more upset, however, C group (cast AISI 1050-AISI 304) specimens represent less and this is due to forgability. As the specimens are forged before welding operation, their forgability increases and the steel with greater forgability leads to greater amount of weld upset. Another important issue is the difference of amount of upset between themselves which can be considered as medium carbon steel and austenitic stainless steel. The amount of upset is more in medium carbon steel and this is directly related to the high temperature strength of the material.

5.4. Microstructural Examination of Friction-Welded Specimens

The microstructures of the base metals, HAZ (heat affected zone) and weld interface of each group, say, forged AISI 1050 and investment cast AISI 1050 steel and AISI 304 steel are shown in Figure 5.75-5.110.

5.4.1. Microstructures of Forged AISI 1050-AISI 304 Combination

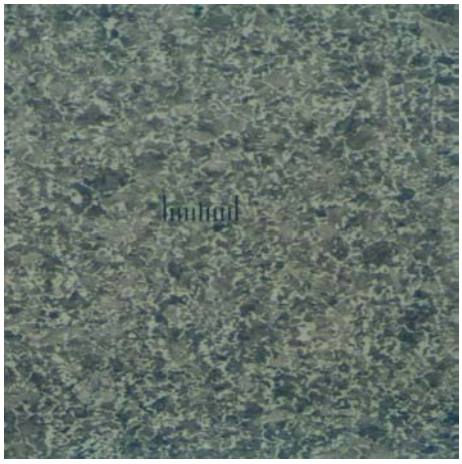

Figure 5.75. F1-AISI 1050-base metal-50X

Figure 5.76. F1-AISI 304-HAZ-100X

In the Figure 5.76 it is seen that in the vicinity of weld interface there is a sharp bend in the flow lines. This is because plastic deformation is restricted to very narrow zone.

Figure 5.77. F1-MML-500X

Figure 5.77 suggests that a mechanically mixed layer (MML) was emerged between the AISI 304-AISI 1050. Moreover this layer is continuous and responds nital etch.

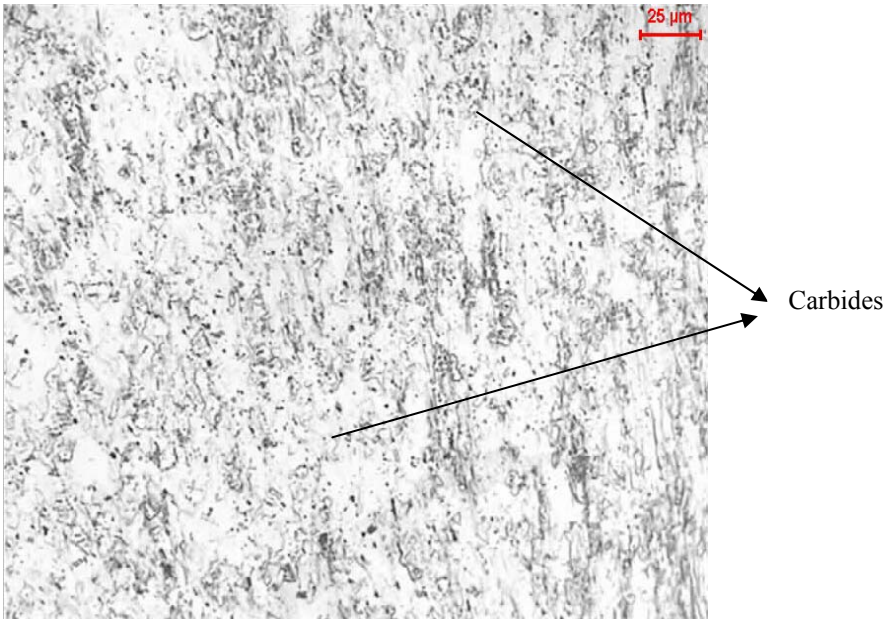

Figure 5.78. F1 AISI 304-HAZ-400X

HAZ (heat affected zone) of the stainless steel obtains carbide grains which are seen as black points in the Figure 5.78.

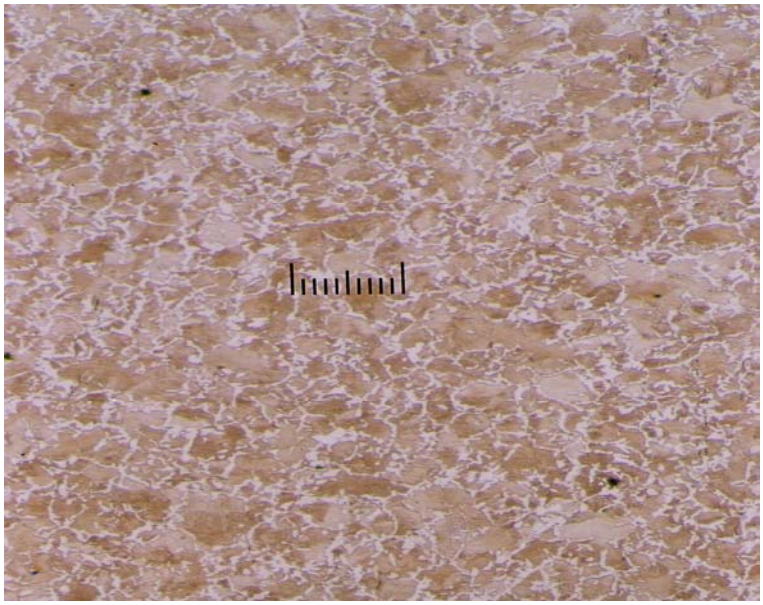

Figure 5.79. F2-AISI 1050-base metal-100X

As seen in the Figure 5.79, base metal of medium carbon steel consists of ferrite (light areas) and pearlite (dark areas) with fine grain structure.

Figure 5.80. F2-AISI 1050-HAZ-50X

Figure 5.80 shows that grain size becomes smaller as it is close to the welding interface and this creates grain refined region in the HAZ of medium carbon steel.

Figure 5.81. F2-AISI 304-HAZ-50X

In Figure 5.81 it is obvious that flow lines direction is changed in the HAZ (heat affected zone) of the AISI 304.

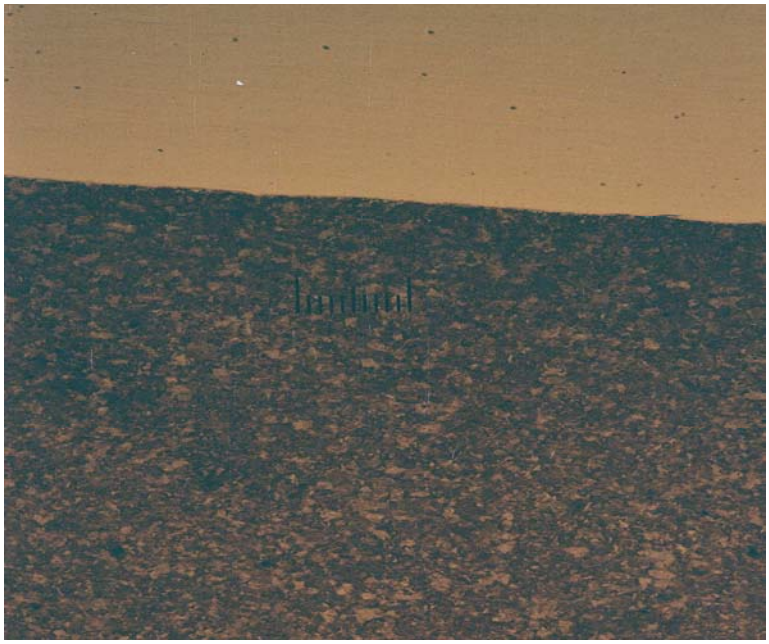

Figure 5.82. F2-welding interface-50X

In Figure 5.82 dark area shows medium carbon steel and white area is stainless steel. It seems that there is uniform dark etching layer in the side of AISI 1050 steel.

Figure 5.83. F3-AISI 1050-HAZ-100X

Figure 5.83 explains that the size of grain becomes smaller in the HAZ zone of AISI 1050.

Figure 5.84. F3-AISI 304-HAZ-500X

Figure 5.84 shows that flow lines direction is changed in the HAZ of the AISI 304.

Figure 5.85. F3-AISI 304-HAZ

Some carbide grains are seen in the Figure 5.85. What is more, elongated microstructure is observed in the same figure.

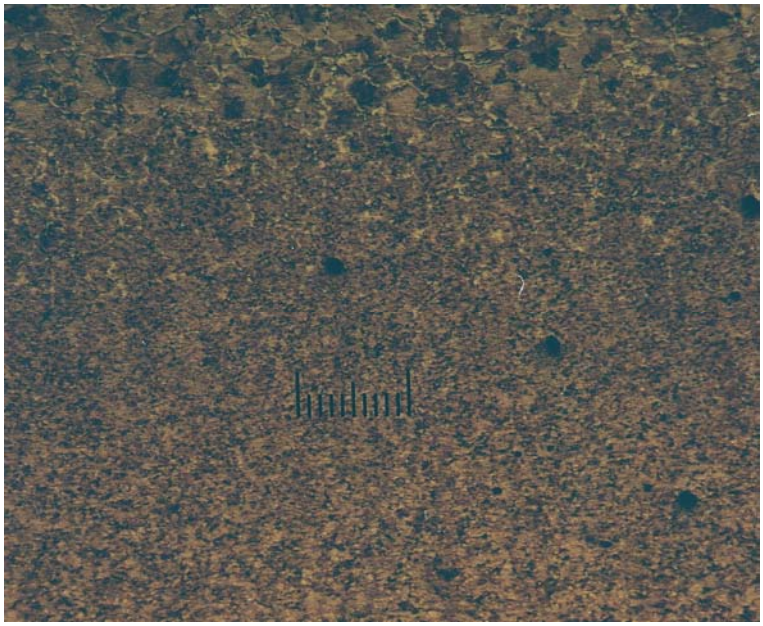

Figure 5.86. F4-AISI 1050-HAZ-50X

As seen in Figure 5.26, in the HAZ of medium carbon steel of F4 grains begin to coarsen as being closer to base metal.

Figure 5.87. F5-AISI 304-HAZ-100X

A change in the flow direction is seen for the HAZ (heat affected zone) of austenitic stainless steel in Figure 5.87. This is a consequence of temperature gradient in this narrow HAZ.

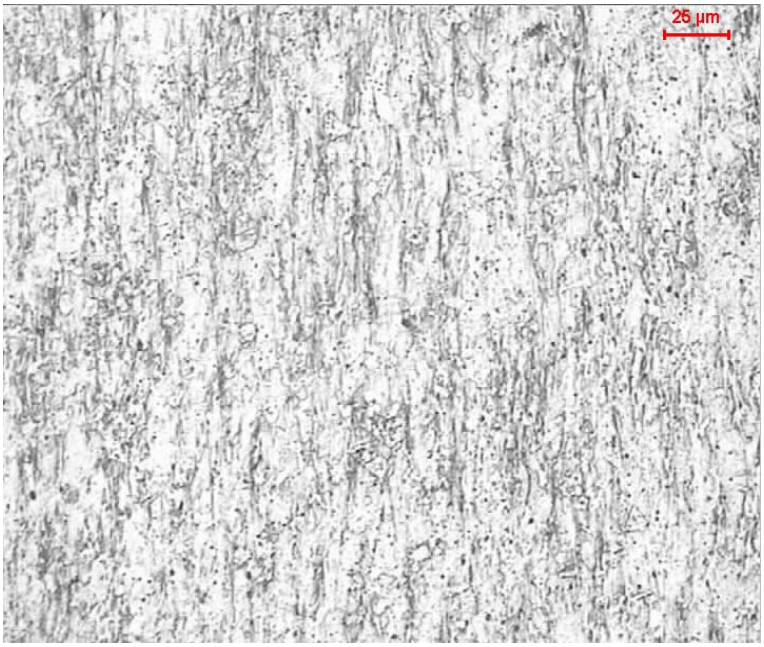

Figure 5.88. F5-AISI 304-HAZ-400X

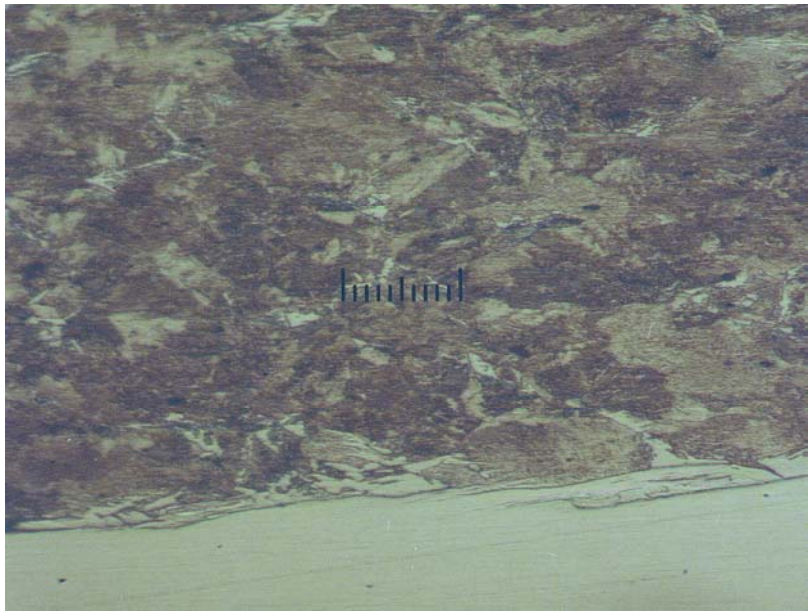

Figure 5.89. F5-welding interface-500X

By careful examination the microstructure of welding interface of F5, martensite formation can be recognized. Because stainless steel and MML (mechanically mixed layer) do not respond to nital etch, they seem as white area in the Figure 5.89.

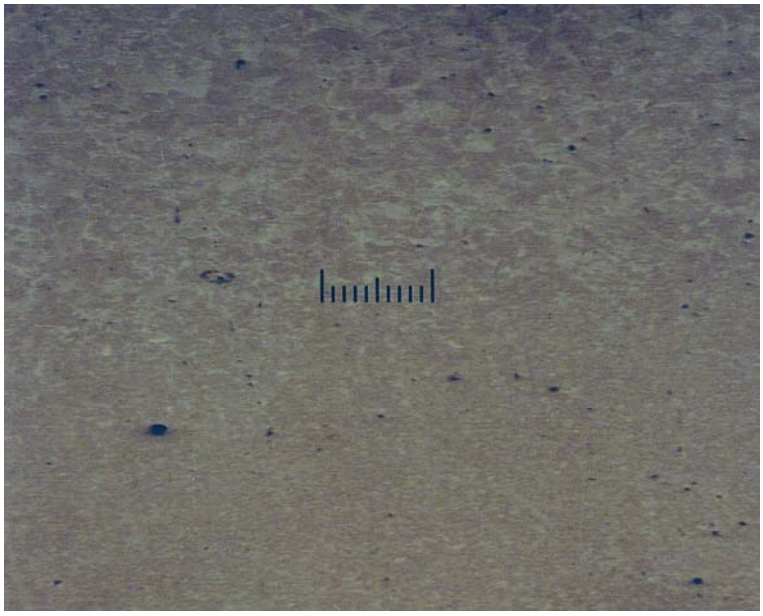

Figure 5.90. F6-AISI 1050-HAZ-50X

In the Figure 5.90 the grain size becomes smaller proportionally to the distance of weld interface. That can be explained with plastic deformation at high temperature.

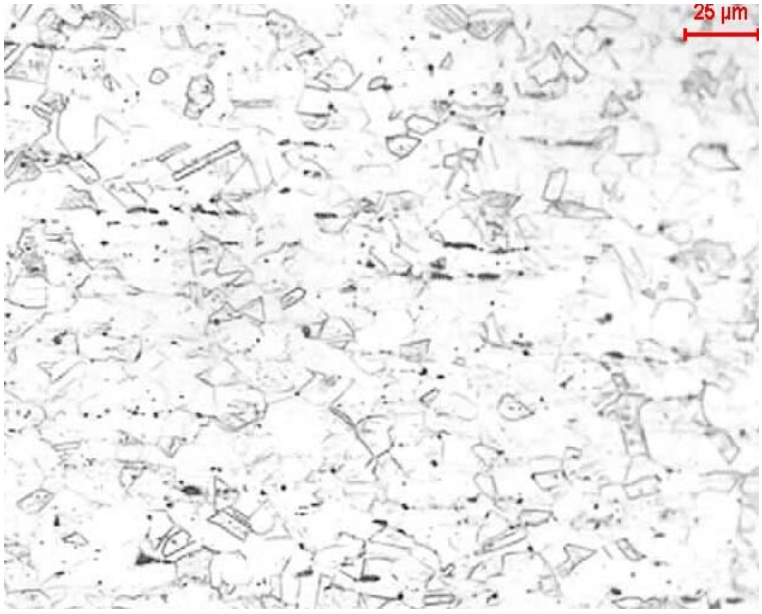

Figure 5.91. F6-AISI 304-base metal

In the Figure 5.91 it is clearly shown that the microstructure consists of equiaxed austenitic grain structure with annealing twins.

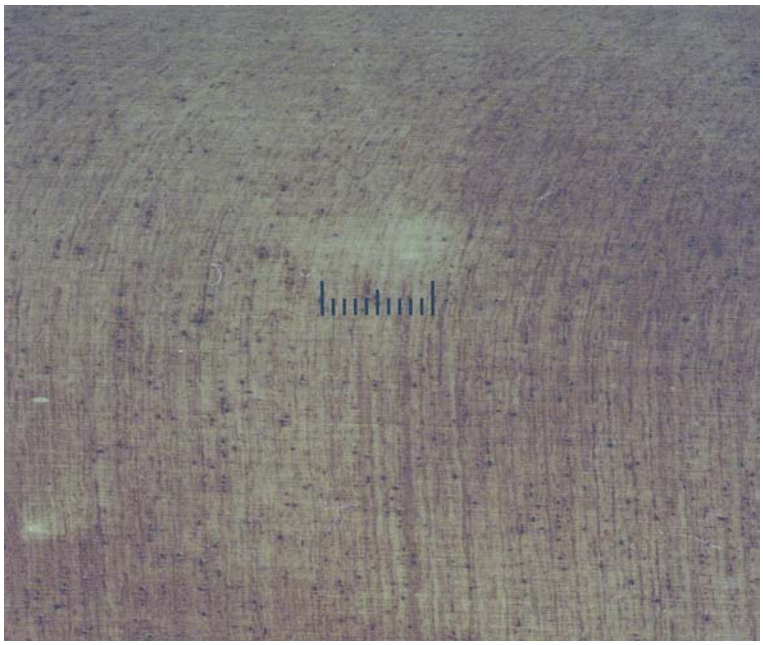

Figure 5.92. F6-AISI 304-HAZ-50X

Figure 5.92 represents that flow direction is sharply changed in the vicinity of weld interface with containing some carbide grains.

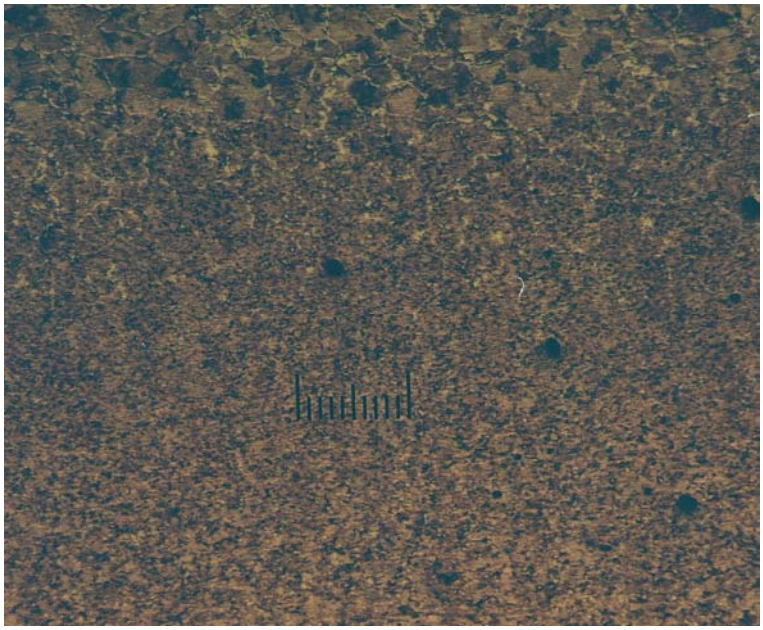

Figure 5.93. F7-AISI 1050-50X

Figure 5.93 informs that because of excessive heat generation more martensite formation is seen in medium carbon steel side.

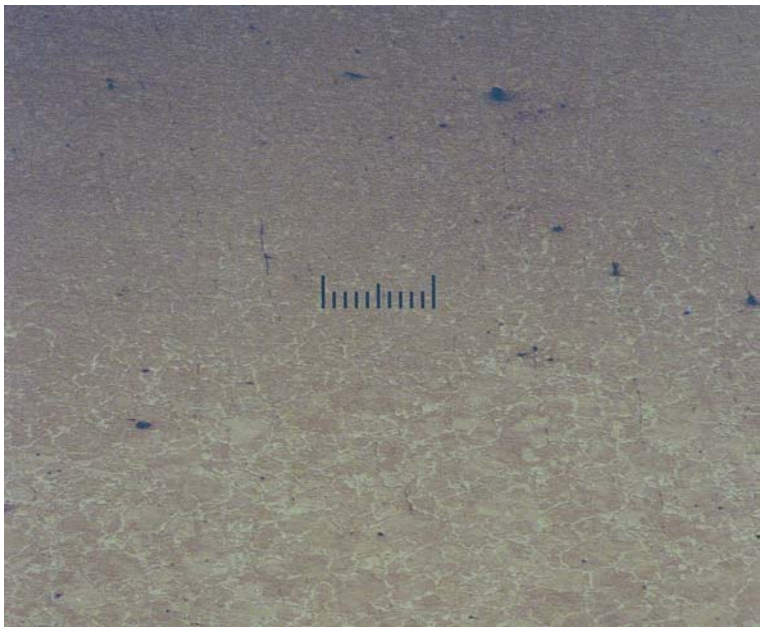

Figure 5.94. F8-AISI 1050-HAZ-50X

Figure 5.94 explains that grain size coarsens as going to the base metal from the weld interface.

5.4.2. Microstructures of Cast AISI 1050-AISI 304 Combination

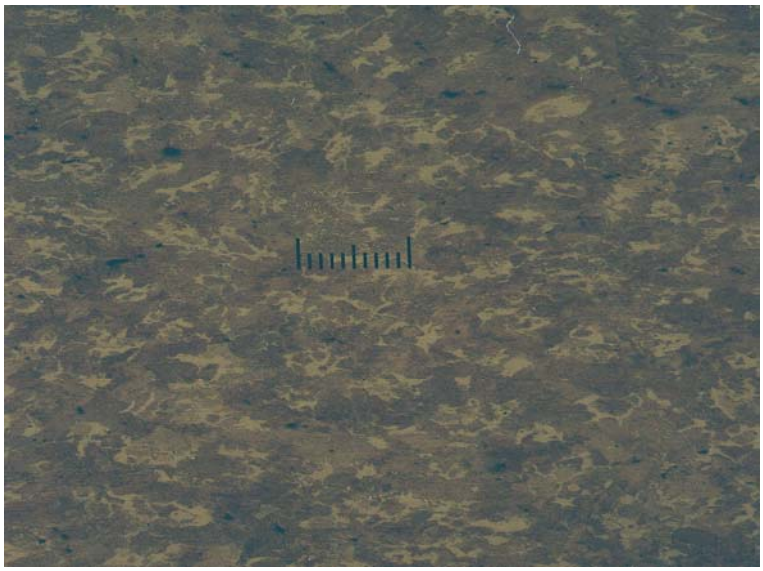

Figure 5.95. C1-AISI 1050-base metal-100X

Cast medium carbon steel consists of the same microstructure known as pearlite surrounded by ferrite network. However this is not a fine grain structure as forged one in Figure 5.95.

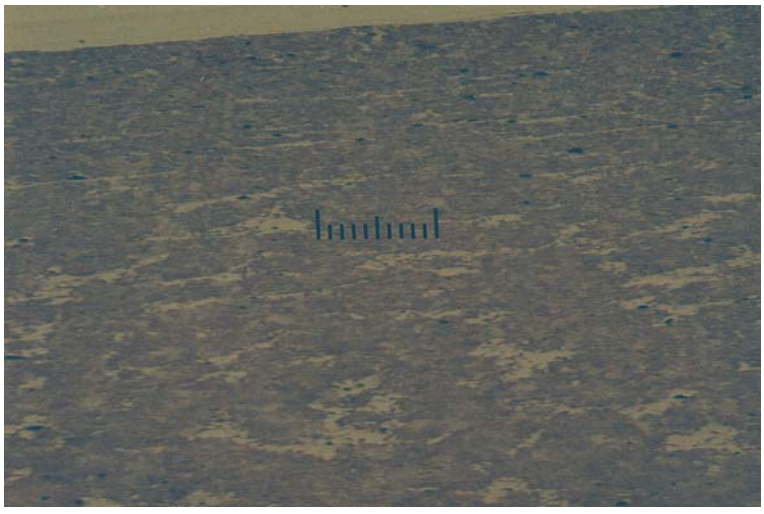

Figure 5.96. C1-AISI 1050-HAZ-100X

In the Figure 5.96 it is very clear that grain size decreases as going to weld interface.

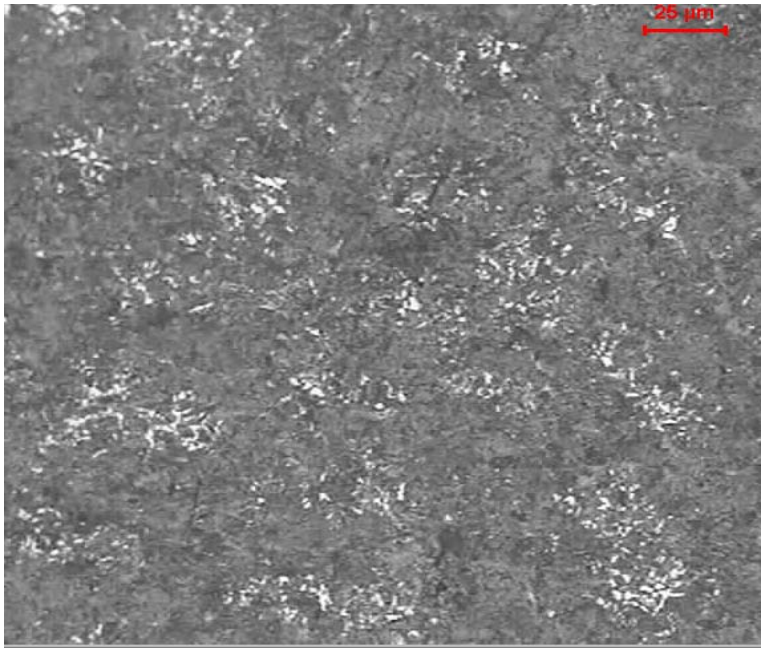

Figure 5.97. C2-AISI 1050-HAZ

Figure 5.97 indicates that the size of grains reduces with effect of pressure at high temperature through the HAZ.

Figure 5.98. C2-AISI 304-HAZ-100X

The change in the flow pattern is clearly seen in the HAZ of the austenitic stainless in Figure 5.98.

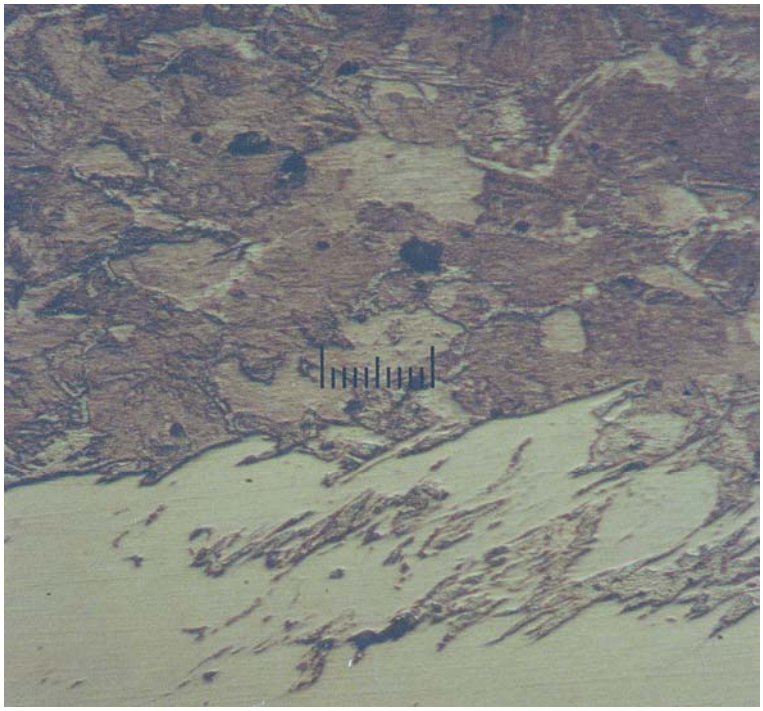

Figure 5.99. C2-welding interface-500X

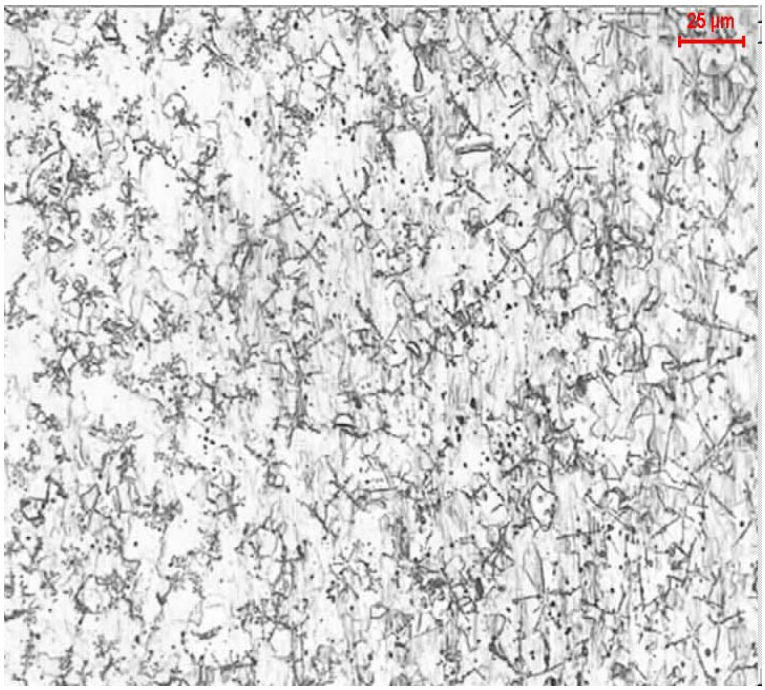

Figure 5.100. C3-AISI 304-HAZ

By examining the HAZ of stainless steel side of C3 in Figure 5.100, it is observed that a carbon migration from medium carbon steel to stainless steel was emerged.

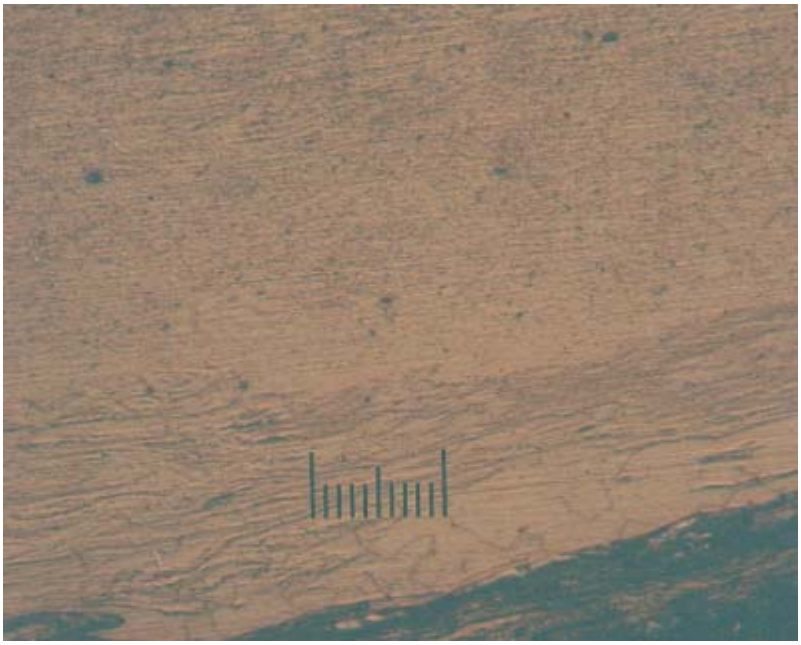

Figure 5.101. C3-AISI 304-welding interface-500X

Mixing of AISI 1050 into AISI 304 is clearly indicated in Figure 5.101.

Figure 5.102. C4-AISI 304-HAZ-100X

Because heat is restricted to the narrow HAZ, Figure 5.102 exhibits those parallel banded features in the stainless steel side of weld interface.

Figure 5.103. C4-welding interface-500X

Figure 5.103 shows that there is an equiaxed grain structure within MML (mechanically mixed layer). Moreover, grains in the vicinity of interface of AISI 1050 side become smaller in size.

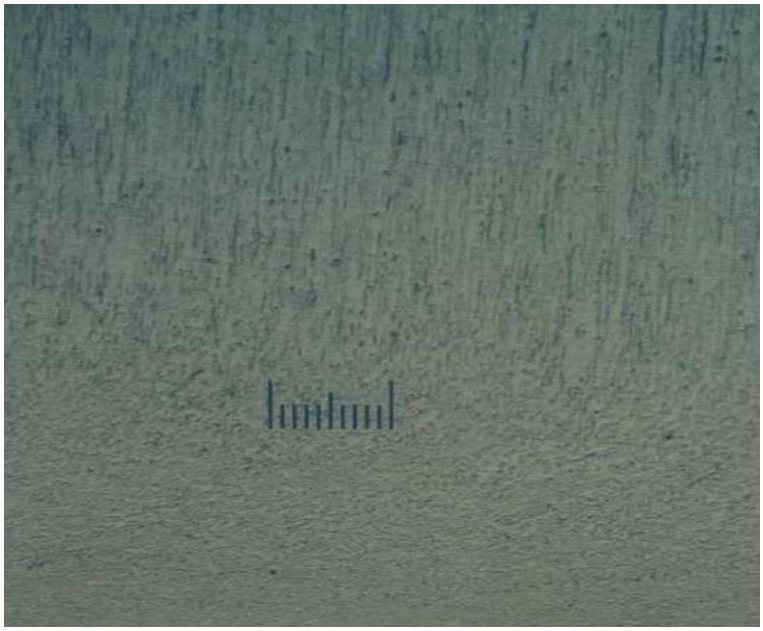

Figure 5.104. C5-AISI 304-HAZ-50X

Figure 5.104 represents the HAZ of AISI 304 specimen with change in flow direction.

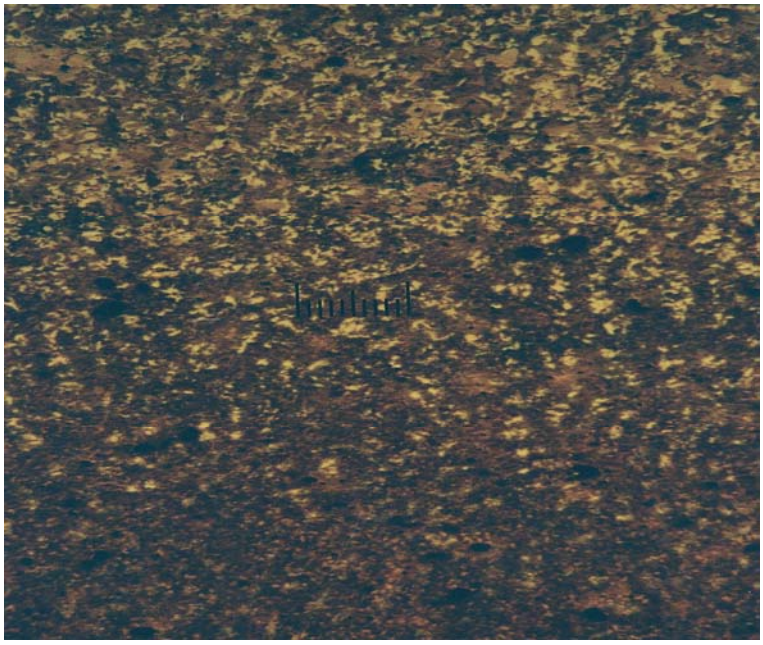

Figure 5.105. C6-AISI 1050-HAZ-50X

Figure 5.105 indicates that ferrite grains become less in total amount as being adjacent to the weld interface. At the same time pearlite grains become smaller in size.

Figure 5.106. C6-AISI 1050-near weld interface-500X

Figure 5.106 shows that some martensite is formed at the interface of AISI 1050 because of high cooling rate in this material.

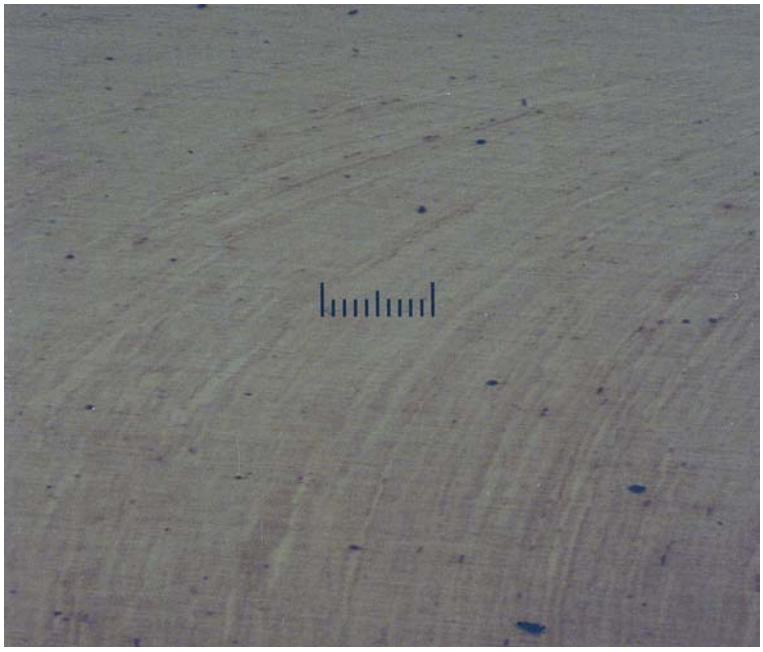

Figure 5.107. C6-AISI 304-HAZ-50X

Flow pattern changes as being closer to the interface in Figure 5.107. This pattern is just same as the direction of upset .

Figure 5.108. C7-AISI 1050-base metal and HAZ-100X

Figure 5.108 indicates that unaffected base material has pearlite surrounded by ferrite; however, as going through base material to the weld, grains become smaller in size.

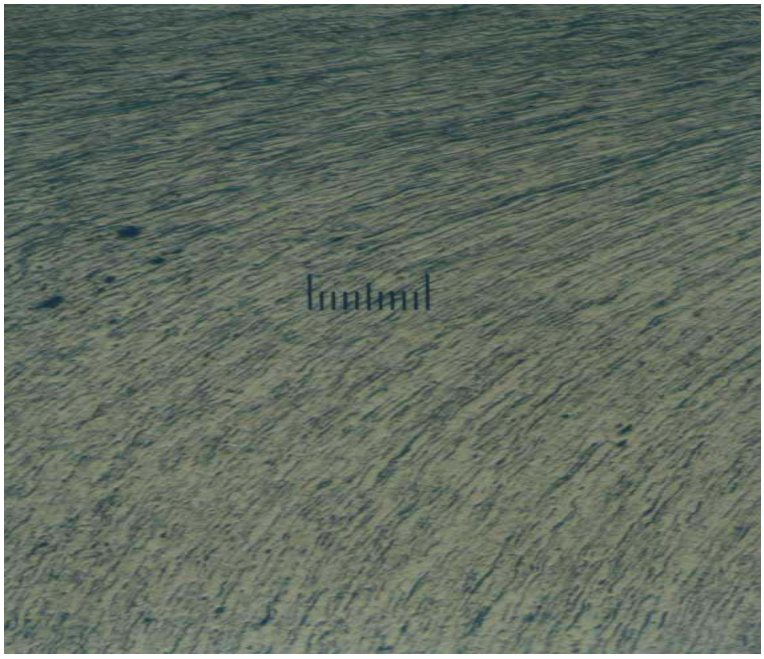

Figure 5.109. C8-AISI 304-HAZ-100X

Change in flow direction is very obvious in Figure 5.109 because of high temperature gradient.

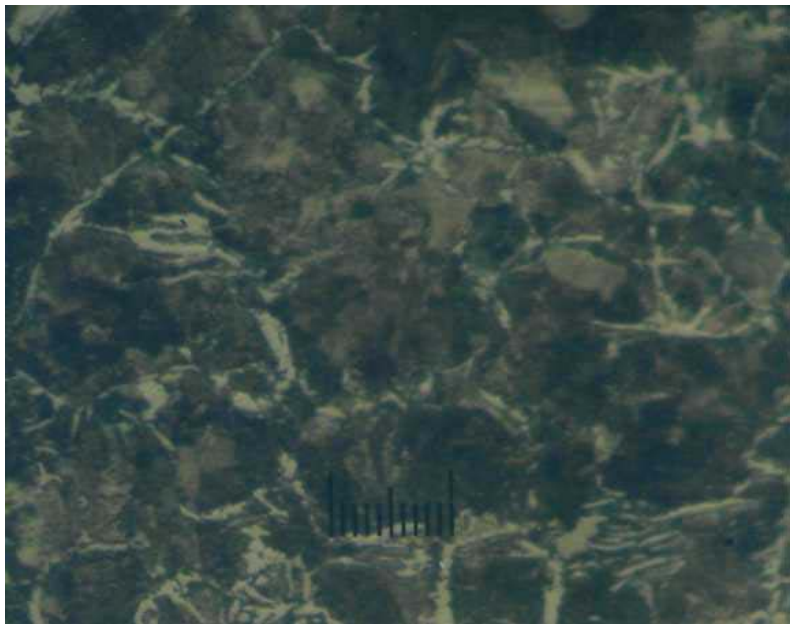

Figure 5.110. C8-AISI 1050-near weld interface-500X

Figure 5.110 shows that martensite is formed near weld interface in the AISI 1050 side of the weldment.

5.4.3. Examination of Microstructure in Interface of F Group

The microstructures of weld interfaces of forged AISI 1050-AISI 304 (F group) are shown in Figure 5.111-5.117.

Figure 5.111. F1 MML (10-12-40)

It is very clear from the above that a mechanically mixed layer (MML) was formed when the process parameters are as F1.

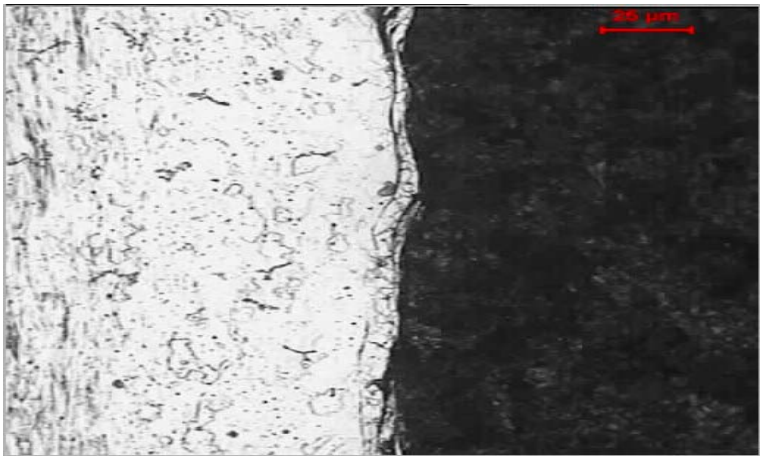

Figure 5.112. F2 Recrystallized region and MML (14-17-25)

Figure 5.112 shows that a recrystallized region and MML (mechanically mixed layer) were produced in the parameters of F2.

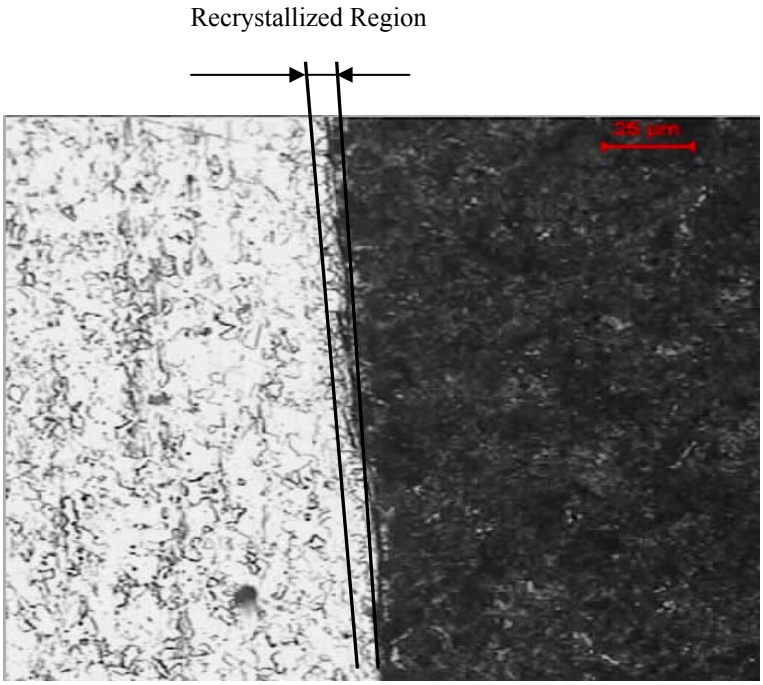

Figure 5.113. F3 Recrystallized region (14-17-40)

It is very difficult to etch HAZ (heat affected zone) of AISI 304 steel, therefore HAZ of AISI 1050 seems dark with this etching agent in Figure 5.113. In general high axial pressures lead the refinement of austenitic grains by hot working prior to their cooling and one may expect the resulting microstructure to be less brittle [38].

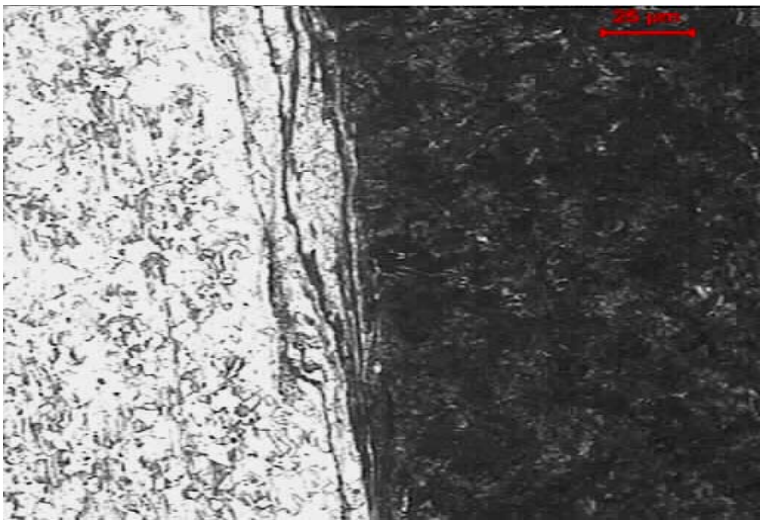

Figure 5.114. F4 MML (14-12-40)

Some mixing between two parent materials is seen in Figure 5.114, however this is mainly observed from the AISI 1050 because of high temperature strength.

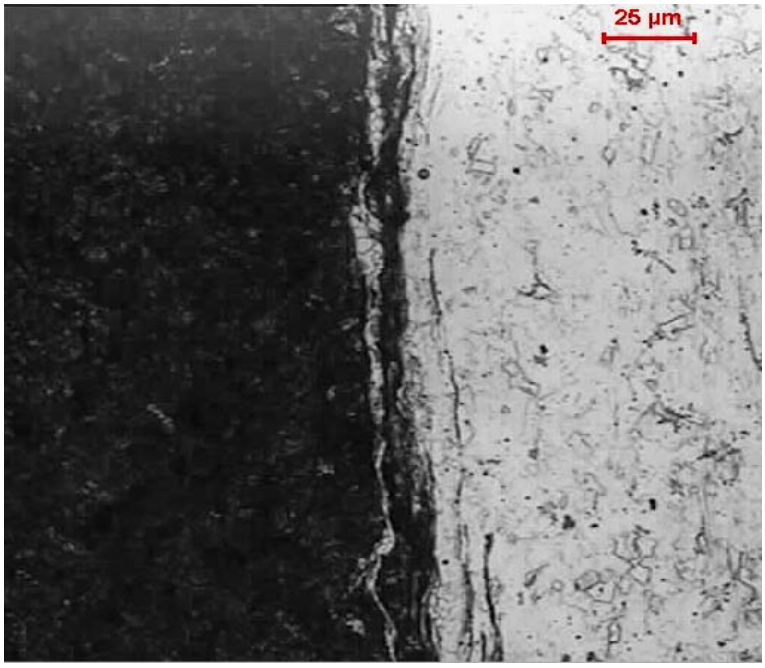

Figure 5.115. F5 MML (10-17-25)

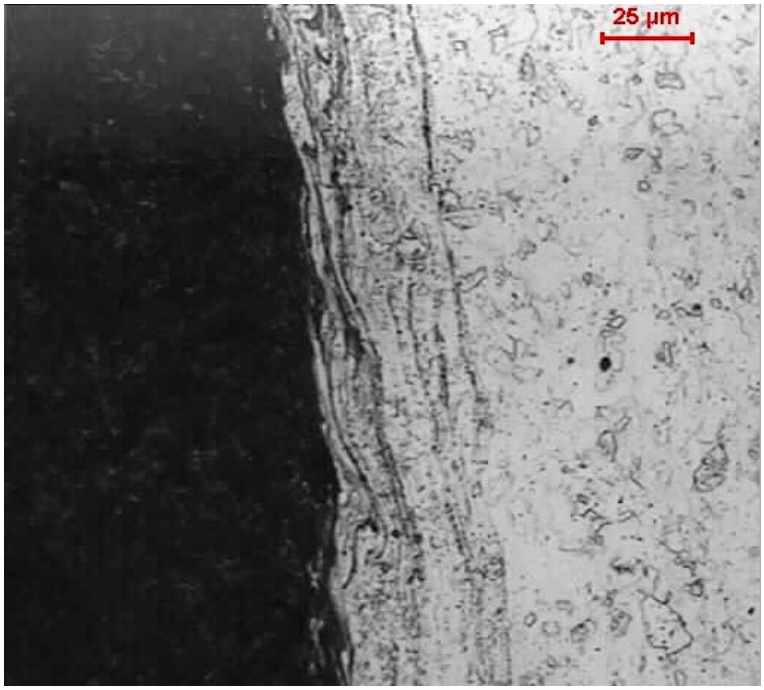

Figure 5.116. F6 MML (10-12-25)

Mechanically mixed layer (MML) which is an indication of strong interlocking between the two mating material is seen in Figure 5.115 and 5.116. The width of this layer changes depending on the parameters, mainly with forge pressure.

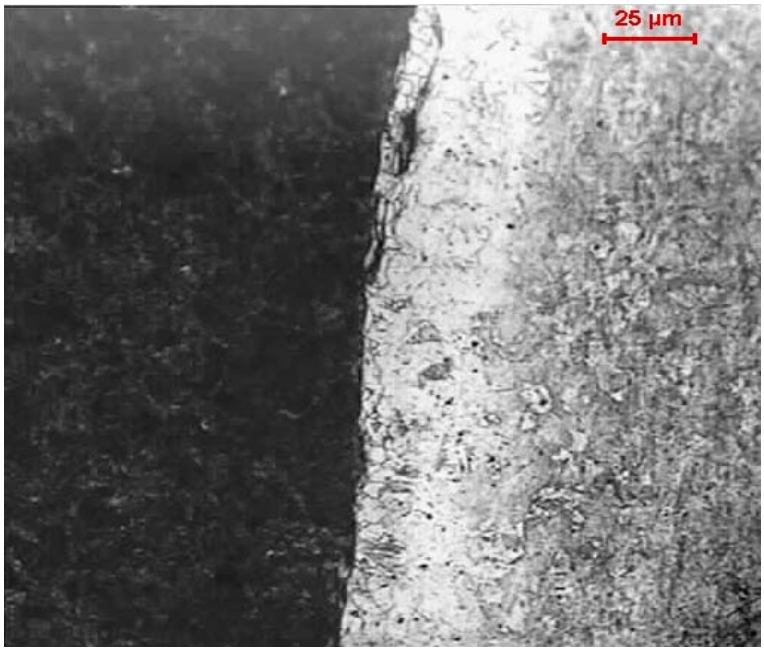

Figure 5.117. F7 Recrsytallized region (10-17-40)

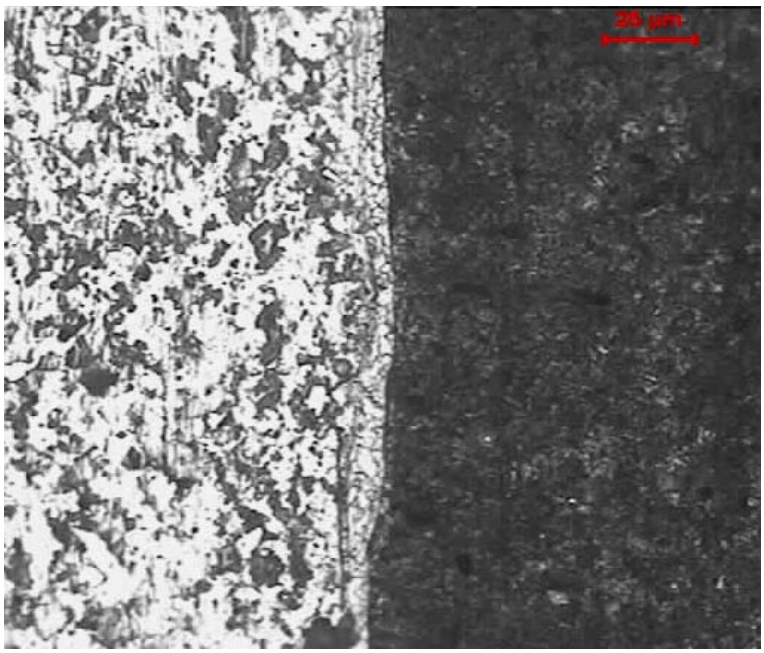

Figure 5.118. F8 Recrystallized region (14-12-25)

A recrystallized region in the vicinity of weld line is very obvious from the Figure 5.118; however, some martensite is formed in the austenite matrix.

5.4.4. Examination of Microstructure in Interface of C Group

The weld interfaces of investment cast AISI 1050-AISI 304 specimens (C group) are shown in Figure 5.119-5.126.

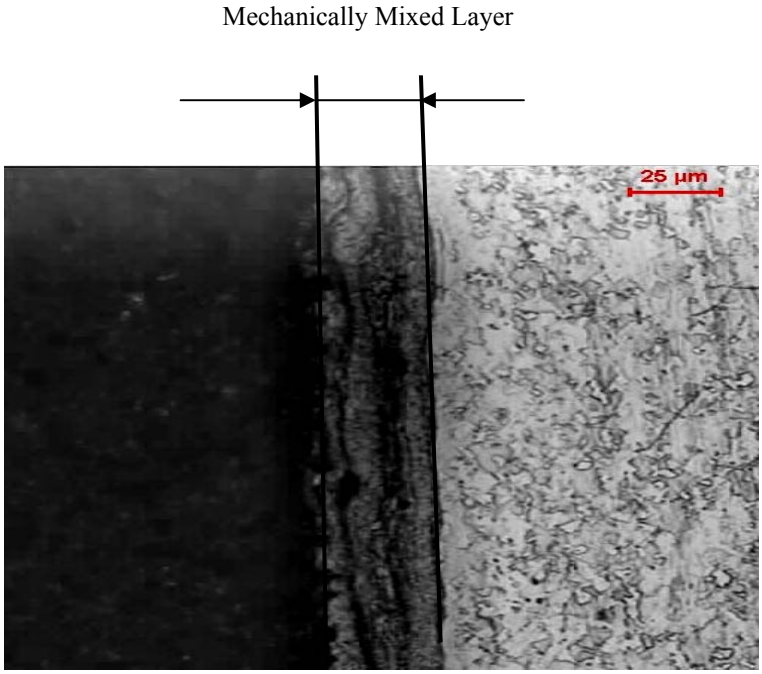

Figure 5.119. C1 MML (10-12-40)

Mixing of AISI 1050 steel into AISI 304 steel is clearly indicated in Figure 5.119 but the width of this mixing layer is relatively larger than that of F1.

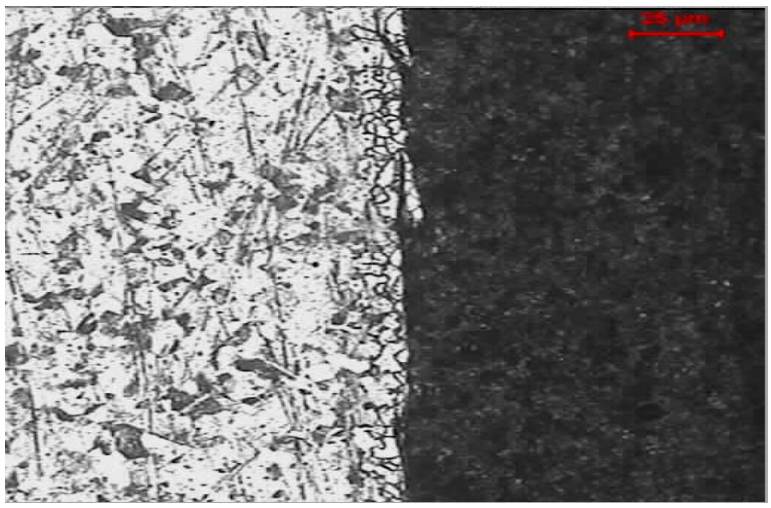

Figure 5.120. C2 Recrystallized region (14-17-25)

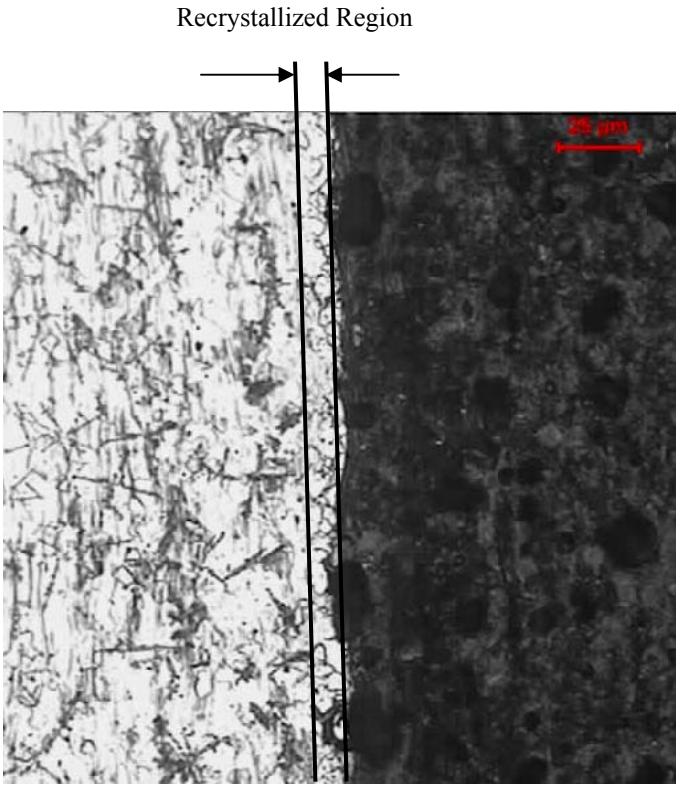

Figure 5.121. C3 Recrystallized region (14-17-40)

The phenomena of recrystallization is seen in the C2 and C3 which is mainly emerged in the austenitic stainless steel side.

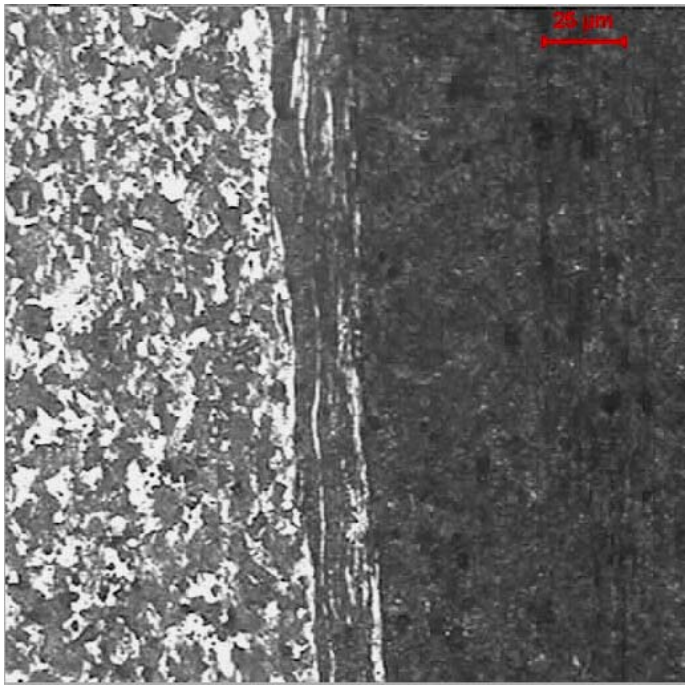

Figure 5.122. C4 MML (14-12-40)

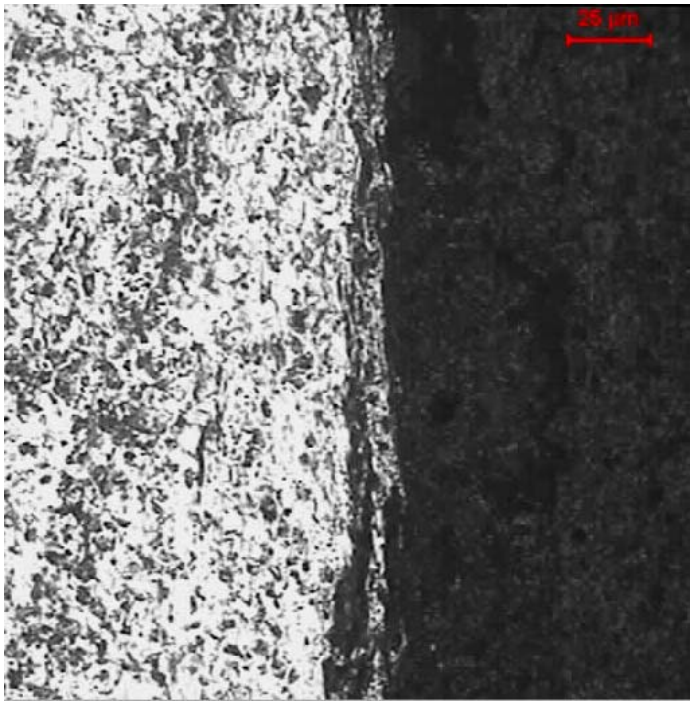

Figure 5.123. C5 MML (10-17-25)

Figures 5.122 and 5.123 inform that because of cooling from the high temperature in a very short time, martensite can be formed in the austenitic stainless steel.

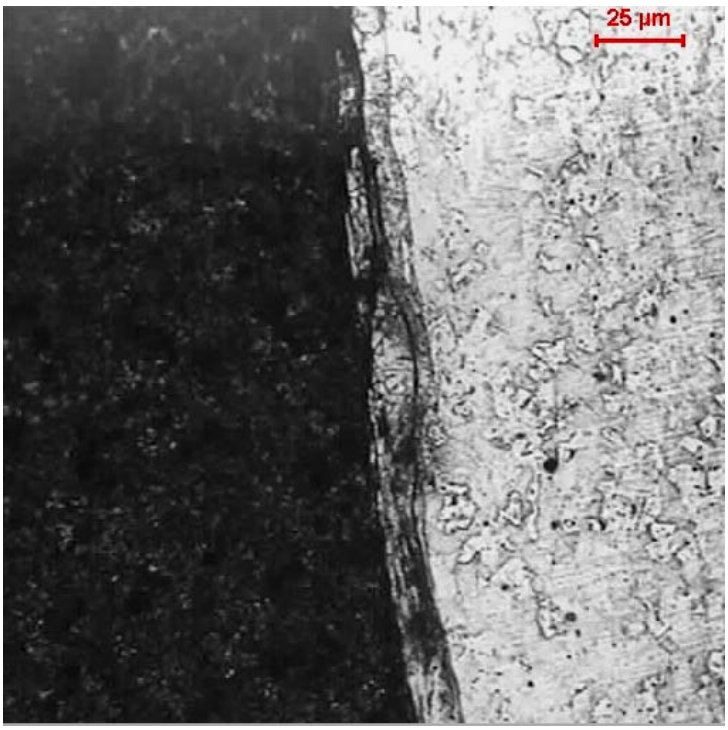

Figure 5.124. C6 MML (10-12-25)

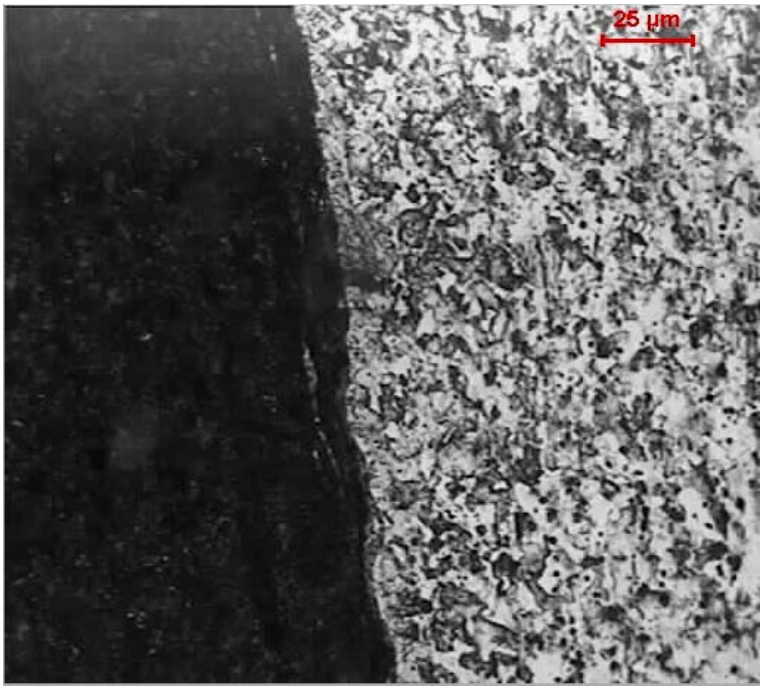

Figure 5.125. C7 MML (10-17-40)

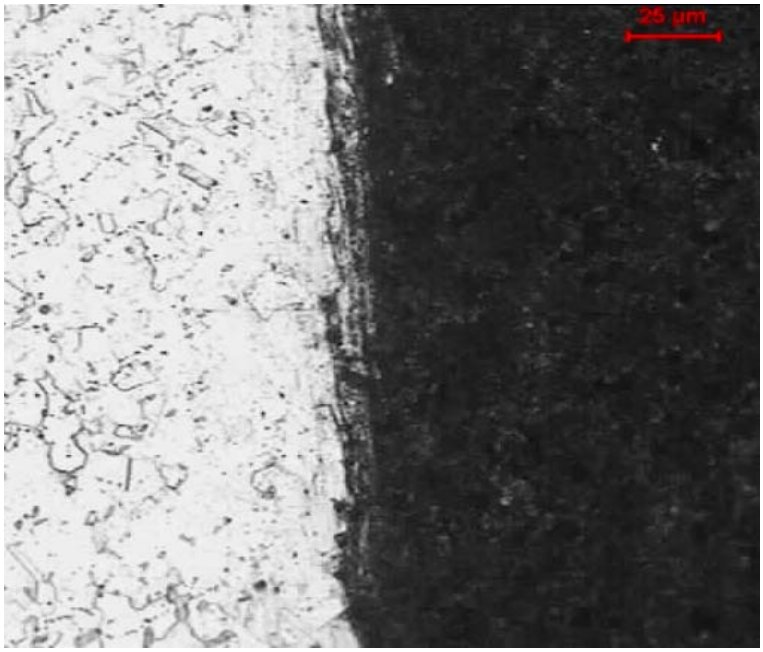

Figure 5.126. C8 MML (14-12-25)

The main difference between the Figures 5.125 and 5.126 is the formation of martensite which is a result of the cooling phenomena from very high temperature.

5.5. SEM and EDS Analysis of Friction-Welded Specimens

Scanning electron microscopy (SEM) and energy dispersive spectroscopy (EDS) analysis were performed by TUBİTAK Marmara Research Center in order to understand the phases that occurred during welding in the welding interface. SEM images were taken from F3, F6, C1, C6 and EDS analysis was done with respect to SEM images. After analyzing SEM images and EDS analysis in detail, the phases that occur during welding process were predicted by using Schaeffler Diagram which provides information on the welding properties of the various types of microstructure, as a function of what alloying elements they contain. The Schaeffler diagram is indispensable in the case of "dissimilar" joins. By these it is explained welded joins between higher-grade CrNi steel and low-cost structural steel.

5.5.1. SEM Analysis of F Group

The SEM (scanning electron microscopy) images of the F3 and F6 specimens are shown in Figure 5.127-5.131

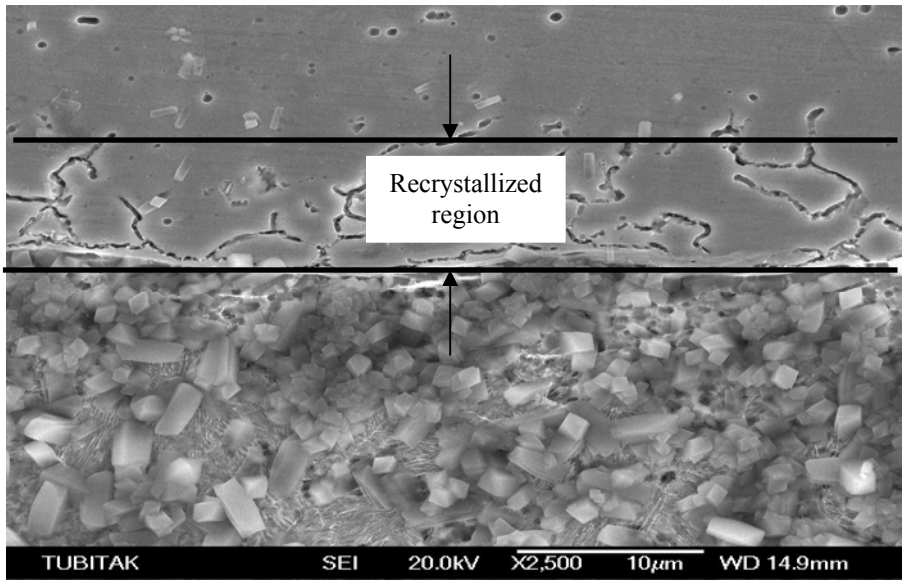

Figure 5.127. SEM image of weld interface of F3

The recrystallized region including carbides in a matrix of austenite can be clearly observed in Figure 5.127.

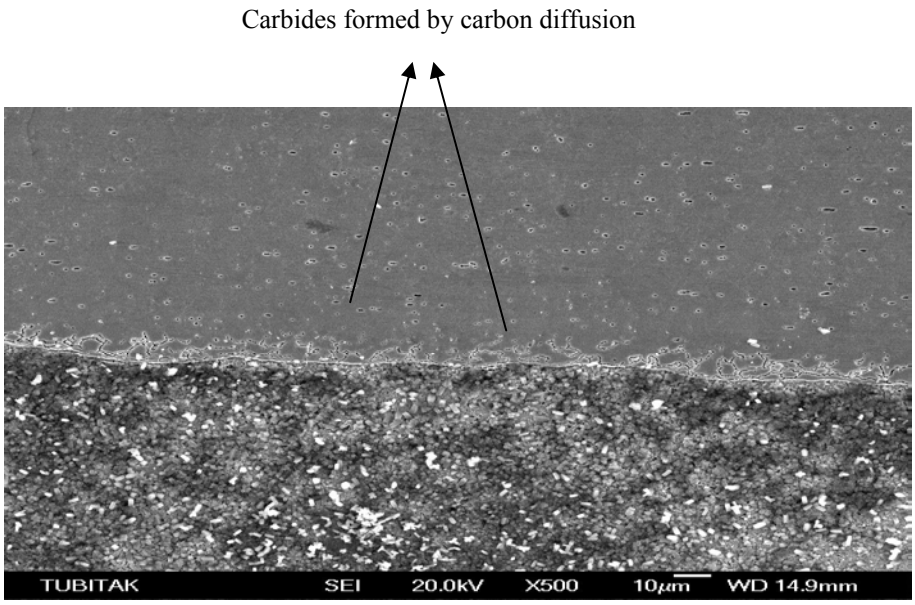

Figure 5.128. SEM image of weld interface of F3

Grain refining is observed adjacent to the weld interface in Figure 5.128. This is because the material at the interface was heated to a high temperature and subsequently cooled at a faster rate due to the temperature gradient between the interface and base metal [55].

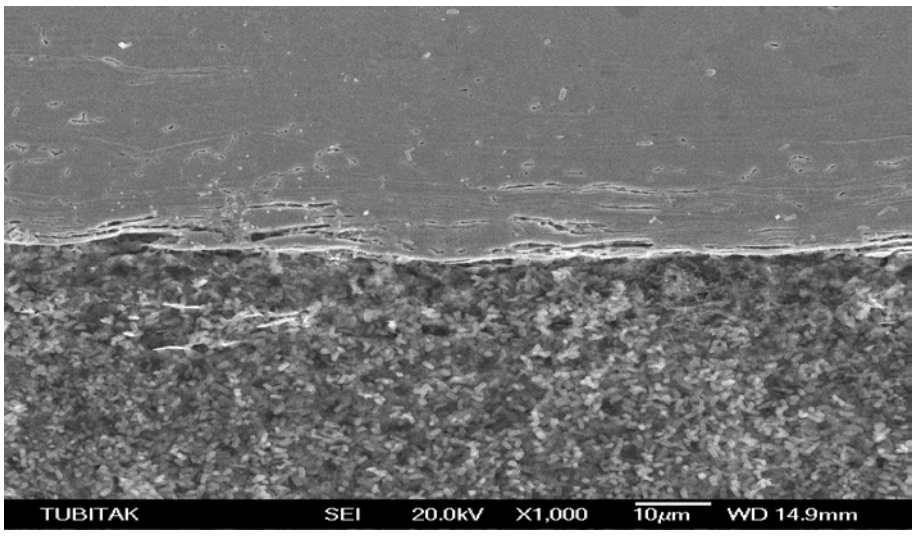

Figure 5.129. SEM image of weld interface of F6

HAZ of AISI 1050 steel consists of reduction in grain size with effect of high axial pressure at high temperature and a grain refined zone in AISI 1050 side and this can be clearly seen in Figure 5.129.

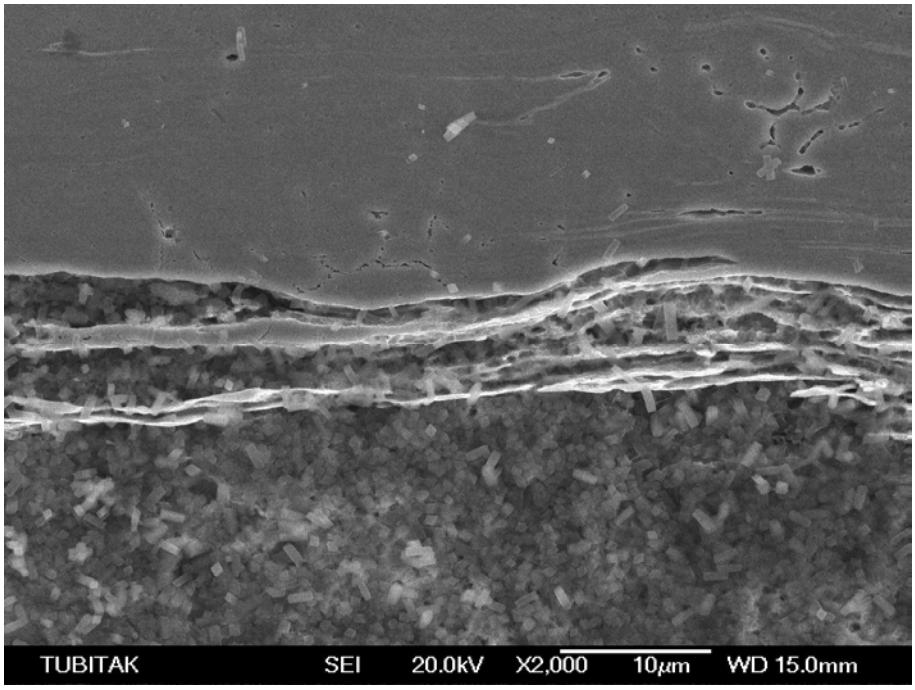

Figure 5.130. SEM image of weld interface of F6

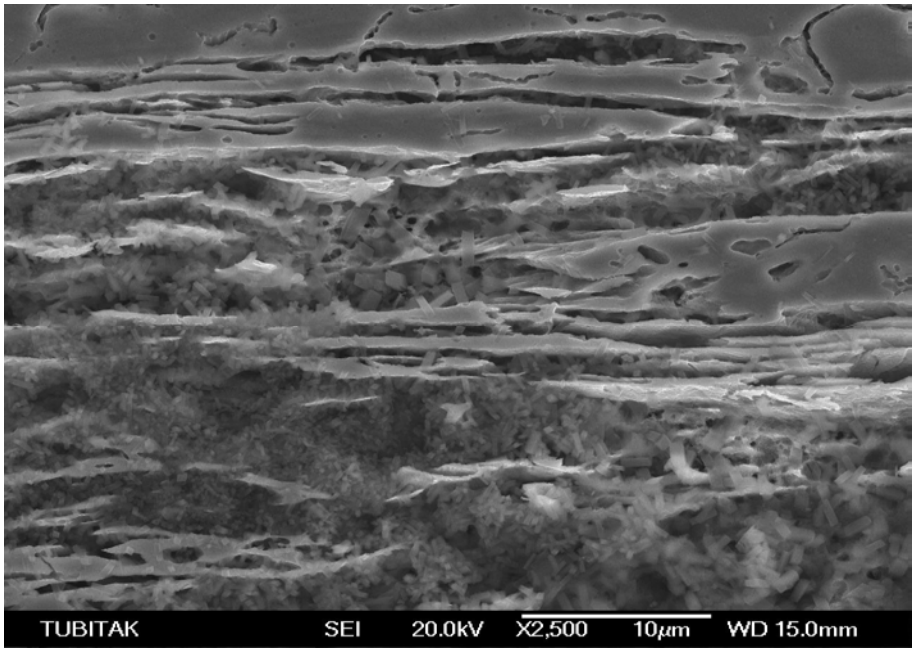

Figure 5.131. SEM image of weld interface of F6

Figures 5.130 and 5.131 illustrate the MML (mechanically mixed layer) which has ability of interlocking between the two mating materials.

5.5.2. SEM Analysis of C Group

The SEM (scanning electron microscopy) images of the F3 and F6 specimens are shown in Figure 5.32-5.137.

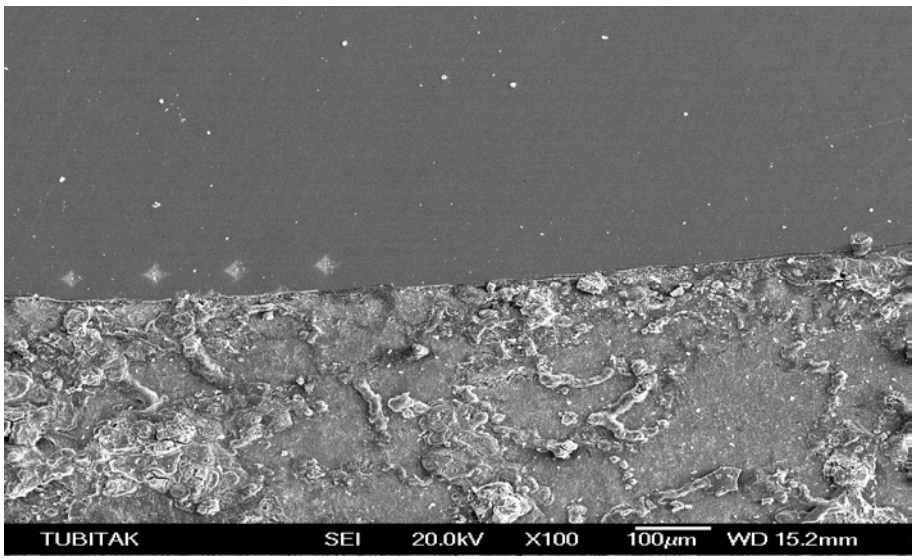

Figure 5.132. SEM image of weld interface of C3

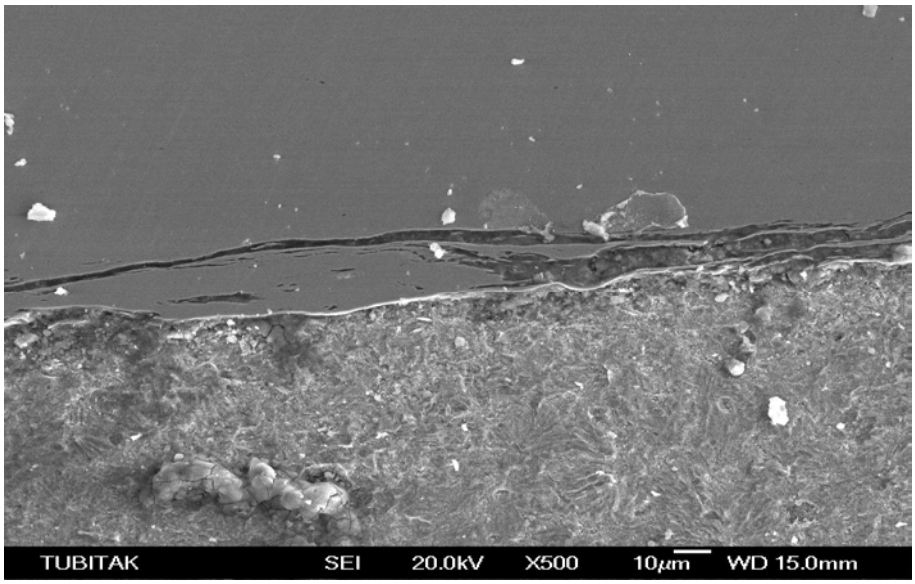

Figure 5.133. SEM image of weld interface of C3

During welding, an interface layer which is generally martensitic is formed in stainless steel side and the width of this layer is not uniform through the interface.

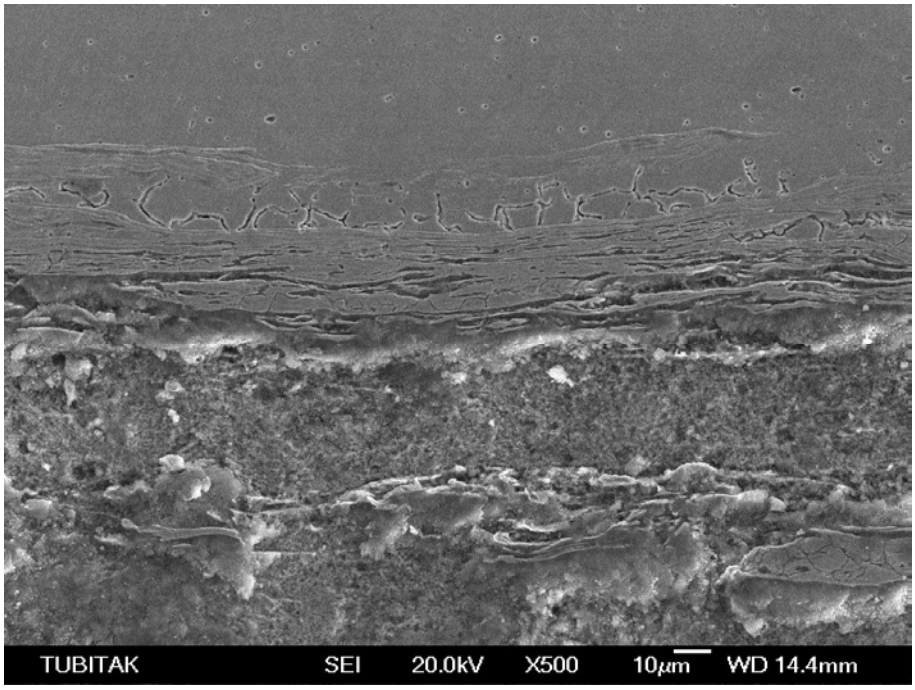

Figure 5.134. SEM image of weld interface of C1

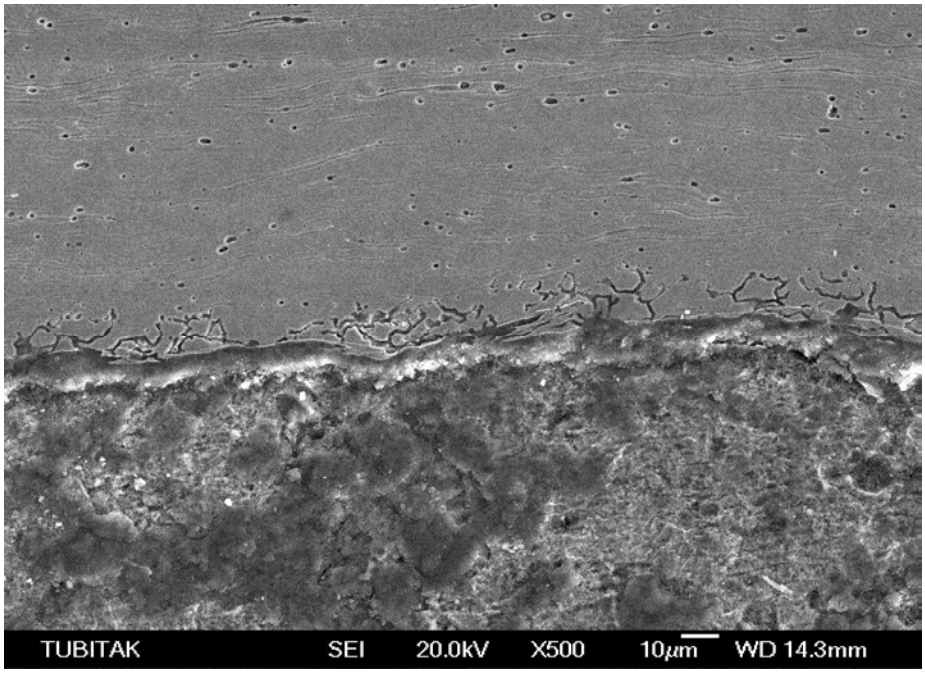

Figure 5.135. SEM image of weld interface of C1

In Figures 5.134 and 5.135 it is shown that mechanically mixed layer was emerged.

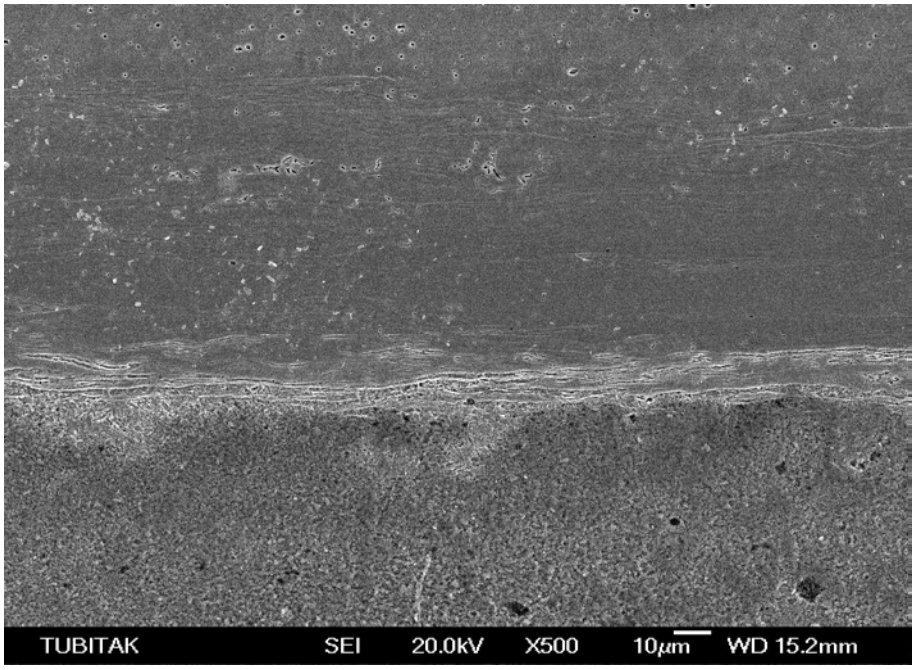

Figure 5.136. SEM image of weld interface of C3

In the Figure 5.136, it seems that there are some carbide grains and this can be attributed to the carbon diffusion which emerged during welding.

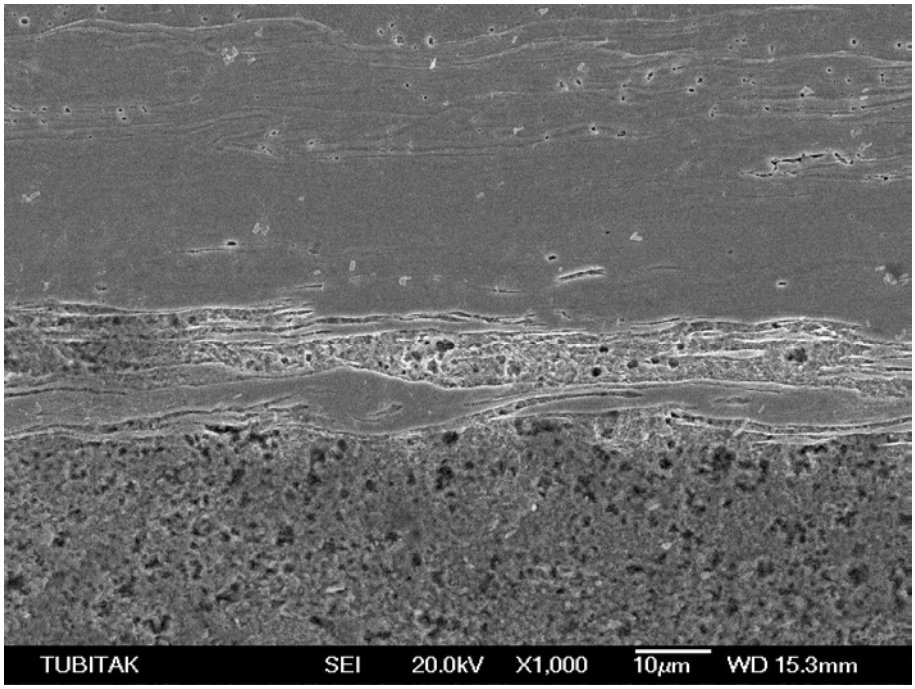

Figure 5.137. SEM image of weld interface of C3

5.5.3. EDS Analysis of F Group

The results of EDS analysis of F3 and F6 and distributions of elements within the determined location are shown in Figure 5.138-5.141.

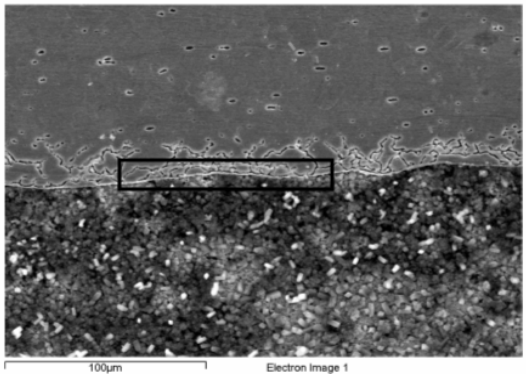

Figure 5.138. EDS analysis location in F3

Table 5.11. Results of EDS analysis in F3

Element	Weight%	Atomic%
Si K	0,45	0,88
Cr K	11,32	12,04
Mn K	2,07	2,08
Fe K	80,52	79,70
Co K	1,08	1,01
Ni K	4,56	4,29
Totals	100	

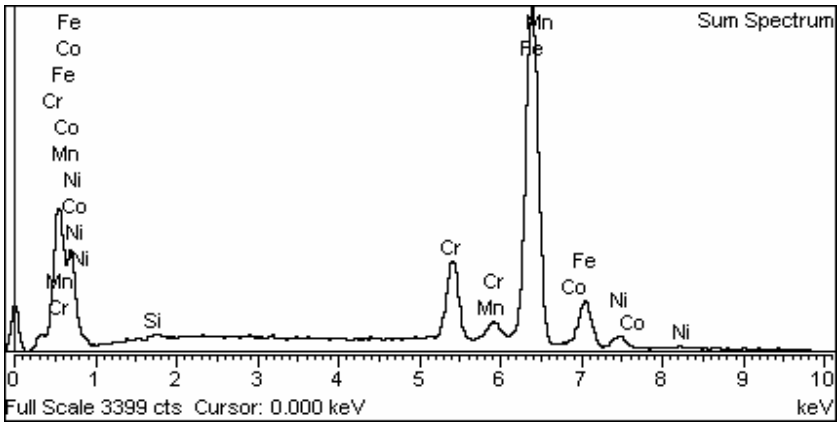

Figure 5.139. Spectrum of elements in weldment of F3

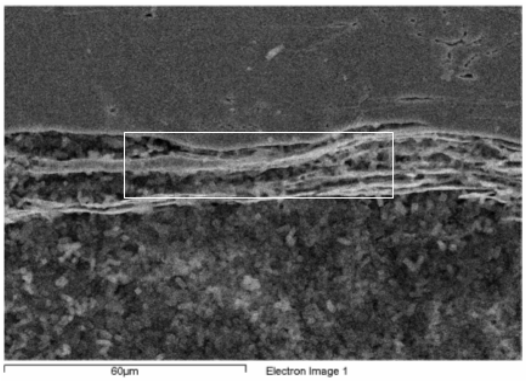

Figure 5.140. EDS analysis location in F6

Table 5.12. Results of EDS analysis in F6

Element	Weight%	Atomic%
Si K	0,27	0,53
Cr K	5,89	6,30
Mn K	0,86	0,87
Fe K	89,44	89,05
Co K	1,05	0,99
Ni K	2,24	2,12
Mo L	0,25	0,14

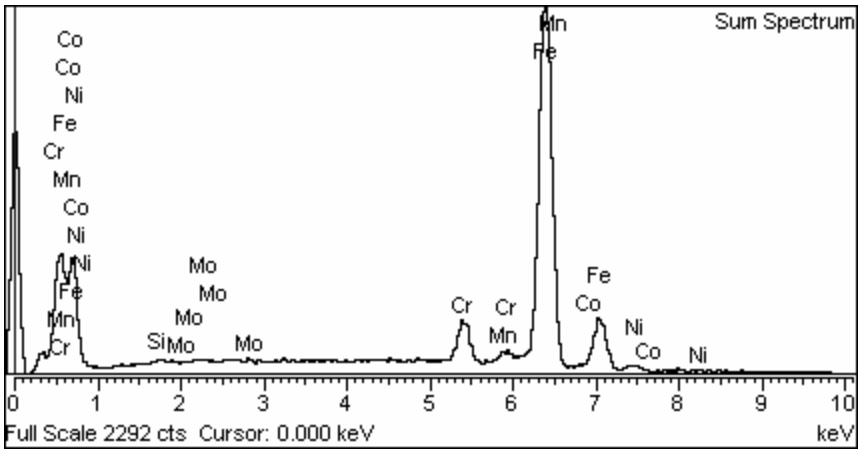

Figure 5.141. Spectrum of elements in weldment

The difference in the weight of alloying elements can be clearly seen by analyzing spectrum of elements. This is because welding process parameters are different from each other.

5.5.4. EDS Analysis of C Group

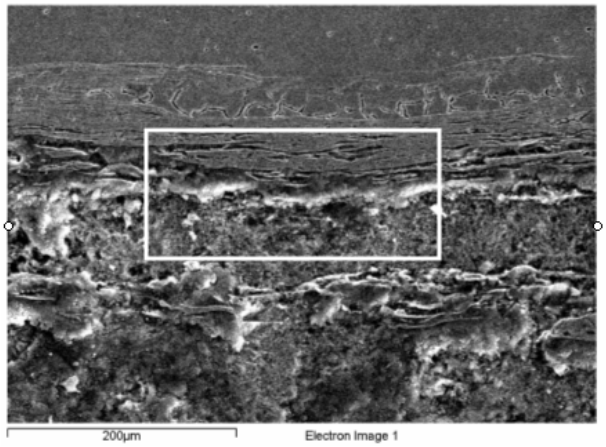

Figure 5.142. EDS analysis location in C1

Table 5.13. Results of EDS analysis in C1

Element	Weight%	Atomic%
O K	6,56	19,61
Si K	0,30	0,52
Cr K	4,16	3,82
Mn K	0,91	0,79
Fe K	85,39	73,08
Co K	0,69	0,56
Ni K	1,98	1,61
Totals	100	

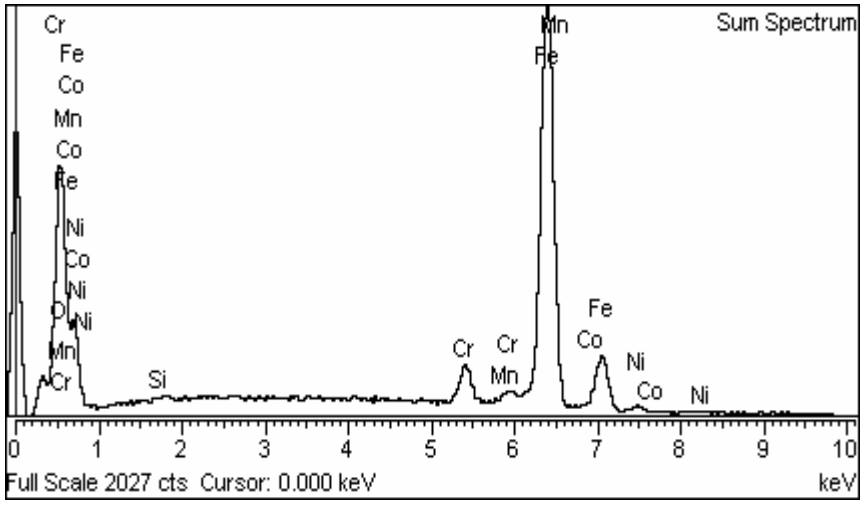

Figure 5.143. Spectrum of elements in weldment

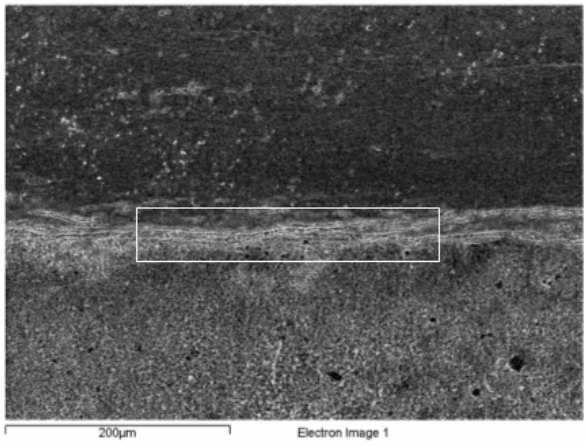

Figure 5.144. EDS analysis location in C3

Table 5.14. Results of EDS analysis in C3

Element	Weight%	Atomic%
Si K	0,38	0,76
Cr K	2,90	3,09
Mn K	1,07	1,08
Fe K	94,23	93,72
Ni K	1,43	1,35
Totals	100	

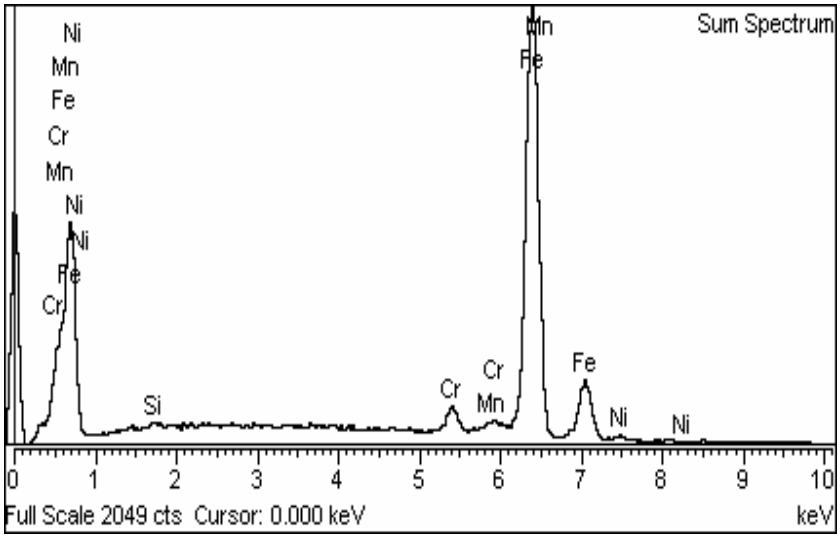

Figure 5.145. Spectrum of elements in weldment

5.6. Evaluation of EDS Analysis

In order to determine the main phases that occurred during the process, one needs the results of EDS analysis for a certain location in a welding line. Therefore EDS analysis results will be needed and used in Schaeffler diagram. The Shaeffler diagram can be used to determine the type of microstructure that can be expected when a metal and parent metal of differing compositions are mixed together in a weld. To do that, “Nickel Equivalent” and “Chromium Equivalent” are needed. After calculations of equivalents, the points are marked and the locations of points the give the phases. The formulas for the “Nickel Equivalent” and “Chromium Equivalent” are as follows:

$$N.E.= Ni\ \% + 30\times C\ \% + 0{,}5\times Mn\ \% \tag{5.5}$$

$$CHR.E.= Cr\% + Mo\ \% + 1{,}5\times Si\% + 0{,}5\times Nb\ \% \tag{5.6}$$

In the light of this information “Nickel Equivalent” and “Chromium Equivalent” are calculated for F3, F6, C1 and C3 as in Table 5.15..

Table 5.15. Determination of nickel equivalent and chromium equivalent

Specimen	Nickel Equivalent	Chromium Equivalent
F3	=4,56+0,5×2,07=5,595	=11,32+1,5×0,45=11,995
F6	=2,24+0,5×0,86=2,67	=5,89+0,25+1.5×0,257=6,541
C1	=1,98+0,5×0,91=2,435	=4,16+1,5×0,3=4,61
C3	=1,43+0,5×1,07=1,965	=2,9+1,5×0,38=3,47

After this simple calculation the coordinates are marked in the diagram. Based on the location of this point, Figure 5.146 reveals that some martensite is formed at the weld interface because of decrease in temperature in very short time, say, rapid cooling rate.

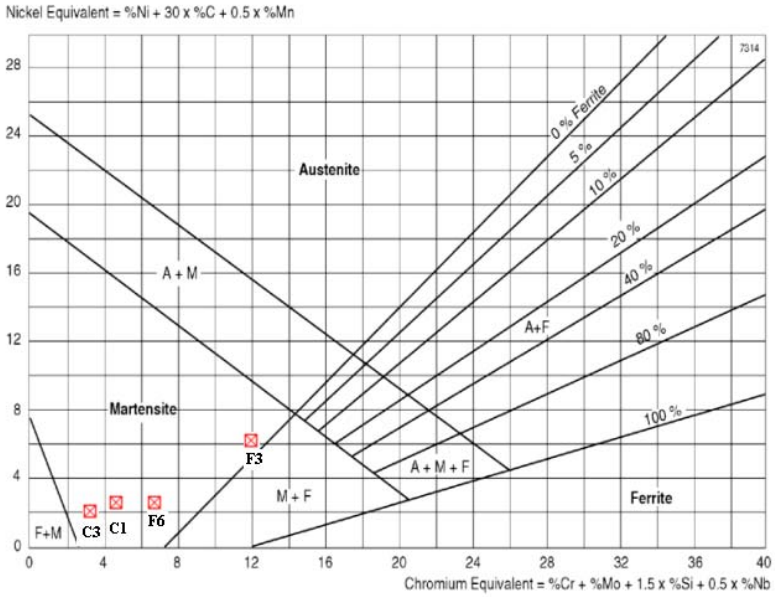

Figure 5.146. Schaeffler diagram [56]

6. CONCLUSIONS

In the view of mechanical properties, for both C group (cast AISI 1050-AISI 304) and F group (forged AISI 1050-AISI 304) the fracture was obtained in base metal, not at the weld interface. The weldments exhibited higher strength than the base metals which means weld quality is superior to other welding process for both of F and C group. The joint strength in F group was more than that of C group as expected due to work hardening which took place during manufacturing forged medium carbon specimens.

What is more, parameters optimization study showed that friction pressure and forge pressure are the most significant parameters for the forged AISI 1050-AISI 304 material pair, however for investment cast AISI 1050-AISI 304 material combination not only friction pressure and forge pressure are the most important factors but also friction time. Parameter optimization at the end of 2^3 factorial design suggested that maximum tensile strength is obtained when friction pressure is between 10-14 sec, friction pressure is 17 bar and forge pressure is 25 bar. Together with, the results were different for C group which suggest friction pressure time as 10 sec, friction pressure as 12 bar and forge pressure as 25 bar.

The evaluation of hardness distribution across the horizontal plane and vertical plane for F and C group gives some interesting results. To begin with, the hardness values in the HAZ of C group are higher than those of F group. This is probably due to recrystallization phenomena which is known as softening process. It is to be noted that forging pressure aids grain refinement and because forging pressure is more effective in the forged parts, recrystallization becomes effective in forged parts. Secondly, almost in the all vertical hardness profiles represent an increase in AISI 1050 parts due to higher cooling rates at the outer faces and a little decrease in the AISI 304 parts due to stainless steel is not hardenable by heat treatment. Statistical approach from the perspective of hardness profiles shows that friction time and friction pressure should be kept as large as possible for minimizing the hardness at the centre whose excessive values can lead to notch effect in the this region. This is somewhat reasonable with the results explained above.

Metallographic examination of the specimens can be classified into three regions: the plastic deformed zone (PDZ) around the welding line, partially deformed zone (PADZ) and unaffected parent material. In the AISI 1050 parts of F group it is clearly seen PDZ contains martensite, PADZ obtains reduction in grain size with increase in pearlite and decrease in ferrite, and undeformed zone obtains more homogeneous mixture of pearlite and ferrite than the cast AISI 1050 parts. Together with, PDZ includes a rapid change in flow direction in AISI 304 parts of both F and C groups. This is mainly based on the high temperature gradient within this zone in which flow is produced radially outwards parallel to the interface. Another aspect was the carbide grains occurred as a result of carbon diffusion from AISI 1050 to AISI 304. Microstructure of stainless steel of cast group shows that martensite is formed at high friction pressure and short friction time due to occurrence of high cooling rates.

SEM Analysis proved that there was a mechanically mixed layer in the specimens in which the hardness was maximum at the interface, on the other hand, there was an equiaxed grain layer in which the hardness value was at minimum level. This is confirmed by the EDS analysis by using Schaeffler Diagram that always some martensite was formed in the MML (mechanically mixed layer).

Taking all the metallurgical and mechanical properties into consideration, friction welding of forged AISI 1050 steel became more effective compared to the investment cast AISI 1050 steel.

7. REFERENCES

1. Kim, S., S. Jung and S. Chur, "Mechanical Properties of Copper to Titanium Joined by Friction Welding", *Journal of Materials Science*, Vol. 38, pp.1281-1287, 2003.

2. Bahrani, A. S. and B. Crossland, "Friction Welding", *Welding and Joining*, Vol. 3, pp. 61-66, 1976.

3. ASM Publications, *Metal's Handbook*, 9th Edition, Vol. 6, Metals Park, Ohio, 1983.

4. Ellis, R. G., "Recent Developments in Friction Welding", *Welding Journal*, pp. 582-589, 1975.

5. Vill, V. I., *Friction Welding of Metals*, American Welding Society, Newyork, 1962.

6. Rao, P. N., *Manufacturing Technology: Foundry, Forming and Welding*, McGraw-Hill, 1987.

7. Koenigsberger, F. and J. R. Adair, *Welding Technology*, MacMillan, London, 1966.

8. Dunkerton, S. B., "Toughness Properties of Friction Welds in Steels", *Welding Research*, AWS, pp. 193-202, August 1986.

9. Thompson Friction Welding, Friction Welding all Around the World, http://www. th-ompson-friction-welding.co.uk/tfwlit/TFW_brochure.pdf, 2004.

10. American Welding Society, *Welding Handbook*, Vol. 3, Miami, 1976.

11. Manufacturing Technology Inc., http://www.mtiwelding.com, 2005.

12. Kinley, W., "Inertia Welding: Simple In Principle and Application", *Welding and Materials Fabrication*, pp. 585-589, October 1979.

13. ASM Publications, *Metal's Handbook*, 10th Edition, Vol. 6, Metals Park, USA, 1994.

14. Walloe, S. J., E. Massoni and L. D. Alvise, "Finite Element Modeling of the Inertia Friction Welding Process Between Dissimilar Materials", *Journal of Material Processing Technology*, Vol. 125-126, pp. 387-391, March 2002.

15. Begg, H. C. and B. A. Humphrey, "Rotational Friction Welding", *Engineering Technical File*, Vol. 91, pp. 1-4, July 1981.

16. Ganowski, F. N., "Practical Considerations for Friction Welding", *Welding Engineer*, May 1973.

17. Sahin, A. Z., "A 3D Numerical Study of Heat Conduction in Friction Welding Process", *Mathematical and Computational Applications*, Vol. 1, No. 1, pp. 111-116, 1996.

18. Sahin, A. Z., B. S. Yibas, M. Ahmed and J. Nickel, "Analysis of Friction Welding Process in Relation to the Welding of Copper and Steel Bars", *Journal of Materials Processing Technology*, Vol. 82, pp. 127-136, March 1997.

19. Nicholas, E. D., "Friction Welding", *Engineering*, Vol. 243, pp. 275-278, September 1970.

20. Sahin, A. Z., B. S. Yibas, M. Ahmed and J. Nickel, "Investigation into the Properties of Friction-Welded Aluminum Bars", *Journal of Materials Processing Technology*, Vol. 54, pp. 76-81, 1995.

21. Welding Advisers, Friction Welding: Low Cost High Yield, http: //www.welding-advisers.com/Friction-welding.html, 2004.

22. Kuruzar, D., “Joint Design for the Friction Welding Process”, *Welding Journal*, pp. 31-35, June 1979.

23. Duffin, F. D. and A. S. Bahrani, “The Mechanics of Friction Welds in Steels”, Metal Construction, pp. 267-271, June 1974.

24. Interface Welding, The Process, http://www.interfacewelding.com, 2005.

25. GB Federal Machines Limited, Friction Welding Applications in the Automotive Industry, http://www.gbfederal.co.uk/allreports4.html, 2004.

26. Ellis, R. G., “Friction Welding: Where the Industry Uses It?”, *Welding Design and Fabrication*,Vol. 6, pp. 78-81, 1976.

27. Scaglia Company, http://www.scaglia.it/en_cylinder.htm, 2005.

28. Aritoshi, M. and K. Okita, “Friction Welding of Dissimilar Materials”, *Welding International*, Vol. 17, pp. 271-275, 2003.

29. Staffelini, G., M. Pellizzari and N. Bernardi, “Microstructure and Impact Behavior of ASTM A105/AISI 304 L Friction Weldments”, *Materials Science and Technology*, Vol. 20, pp. 634-640, May 2004.

30. Ellis, R. G., “Some Recent Applications of Friction Welding”, *Welding and Metal Fabrication*, pp. 207-213, May 1977.

31. TBS Tecnishitube, http://www.tps-technitube.de/Products/Drill-Pipe, 2005.

32. Oberle, T. L. and M. R. Calton, *Turbochargers*, United States Patent Office, Patent No: 3 421 201, Jan 1969.

33. Fukumoto, S., H. Tsubakino, K. Okita, M. Aritoshi and T. Tomita, "Microstructure of Friction Weld Interface of 1050 Aluminum to Austenitic Stainless Steel", *Materials Science and Technology*, Vol. 14, pp. 333-338, April 1988.

34. Mannion, B. and L. Mannin, Trends in the Welding Industry, http://profusiononline.com/pdf/fc-mar99.pdf, 2005.

35. Kobayashi, A., K. Iwase, K. Tadauchi and T. Sakurai, "Study on the Amount of Upset of Friction Welding", *Strength of Materials*, Vol. 32, pp. 285-290, July 1989.

36. Yeom, J. T., J. H. Park, J. W. Lee and N. K. Park, "Characterization of Friction Welding for IN713LC and AISI 4140 Steel", *Materials Science Forum*, Vol. 449, pp. 53-56, 2004.

37. Lipa, M. and R. G. Ellis, "Test for Resistance and Friction Butt Welds", *Welding in the World*, Vol. 16, pp. 31-41, 1978.

38. Murti, G. K. and S. Sunderasan, "Parameter Optimization in Friction Welding Dissimilar Materials", Metal Construction, pp. 331-335, June 1983.

39. Reliability Analysis Center, Design of Experiments, http://rac.alionscience/com/pdf/START2001-3.PDF, 2005.

40. Sionng, H. L. and N. Ann, Understanding Statistical Design and Analysis of Experiment in the Classroom, http://www.stat.auckland.ac.nz/~iase /publications/2/Topic2o .pdf, 2005.

41. Noordegeraaf A. V., M. Nielen and P. C. Kleijinen, "Sensitivity Analysis by Experimental Design and Metamodelling: Case Study on Simulation in National Animal Disease Control", *European Journal Operational Research*, Vol. 146, pp. 433-443, April 2002.

42. Guo, Y., *Construction of Efficient Fractional Factorial Mixed-Level Designs*, Master Thesis, Florida State of University, http://etd.lib.fsu.edu/theses/available/etd-111212 003-230640/unrestricted/YongGuo_Thesis.pdf, 2005.

43. Anderson, M. J. and P. J. Whitcomb, Make Breakthrough Improvements with Design of Experiments, http://www..statease.com/pubs/plastics.pdf, 2005.

44. Sherrill, T., J. Snider, N. Terpstra, C. Vanderpool and W. Schmidt, Accelerating Assay Development Using Experimental Design and Integrated Liquid Handling, http://www.labautomation.org/ConferencePDFs/fg.pdf, 2005.

45. New Mexico Institute of Mining and Technology, http://infohost.nmt.edu/~design /ByChapter/Factorial.htm, 2005.

46. Speedy, A., Design and Analysis of Experiments, http://www.fao.org/ag/AGA/AGA-P/FRG/AHPP126/Ch8.pdf, 2005.

47. University of Leeds, Normal Probability Plots, http://www.maths.leeds.ac.uk/~john/ 3713/ho-4.pdf, 2005.

48. Lawson, J., S. Grimshaw and J. Burt, "A Quantitative Method for Identifying Active Contrasts in Unreplicated Factorial Designs Based on the Half-Normal Plot", *Computational Statistics & Data Analysis*, Vol. 26, pp. 425-436, 1998.

49. Engineering Statistics Handbook, Half-Normal Probability, http://www.itl.nist.gov/d-iv898/handbook/pri/section5/pri598.htm, 2005.

50. Otmanbölük, A. N., "Sürtünme Kaynağı Prosesleri Üzerine Bir Araştırma", Denizli Materials Symposium, Denizli, pp 507-511, 2-4 April 1997.

51. Gürleyik, M. Y., *Sürtünme Kaynağının Kinetik ve Pratiği*, Ph..D. Dissertation, Karadeniz Institute of Science and Engineering, 1971.

52. Satyarayana, V. V., G. M. Reddy and T. Mohandas, “Dissimilar Metal Friction Welding of Austenitic-Ferritic Stainless Steels”, *Journal of Materials Processing Technology*, pp. 1-10, 2004.

53. American Society of Materials, Heat Treater’s Guide, 1995.

54. Taschenbuch Mechanishe Verbindunselemente, Beult-Vertrieb GMBH, 1973.

55. Rajamani, G. P., M. S. Shunmugam and K. P. Rao, “Parameter Optimization and Properties of Friction Welded Quenched and Tempered Steel”, Welding Journal, pp. 225-230, June 1992.

56. Key to Steel, http://www.key-to-steel.com/Articles/Art50.htm, 2005.